



**João Gonçalves Neto**

**Modeling of suspension copolymerization of  
poly(vinyl acetate-co-methyl methacrylate) for  
vascular embolization procedures**

**Dissertação de Mestrado**

Thesis presented to the Programa de Pós-graduação em Engenharia de Materiais e Processos Químicos e Metalúrgicos, do Departamento de Engenharia Química e de Materiais da PUC-Rio in partial fulfillment of the requirements for the degree of Mestre em Engenharia de Materiais e Processos Químicos e Metalúrgicos.

Advisor : Prof. Amanda Lemette Teixeira Brandão  
Co-advisor: Dr. Gustavo Dias Azevedo

Rio de Janeiro  
August 2020



**João Gonçalves Neto**

**Modeling of suspension copolymerization of  
poly(vinyl acetate-co-methyl methacrylate) for  
vascular embolization procedures**

Thesis presented to the Programa de Pós-graduação em Engenharia de Materiais e Processos Químicos e Metalúrgicos da PUC-Rio in partial fulfillment of the requirements for the degree of Mestre em Engenharia de Materiais e Processos Químicos e Metalúrgicos. Approved by the Examination Committee:

**Prof. Amanda Lemette Teixeira Brandão**

Advisor

Departamento de Engenharia Química e de Materiais – PUC-Rio

**Dr. Gustavo Dias Azevedo**

IQ/UFRJ

**Prof. Roberto Ribeiro de Avillez**

Departamento de Engenharia Química e de Materiais – PUC-Rio

**Dr. João Batista de Paiva Soares**

UA

**Dr. José Carlos Costa da Silva Pinto**

UFRJ

Rio de Janeiro, August the 25th, 2020

All rights reserved.

## João Gonçalves Neto

Majored in **Chemical Engineering** by the Pontifical Catholic University of Rio de Janeiro (Rio de Janeiro, Brazil) and in **Generalist Engineering** by the École Centrale de Marseille (Marseille, France).

### Bibliographic data

Gonçalves Neto, João

Modeling of suspension copolymerization of poly(vinyl acetate-co-methyl methacrylate) for vascular embolization procedures / João Gonçalves Neto; advisor: Amanda Lemette Teixeira Brandão; co-advisor: Gustavo Dias Azevedo. – 2020.

144 f: il. color. ; 30 cm

Dissertação (mestrado) - Pontifícia Universidade Católica do Rio de Janeiro, Departamento de Engenharia Química e de Materiais, 2020.

Inclui bibliografia

1. Engenharia Química – Teses. 2. Engenharia de Materiais – Teses. 3. Método dos Momentos. 4. Modelagem Cinética de Polimerização. 5. Modelagem Baseada em Difusão. 6. Agente Embólico. 7. Efeitos Viscosos. I. Lemette Teixeira Brandão, Amanda. II. Dias Azevedo, Gustavo. III. Pontifícia Universidade Católica do Rio de Janeiro. Departamento de Engenharia Química e de Materiais. IV. Título.

CDD: 620.11

To my parents and sister, whose unconditional love and support helps me live  
one day at a time and gives me strength accomplish anything.

## Acknowledgments

I am deeply grateful to my family for always being present, loving and understanding.

I would like to express my gratitude to all members of LaMAC, distinctively my soul sister Annita Fidalgo, Artur Serpa, Caio Grossi, Carlos Castanho, Isabelle Valim and Manoela Fandiño for all the good times and daily delights.

I would like to offer my special thanks to the Cookie Tasters, Fernanda Limonge, Isabela Bastos and Júlia Ribeiro, for the everlasting friendship.

I would particularly like to thank Fernanda Gonçalves, Igor Weilemann and William Guedes for being friends for all moments.

Special thanks to Carol Langenegger and Matheus Ferreira, for a friendship that crossed oceans.

I am deeply grateful to Brunno Santos, for all encouragement, motivation and support.

I would like to show my greatest appreciation to my advisor Gustavo Azevedo, for the patience, trust and enthusiasm, whose mentoring was essential and helped getting me where I am today.

I owe my most profound gratitude to my advisor Amanda Lemette, for not only accepting and guiding me from the beginning, but also for always being there for me. Words will never be enough to describe how deeply I admire and respect you as a professional and as a dear friend.

This study was financed in part by the Coordenação de Aperfeiçoamento de Pessoal de Nível Superior - Brasil (CAPES) - Finance Code 001.

## Abstract

Gonçalves Neto, João; Lemette Teixeira Brandão, Amanda (Advisor); Dias Azevedo, Gustavo (Co-Advisor). **Modeling of suspension copolymerization of poly(vinyl acetate-co-methyl methacrylate) for vascular embolization procedures**. Rio de Janeiro, 2020. 144p. Dissertação de Mestrado – Departamento de Engenharia Química e de Materiais, Pontifícia Universidade Católica do Rio de Janeiro.

The treatment of vascularized tumors through vascular embolization is sensible to the polymeric particles used during procedure. These embolic agents have attributes, like size and morphology, which play a significant role on the success of this technique and can promote complications when not well dimensioned. Among the many options available, spherical particles of poly(vinyl acetate-co-methyl methacrylate) present most desired characteristics after alkaline hydrolysis treatment. Being relatively new, the literature lack studies related to the kinetics of production of this material. Therefore, this research investigated the copolymerization kinetics of poly(vinyl acetate-co-methyl methacrylate) production. In the mathematical development, the method of moments was used assuming quasi-steady state for the free radical species. Additionally, the model includes the viscous effects through the diffusion of the involved molecules, which is usually accounted empirically. It was possible to use the physical properties of the monomers as well as the homopolymerization kinetic parameters in the copolymerization. However, as reported in the literature, some parameters are sensible to the system and some viscous effects affect the copolymerization differently. Therefore, some parameters were reestimated. It was possible to predict the conversion, average molecular weights and composition. Consequently, the model was capable of representing the kinetics of the suspension copolymerization of poly(vinyl acetate-co-methyl methacrylate), meaning it could be used to improve the production of this polymer as an embolic agent for vascular embolization procedure. As far as known by the author, this is the first study to successfully perform the kinetic modeling of this specific system.

## Keywords

Method of Moments; Polymerization Kinetic Modeling; Embolic Agent; Diffusion-Based Framework; Viscous Effect.

## Resumo

Gonçalves Neto, João; Lemette Teixeira Brandão, Amanda; Dias Azevedo, Gustavo. **Modelagem da copolimerização em suspensão de poli(acetato de vinila-co-metacrilato de metila) aplicado em procedimentos de embolização vascular**. Rio de Janeiro, 2020. 144p. Dissertação de Mestrado – Departamento de Engenharia Química e de Materiais, Pontifícia Universidade Católica do Rio de Janeiro.

O processo de tratamento de tumores por embolização vascular é sensível ao conjunto de partículas poliméricas empregado, ditos agentes embólicos, cujos fatores como tamanho e morfologia influenciam no sucesso do procedimento e podem ocasionar complicações quando mal dimensionados. Partículas esféricas de poli(acetato de vinila-co-metacrilato de metila) apresentam a maioria das características desejadas após tratamento por hidrólise alcalina. Este material é relativamente novo, o que significa que há uma lacuna de conhecimento em relação ao estudo dos fenômenos que regem sua cinética. Dessa forma, o presente trabalho investigou a cinética de copolimerização responsável pela sua produção. No desenvolvimento matemático, o método dos momentos foi utilizado assumindo estado quase-estacionário para as espécies radicalares. Além disso, o modelo considera difusão das moléculas no meio para contabilização dos efeitos viscosos, comumente determinados empiricamente. Constatou-se que as características físicas dos monômeros, assim como os parâmetros cinéticos da homopolimerização, puderam ser utilizados na copolimerização. Entretanto, como relatado na literatura para outros sistemas, os efeitos viscosos se comportam de forma consideravelmente diferente na copolimerização, sendo necessário a reestimação de alguns parâmetros relativos aos mesmos. Assim, foi possível reproduzir de forma adequada perfis de conversão, massas molares médias e composição do copolímero. Concluiu-se que o modelo proposto é capaz de representar a cinética da copolimerização em suspensão do poli(acetato de vinila-co-metacrilato de metila), possibilitando um melhor controle das características do copolímero aplicado ao procedimento de embolização vascular. Até onde se tem conhecimento, este é o primeiro trabalho que investiga e implementa com sucesso a modelagem cinética desse sistema.

## Palavras-chave

Método dos Momentos; Modelagem Cinética de Polimerização; Modelagem Baseada em Difusão; Agente Embólico; Efeitos Viscosos.

## Table of contents

<b>1</b>	<b>Introduction</b>	<b>19</b>
1.1	Objectives	21
1.2	Thesis outline	21
<b>2</b>	<b>Literature review</b>	<b>22</b>
2.1	Basic concepts of polymers	22
2.1.1	Characteristics and classification	22
2.1.2	Free-radical polymerization	27
2.1.3	Viscous effects	30
2.1.4	Polymerization techniques	32
2.2	Vascular embolization	33
2.2.1	History and applications	34
2.2.2	Embolic agents	36
2.3	Free radical polymerization modeling	38
2.3.1	Free volume theory	41
2.3.2	Diffusion-controlled reactions	43
2.4	Parameter estimation	49
2.4.1	Estimation algorithm	49
2.4.2	Statistical evaluation	52
2.5	Concluding remarks	52
<b>3</b>	<b>Model development</b>	<b>54</b>
3.1	Homopolymerizations	55
3.1.1	Balance equations	56
3.1.2	Viscous effects	61
3.2	Copolymerizations	62
3.2.1	Balance equations	65
3.2.2	Viscous effects	82
3.3	Model parameters	86
3.4	Program structure	90
3.5	Concluding remarks	92
<b>4</b>	<b>Experimental procedure of collected data</b>	<b>93</b>
4.1	Poly(vinyl acetate)	93
4.2	Poly(methyl methacrylate)	95
4.3	Poly(vinyl acetate-co-methyl methacrylate)	96
4.4	Concluding remarks	97
<b>5</b>	<b>Simulation Performances</b>	<b>98</b>
5.1	Estimation process	98
5.2	Polymerization prediction	101
5.2.1	Poly(vinyl acetate)	101
5.2.2	Poly(methyl methacrylate)	105
5.2.3	Poly(vinyl acetate-co-methyl methacrylate)	108

5.3	Concluding remarks	117
6	Conclusions	119
7	Future perspectives and suggestions	121
	Bibliography	121
A	Mathematical equivalences	133
B	Copolymerization moments valid combinations	134
C	Values of model parameter in the confidence regions	136
D	Monomer, volume and initiator charts	140

## List of figures

Figure 2.1	Example of polymer definition.	23
Figure 2.2	Chain structure classification of polymers. (a) Linear, (b) Branched, (c) Cross-linked, (d) Network. Adapted from Callister & Rethwisch, 2013 [1].	24
Figure 2.3	Examples of homopolymer and copolymer structures.	25
Figure 2.4	Example of step-growth polymerization. Synthesis of PET [1].	26
Figure 2.5	Simplified illustration of chain reaction polymerization stages.	27
Figure 2.6	Benzoyl peroxide decomposition reaction and possible parallel reactions. Adapted from Su, 2013 [29].	31
Figure 2.7	Illustration of a smart tip catheter being maneuvered to a target blood vessel. (a) Catheter placement; (b) Tip activation; (c) Bend adjustment; (d) Vessel selection; (e) Steer; (f) Tip deactivation; Adapted from Selvaraj & Takahata, 2020 [44].	34
Figure 2.8	Illustration of vascular embolization procedure in the treatment of uterine fibroid. Adapted from Hu et al, 2019 [8].	35
Figure 2.9	Vinyl alcohol tautomer equilibrium. Adapted from Ced-erstav & Novak, 1994 [61].	37
Figure 2.10	Illustration of belt saponification of poly(vinyl acetate) to generate poly(vinyl alcohol) particulates. (a) Mixing vessel; (b) Cover plate; (c) Discharge; (d) Conveyor belt; (e) Mill; (f) Washing vessel. Adapted from Hallensleben et al, 2015 [12]	38
Figure 2.11	Monomers and polymer molecular structure used in the study performed by Oliveira et al, 2011 [13] and Azevedo, 2019 [14].	39
Figure 2.12	Commercialization cycle of new processes and products. Adapted from Al-Harathi [63].	40
Figure 2.13	Cage effect geometry illustration. Adapted from Kiparis-sides [36].	43
Figure 2.14	Gel effect geometry illustration. Adapted from Kiparis-sides [36].	46
Figure 2.15	Glass effect geometry illustration. Adapted from Kiparis-sides [36].	47
Figure 2.16	Example of expected behavior of $k_t$ due to gel effect. Adapted from Achilias, 2007 [72].	48
Figure 2.17	Example of expected behavior of $f$ and $k_p t$ due to cage and glass effects. Adapted from Achilias, 2007 [72].	48
Figure 2.18	Simplified diagram of the parameter estimation process.	49
Figure 2.19	Illustration of PSO vector composition.	51
Figure 2.20	PSO implementation diagram.	51
Figure 3.1	Flowchart of the model development process for all polymerization systems.	54
Figure 3.2	Representation of P and Q polymer chain types.	63

Figure 4.1	Illustration of the experimental structure used.	94
Figure 5.1	Vinyl acetate estimation progress at each iteration.	99
Figure 5.2	Methyl methacrylate estimation progress at each iteration.	100
Figure 5.3	Poly(vinyl acetate-co-methyl methacrylate) estimation progress at each iteration.	100
Figure 5.4	Conversion over time for the experimental data and model prediction of vinyl acetate homopolymerization.	102
Figure 5.5	Gel effect present in the simulation of PVAc.	103
Figure 5.6	Cage and glass effects present in the simulation of PVAc.	103
Figure 5.7	Final average molecular weights for the experimental data and model prediction in the homopolymerization of vinyl acetate.	104
Figure 5.8	Average molecular weights evolution in the simulation of PVAc.	104
Figure 5.9	Conversion over time for the experimental data and model prediction of methyl methacrylate homopolymerization.	105
Figure 5.10	Gel effect in methyl methacrylate modeling.	106
Figure 5.11	Cage and glass effects in methyl methacrylate modeling.	106
Figure 5.12	Final average molecular weights for the experimental data and model prediction in the homopolymerization of methyl methacrylate.	107
Figure 5.13	Average molecular weights evolution in the simulation of PMMA.	107
Figure 5.14	Conversion over time for the experimental data and model prediction of poly(vinyl acetate-co-methyl methacrylate copolymerization).	111
Figure 5.15	Conversion over time for the copolymerization. The vertical red line indicates the start of the extrapolated region.	112
Figure 5.16	Gel effect in P(VAc-co-MMA) modeling. The vertical red line indicates the start of the extrapolated region.	113
Figure 5.17	Cage effect in P(VAc-co-MMA) modeling. The vertical red line indicates the start of the extrapolated region.	114
Figure 5.18	Glass effect in P(VAc-co-MMA) modeling. The vertical red line indicates the start of the extrapolated region.	114
Figure 5.19	Model prediction and experimental data on the copolymer composition.	115
Figure 5.20	Final average molecular weights of experimental data and model prediction in the copolymerization of P(VAc-co-MMA).	116
Figure 5.21	Average molecular weights in the simulation of P(VAc-co-MMA).	116
Figure 5.22	Monomers consumption through the reaction.	117
Figure C.1	Values of the coordinates that were considered to be inside the confidence region.	136
	(C.1(a))	136
	(C.1(b))	136
	(C.1(c))	136
	(C.1(d))	136

Figure C.2 Values of the coordinates that were considered to be inside the confidence region, continuation.	137
(C.2(a))	137
(C.2(b))	137
(C.2(c))	137
(C.2(d))	137
(C.2(e))	137
(C.2(f))	137
Figure C.3 Values of the coordinates that were considered to be inside the confidence region, continuation.	138
(C.3(a))	138
(C.3(b))	138
(C.3(c))	138
(C.3(d))	138
(C.3(e))	138
(C.3(f))	138
Figure C.4 Values of the coordinates that were considered to be inside the confidence region, continuation.	139
(C.4(a))	139
(C.4(b))	139
(C.4(c))	139
(C.4(d))	139
(C.4(e))	139
Figure D.1 Vinyl acetate molar behavior.	140
Figure D.2 Volume behavior.	141
Figure D.3 Initiator molar behavior.	141
Figure D.4 Methyl methacrylate molar behavior.	142
Figure D.5 Volume behavior.	142
Figure D.6 Initiator molar behavior.	143
Figure D.7 Volume behavior.	143
Figure D.8 Initiator molar behavior.	144

## List of tables

Table 3.1	Kinetic parameters gathered from the literature.	86
Table 3.2	Benzoyl peroxyde properties.	87
Table 3.3	Vinyl acetate properties.	87
Table 3.4	Methyl methacrylate properties.	88
Table 3.5	Poly(vinyl acetate) properties.	88
Table 3.6	Poly(methyl methacrylate) properties.	89
Table 3.7	List of estimated variables in each polymerization system.	89
Table 3.8	List of PSO parameters used in the estimation process.	91
Table 4.1	Experimental conditions for PVAc synthesis.	93
Table 4.2	Experimental conditions for PMMA synthesis.	95
Table 4.3	Experimental conditions for P(VAc-co-MMA) synthesis.	96
Table 5.1	PSO execution time.	98
Table 5.2	Results of the estimation for all three polymerizations.	101
Table 5.3	Confidence region of the estimated parameters in the copolymerization considering the well-done experiment hypothesis.	110

## Nomenclature

$[\eta]$	Intrinsic viscosity
$\alpha$	Thermal expansion coefficient above glass transition temperature
$\alpha_0$	Thermal expansion coefficient below glass transition temperature
$\alpha_{seg}$	Parameter accounting segmental diffusion
$\beta$	Cross transfer to polymer parameter
$\delta$	Average root-mean-square end-to-end distance of the polymer chain
$\epsilon_{i0}$	Initiation proportionality constant
$\eta$	Dynamic viscosity
$\gamma$	Live moment variable
$\gamma_j$	Overlap factor
$\lambda$	Live moment variable
$\mu$	Dead moment variable
$\mu_{mix}$	Dynamic viscosity of the mixture
$\omega$	Inertia weight
$\phi_p$	Volume fraction of polymer
$\phi_t$	Cross termination parameter
	Specific mass
$\pi$	Dead moment variable
$\tau$	Characteristic time
$\varphi$	Significance
$\xi_{jp}$	Ratio between the critical molar volume of the jumping unit of species j and of the polymer
$A_\eta$	Multiplicative constant of intrinsic viscosity
$B_\eta$	Exponent constant of intrinsic viscosity
C	Concentration

$C_1$	Acceleration coefficient of best individual component
$C_2$	Acceleration coefficient of best global component
$D$	Concentration of non-active polymeric chain
$D_j$	Diffusion coefficient of species $j$
$D_{pe}$	Effective polymer diffusion coefficient
$DF$	Degree of freedom
$F$	Percent-point function of a Fisher distribution
$f$	Initiator efficiency
$f'$	Monomer functionality
$F_{ni}$	Molar fraction of incorporated monomer $i$
$f_{obj}$	Objective function
$F_{seg}$	Reaction probability of two live polymer chains when their active centers are in close proximity
$G_{ij}$	Parameter of binary interaction between $i$ and $j$
$I$	Initiator concentration
$it_{max}$	Maximum number of iterations
$j_c$	Entanglement spacing between chains
$k_B$	Boltzmann constant
$k_d$	Decomposition kinetic constant
$k_i$	Initiation kinetic constant
$k_p$	Propagation kinetic constant
$k_t$	Total termination kinetic constant
$k_{t,res}$	Residual termination kinetic constants
$k_{tc}$	Kinetic constant of termination by combination
$k_{td}$	Kinetic constant of termination by disproportionation
$k_{tm}$	Kinetic constant of transfer to monomer
$k_{tp}$	Kinetic constant of transfer to polymer
$k_{ts}$	Kinetic constant of transfer to solvent
$k_{tx}$	Kinetic constant of transfer to impurity
$M$	Monomer concentration

$m$	Mass
$M_n$	Number-average molecular weight
$M_w$	Weight-average molecular weight
MMA	Methyl methacrylate
MW	Molecular weight
$N$	Number of moles
$N_A$	Avogadro number
NE	Number of experiments
NP	Total amount of estimated parameters
NY	Number of dependent variables
$P_i^\bullet$	Concentration of active polymeric chain of the first type of size $i$
PET	Poly(ethylene terephthalate)
PMMA	Polymethyl methacrylate
PSO	Particle swarm optimization
PVA	Plyvinyl alcohol
PVAc	Polyvinyl acetate
$Q_i^\bullet$	Concentration of active polymeric chain of the second type of size $i$
$R$	Primary radical
$r_B$	Distance of the chain extremity from the sphere center
$r_b$	Distance where the concentration of chains is representative to that of the reaction medium.
$r_e$	Kuhn's segment length
$R_H$	Hydrodynamic radius
$r_I$	Radius of sphere related to cage effect
$r_i$	Reactivity ration
$r_m$	Effective radius of propagation
$r_t$	Termination radius
S	Solvent
T	Temperature
$T_g$	Glass transition temperature

$V^*$	Critical hole volume
$V_f$	Free volume
$V_{fi}$	Free volume of species $i$
$V_P$	Critical molar volume of the jumping unit of the polymer
VAc	Vinyl acetate
w	Weight fraction
X	Conversion
x	Number fraction
$X_{c0}$	Critical degree of polymerization for the entanglement of polymer chains

*“That’s rather a broad idea,” I remarked.  
“One’s ideas must be as broad as Nature if  
they are to interpret Nature,” he answered.*

**Arthur Conan Doyle, *A Study In Scarlet.***

# 1 Introduction

Materials are present and influence many aspects of everyday life, which makes their study certainly important. This becomes even more evident when pointing out how historical periods of humanity are many times described by society's capability of handling and generating specific materials (Stone Age, Bronze Age, Iron Age, Age of Oil, Nuclear Age, etc) [1].

In recent history, polymeric materials have become notably prominent. Although there are records of production of semi-synthetic plastics as early as 1862, the more consolidated concepts of polymers were developed throughout the twentieth century, due to a rise in academic and economical activities related to plastics and rubbers. Since then, these materials have proven to be versatile, as they are used in different fields, such as domestic and commercial furniture market [2], structural components (aerospace, railway, automotive, naval) [3], surface coating [4], adhesives [5] and many others [6].

In medical field specifically, polymers are important in a procedure called vascular embolization. This technique consists of obstructing blood vessels by injecting embolic agents that may be made of polymer. It is particularly useful in the treatment of uterine myoma, because it blocks the flow that feeds the tumor. As it starts lacking nutrients to sustain itself, the tumor shrinks, sometimes resulting in complete disappearance. Even in cases where the size of the tumor decreases partially, this technique is extremely beneficial to the patient, because it reduces possible risks related to surgical intervention [7, 8].

Considering that the embolic agent is inserted in a biological medium, it must have specific characteristics to ensure not only the success of the procedure, but also the health of the patient. They should present non-toxicity, bio-compatibility, non-antigenicity, among many other properties that can be found in polymers [7, 8]. Besides, it was discovered that the morphology of the embolic agent is important, as spherical shape was proven to generate less aggressive tissue inflammation [9].

A standard material used in the initial development of uterine artery embolization is poly(vinyl alcohol) (PVA) microbeads. It presents most of the desired characteristics when it comes to biological interaction, but not in terms of morphology when produced by classical techniques [9]. This lead to different

polymers being proposed [10, 11], although PVA remained the most financially accessible. A study by Siskin in 2003 [9] has shown that microspheres of PVA solve the morphology problems of the irregular particulates.

PVA is not normally obtained by direct means, therefore it is usually manufactured through polymerization of vinyl compounds, followed by chemical treatment to synthesize the hydroxyl function [12]. A relatively new polymer that can undergo this process is poly(vinyl acetate-co-methyl methacrylate) (P(VAC-co-MMA)) [13]. It can be obtained through suspension polymerization of vinyl acetate (VAc) and methyl methacrylate (MMA) monomers, which results in spherical particles of different sizes. The particle size distribution and morphology are shown to be sensible to the reaction conditions and, in some instances, the polymer conversion can be considerably low. This is not desirable, because the particles size must be in specific size ranges to ensure both procedure effectiveness and patient safety [14]. Therefore, the present conditions lead to a significant economic waste if put in production as it is.

An alternative to better comprehend the phenomena happening during the reaction is to develop a model, because, after validation with experimental data, it can be used to predict the product properties for different conditions without having to perform an enormous quantity of experiments, thereby saving expenses and time. However, the modeling of suspension polymerization systems is usually complex, as it is an heterogeneous process and it involves a considerable amount of reactions. This results in a great quantity of differential equations that are not easily solved. Besides, with the advance of the reaction, there are physical effects that may take place due to a significant change in the medium viscosity, the cage-, gel- and glass-effects [15]. Unfortunately, no study about modeling the suspension copolymerization of poly(vinyl acetate-co-methyl methacrylate) focused vascular embolization applications were found in the literature.

Deterministic and stochastic approaches have already been successfully implemented for other polymerization systems [16, 17, 18, 19, 20]. One of the main models adopted was introduced by the authors Achilias & Kiparissides [21, 22]. In this model the method of moments [23] is applied to limit the infinite DE system and the free-volume theory [24] is used to evaluate the diffusion variation of the species. This variation is then used to account for viscous effects influence over the kinetics [25, 26, 27, 28]. This method is advantageous, because it is based on physical properties of the involved species.

The present study documents a deterministic approach for modeling the suspension copolymerization of poly(vinyl acetate-co-methyl methacrylate) using the model initially proposed by Achilias & Kiparissides.

## 1.1

### Objectives

Considering the previous comments, the following objectives were established for this master's thesis:

- **General Objective:** Modeling the suspension copolymerization of poly(vinyl acetate-co-methyl methacrylate). The model should consider the physico-chemical properties of the monomers and polymer, as well as reaction conditions, such as components initial masses and temperature.
- **Specific Objectives:**
  - To develop the mathematical balance equations system using the method of moments for both homopolymerization and copolymerization.
  - To study the volume-theory and how to implement it on polymerization systems to account for viscous effects.
  - To develop, implement and validate a simulation program for the homopolymerization of poly(vinyl acetate) and of poly(methyl methacrylate) using the proposed model.
  - To develop, implement and validate a simulation program for the copolymerization of poly(vinyl acetate-co-methyl methacrylate) using the proposed model.

## 1.2

### Thesis outline

The present master's thesis is structured in six chapters. **Chapter 1** consists of the introduction, briefly contextualizing the project and establishing its motivations, objectives and outline. **Chapter 2** is the literature review, where the necessary background to understand the project is exposed. **Chapter 3** details the development of the implemented homo- and copolymerization modeling, including theoretical considerations, mathematical developments, programming strategies and parameter data collection. **Chapter 4** is a description of the experiment that resulted in the data used for the modeling. **Chapter 5** presents and discusses all simulation results generated through this research. **Chapter 6** is the conclusion of the thesis and it summarizes the relevant results. **Chapter 7** points out future perspectives for model improvement and applications.

## 2

### Literature review

The focus of this chapter is to expose the state of art related to the main topics as well as to explain the essential concepts needed to better comprehend the developed model. It begins establishing the basic notions related to polymers followed by detailing the vascular embolization process. Other more in-depth aspects are also addressed in this chapter, such as polymerization modeling, kinetics and viscous effects. Lastly, a section concerning parameter estimation is also present.

#### 2.1

##### Basic concepts of polymers

This section establishes the fundamentals of polymers that are needed to better comprehend the themes explored later in this research.

##### 2.1.1

###### Characteristics and classification

Polymers are macromolecules, meaning they are substances that possess high average molecular weights. As the name suggests, they are formed by a repetition of subunits referred as "mers" that are obtained through the reaction of monomers [29]. These subunits are chemically bound, forming long organic chains as illustrated in Figure (2.1).

The monomer molecule must have at least two sites that allow the reaction, so the chain can be formed. The number of bonds a monomer can form is called functionality ( $f'$ )[1]. In styrene, for example, the double bond out of the aromatic ring can be broken so each carbon atom forms the polymeric chain ( $f' = 2$ ).

Depending on the functional groups and the repeating unit structure itself, the chains that form the polymer may interact in different manners, influencing the physical behavior of the final product, such as solubility, hydrophilicity, physical state, heat resistance, flexibility and others [29].

Polymers have a glass-like state, in which they go from solid to rubber-like before melting and vice versa [29]. It happens because, at certain temperatures, some secondary interactions between chains are broken and these chains are

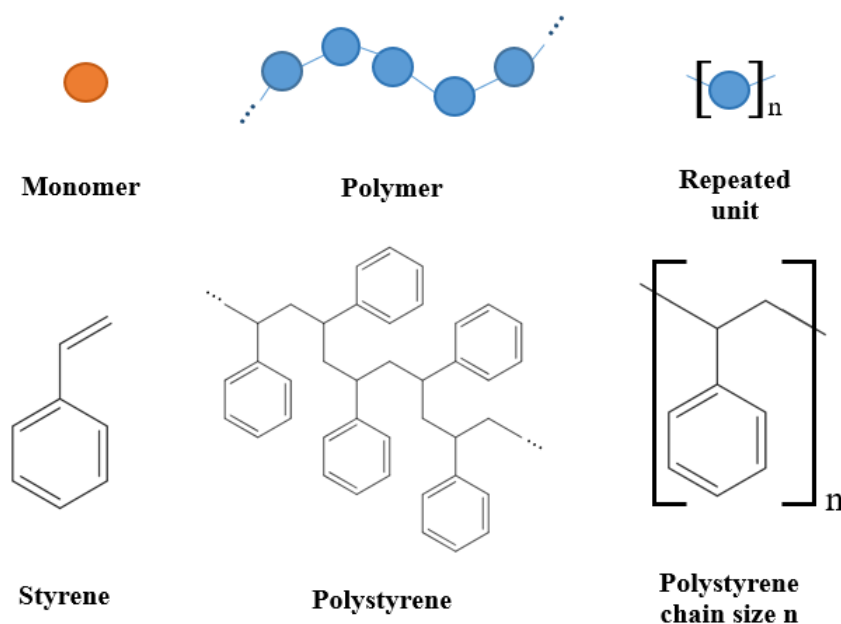


Figure 2.1: Example of polymer definition.

able to move limitedly. This temperature is called glass transition temperature ( $T_g$ ) and it is extremely important, because a polymerization carried out next to the  $T_g$  usually increase the effects of transport phenomena over the reaction kinetics.

The variety of properties related to polymers has lead to a considerable amount of possible classification methods. Some are based on synthesis, structure, mechanical behaviors, composition, etc. For this reason, only the most relevant methods for the research are addressed.

One of the most basic forms of differentiating polymeric materials is through their origin. They are defined as **natural**, when extracted from living organisms (proteins, enzymes, cellulose, etc) and **synthetic**, when obtained through the chemical reaction of monomers (phenol-formaldehyde, polyurethane, epoxies, etc)[1].

Polymers can also be classified according to the structure of the chains. Although different authors may present multiple classifications, there are four major types in this group: linear, branched, cross-linked and network.

The **linear** polymeric chains are formed by covalent bonds and have one beginning and one end. Therefore, this structure allows the chains to arrange themselves and fold in a more compact manner depending on intermolecular forces, usually resulting in tangled chains with possibility of also forming semi-crystalline structures. Polymers of this category are usually denser, such

as poly(methyl methacrylate), (poly(vinyl chloride) and poly(styrene), for example [1].

**Branched** polymers, as the name indicates, are characterized by having a main chain from where other chains begin. Because of these branches, the polymeric chains have less available volume to rearrange themselves, leading to a less dense material like low-density poly(ethylene) [1].

**Cross-linked** polymers are generated when linear polymeric chains form covalent bonds in different positions, meaning no main chain is present. They can be obtained during synthesis or after using nonreversible chemical reactions like rubber vulcanization process [1] and radiation cross-linking of polyolefins [30].

Polymers are considered a **network** when they are formed by a three dimensional net of covalent bonds due to a functionality of three or higher. The result is a final material formed by one big amorphous structure with no identifiable main chain, as illustrated in Figure (2.2). Epoxies are examples of polymers of this category [1].

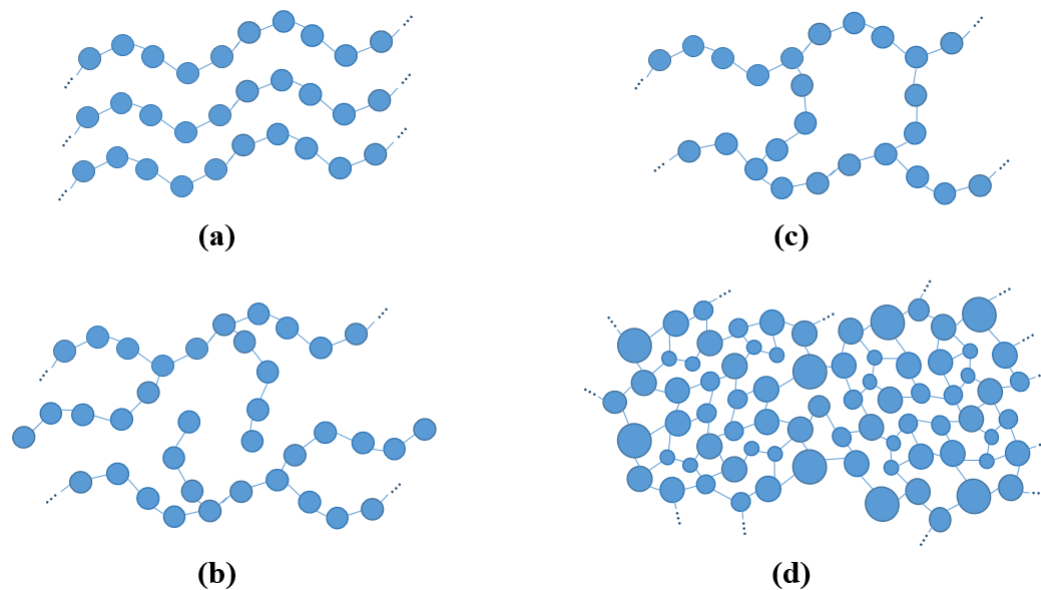


Figure 2.2: Chain structure classification of polymers. (a) Linear, (b) Branched, (c) Cross-linked, (d) Network. Adapted from Callister & Rethwisch, 2013 [1].

Another important classification of polymers is based on their mechanical behavior, the so called thermoplastics, thermosets and elastomers. **Thermoplastic** polymers are rigid at low temperatures and soft or even liquid as temperature rises significantly, giving these materials the possibility of being remolded and recycled after initial production in a reversible process [31]. Lin-

ear and branched polymeric materials fall in this category, because it is usually possible to heat them enough so the secondary interactions are broken while keeping the covalent bonds mostly intact. The result is that polymeric chains are able to move again, reflected in macroscale as a change in physical state [1].

**Thermosets**, on the other hand, do not become softer with heat, signifying they cannot be remolded by temperature after production [31]. In this case, polymeric chains are a network and the temperature needed to change their structure is higher, but also breaks the covalent bonds, degrading the material.

**Elastomers** have elements from both thermoplastics and thermosets. They possess small degrees of cross-linked chains throughout their structure, giving them the possibility of limited rearrange and folding. Consequently, when tension is applied to this material, secondary interactions are broken and the chains are able to unfold. Subsequently, when the force is relaxed, the material return to its previous state, due to the cross-linked points serving as anchors the original configuration [1].

Another classification is related to the monomeric composition. When a polymer is formed by a single type of monomer, it is called an **homopolymer**. On the other hand, if it is composed of two or more different monomer units, it is called a **copolymer**, as illustrated in Figure (2.3). The advantage of using copolymers is that it allows to combine properties that each homopolymer would have individually and adjust them to what is needed [1].

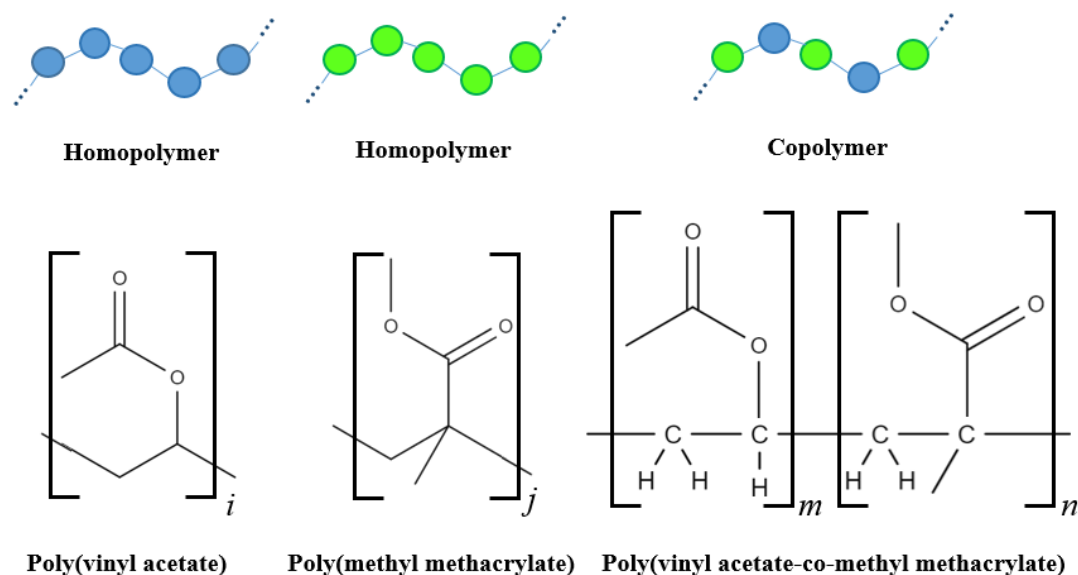


Figure 2.3: Examples of homopolymer and copolymer structures.

Finally, the last classification relevant to this study is related to the chemical mechanism responsible for building up the polymeric chain. There are two major categories, step-growth and chain reaction.

In **step-growth** polymerizations, the monomers present must have at least two functional groups that can react between themselves to form the polymeric chain, usually also forming smaller molecules like the synthesis of poly(ethylene terephthalate) (PET) shown in Figure (2.4) [1]. In the example, it can be noticed the main chain is not only composed of carbon, but also of an element present in the functional group, in this case oxygen.

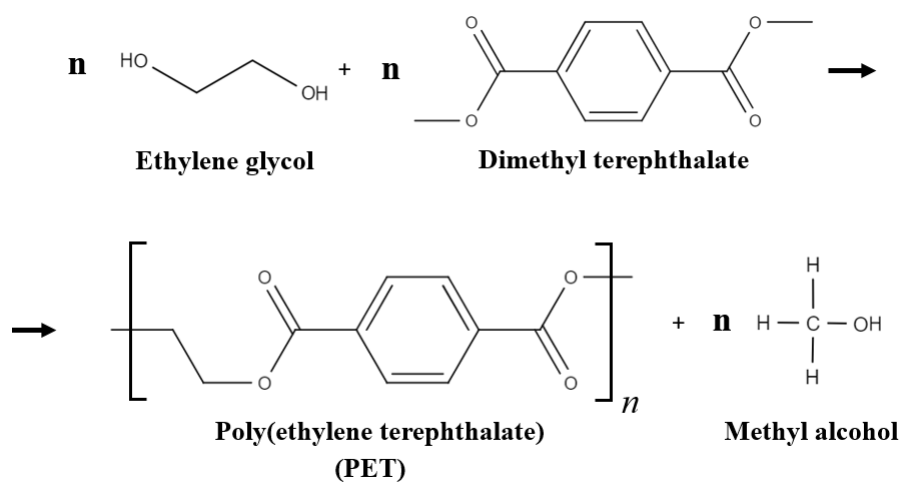


Figure 2.4: Example of step-growth polymerization. Synthesis of PET [1].

**Chain reaction** polymerization is characterized by having the polymer chain growing from an active site [32]. First, the monomer must be initialized to become active. Usually an external agent is used, although in some cases, such as styrene, monomers can autoinitiate. In the second stage, a monomer molecule is incorporated into the chain. The process is repeated, incorporating one monomer at a time, growing the chain in a propagation manner. Finally, the polymerization ends when the active chains deactivate by different possible termination reactions, sometimes being induced by addition of a termination agent to the mixture. The Chain reaction polymerization has some peculiarities depending on which subcategory it belongs [1]. The free-radical polymerization is the most relevant subcategory for this research and its process is illustrated in Figure (2.5), while a better description of each mechanism taking place is shown in the next section.

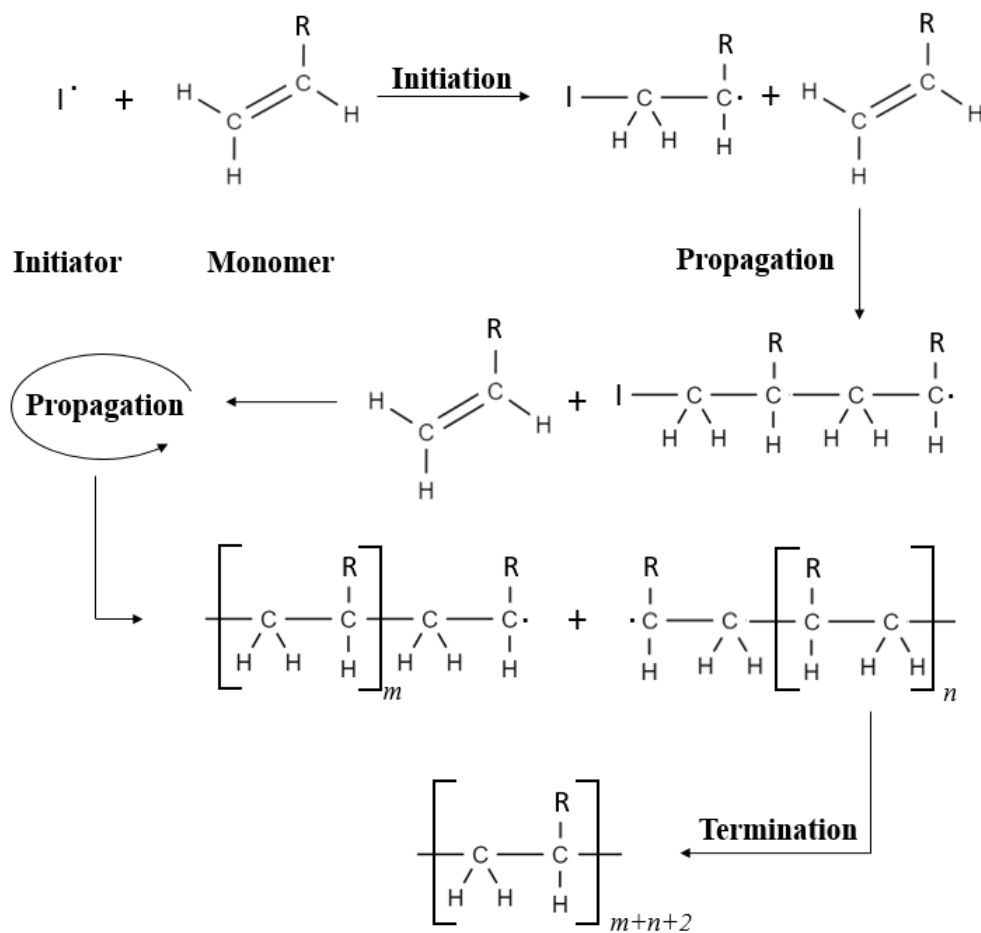


Figure 2.5: Simplified illustration of chain reaction polymerization stages.

### 2.1.2 Free-radical polymerization

The free-radical polymerization is characterized by having the chain reaction being carried out by the generation of free-radicals, meaning that the monomer must have a site that accepts and forms radicals [32]. This is interesting for the polymerization of vinyl-like structures, as the double bonds possess the mentioned property. The kinetics of the three stages are better detailed below.

- **Initiation** - For cases where an initiator is used, this stage happens in two steps. The first is the initiator ( $I$ ) decomposition, where it goes from a stable configuration to the free-radical one ( $R\cdot$ ). As shown in eq. (2-1), depending on its chemical nature of the initiator,  $n$  radical molecules are formed (usually two or more). This process is usually triggered through thermal or photochemical means.

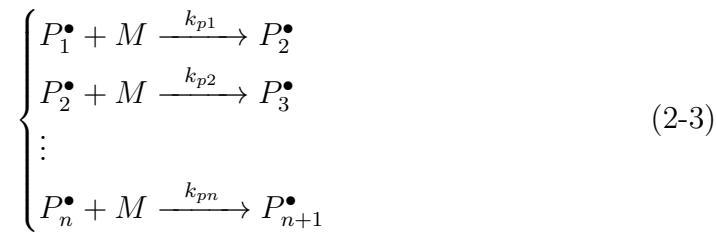


The second step is the monomer activation, where the radical is effectively transferred to a monomer ( $M$ ), as shown in eq. (2-2).



Note that  $P^\bullet$  indicates an active polymeric chain and its subscription indicates the amount of repeating units in its structure, in this case one.

• **Propagation** - In this stage, the active chains, also called "live" chains, react with inactive monomers, growing as shown in eq. (2-3).



As it can be seen, each chain of different size is treated as a different species. Studies have shown the terminal model (or ultimate unit model) can be applied for the polymerization of linear or mostly linear chains [33]. This model considers all polymeric chains of same end unit to be susceptible to the same kinetic rates, independently of their size. Thus, it allows to rewrite the chemical reaction of the polymerization, simplifying the balance development.



• **Termination** - This stage can generate inactive polymeric chains by two major mechanisms. In the termination by **combination**, two live polymers react, generating one inactive polymer, also called "dead" polymer ( $D$ ), as shown in eq.(2-5).



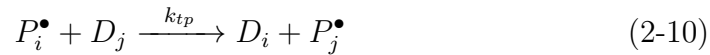
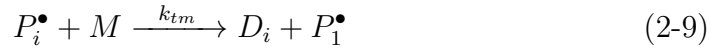
In the termination by **disproportionation**, two live polymers exchange a hydrogen atom and a radical, generating two dead polymers, as presented in eq.(2-6).



The steric hindrance generated by the chemical groups around the polymeric chains determines which termination mechanism will happen [14]. Authors usually represent the terminations constant as  $k_t = k_{tc} + k_{td}$ .

Depending on the species present in the medium, as well as their chemical properties, chain transfer reactions may take place. In these reactions, the

radical is transferred to another molecule, usually being exchanged by a hydrogen, generating a dead polymer. The radical may be transferred to four different species: solvent, impurity, monomer, dead polymers in any position of the chain.



Note that radicals transferred to solvent and impurity are considered lost, also signifying that, when present, these reactions increase the frequency of intermediate and low chain sizes for dead chain [32, 34].

The transfer to polymer reaction has an important role when it is present, because it can generate branching polymeric chains, which increase the average molecular weights of the material, specially the when this reaction leads to long-chains formation [35]. Another important aspect of this reaction is that it reintroduce inactive chains to the reaction dynamics, resulting in a closure problem in the mathematical development of models [36].

During the polymerization reaction, many polymer chains are formed at the same time and they do not necessarily have the same size, resulting in a material with a chain length distribution [1]. As a consequence, there are different forms to define the average molecular weight of a polymer, but the two most common are the number- and weight-average molecular weights ( $M_n$  and  $M_w$ ). Eq.(2-11) and eq.(2-12) show how  $M_n$  and  $M_w$  are calculated.

$$M_n = \frac{\sum_i N_i MW_i}{\sum_i N_i} \quad (2-11)$$

$$M_w = \frac{\sum_i m_i MW_i}{\sum_i m_i} \quad (2-12)$$

where  $MW_i$ ,  $N_i$  and  $m_i$  are the molecular weight, the total number of moles and mass of chains of size  $i$ .

Considering the live and dead polymer chain variables, the number- and weight-average molecular weights of the polymer at any given moment of the process can be expressed in terms of monomer molecular weight ( $MW_0$ ) and the concentration of polymer chains, as represented in eq.(2-13) and (2-14).

$$M_n = \frac{\sum_i N_i MW_i}{\sum_i N_i} = \frac{\sum_i (P_i^\bullet + D_i)(i MW_0)}{\sum_i (P_i^\bullet + D_i)} = MW_0 \frac{\sum_i i(P_i^\bullet + D_i)}{\sum_i (P_i^\bullet + D_i)} \quad (2-13)$$

$$M_w = \frac{\sum_i m_i MW_i}{\sum_i m_i} = \frac{\sum_i N_i MW_i^2}{\sum_i N_i MW_i} = MW_0 \frac{\sum_i i^2(P_i^\bullet + D_i)}{\sum_i i(P_i^\bullet + D_i)} \quad (2-14)$$

### 2.1.3

#### Viscous effects

In some cases, the chain polymerization process is not exclusively controlled by kinetics, because of diffusion properties. In these cases, increase in viscosity due to monomer conversion makes mass transfer phenomena more important, causing three major effects to take place: gel effect, glass effect and cage effect [37].

The **gel effect**, also called Trommsdorff-Norrish effect, happens at low to intermediary conversion levels, where the macromolecules are affected by viscosity increase, but other smaller species are not. As the live chains mobility becomes more limited, the rate of termination reactions decreases [19]. Consequently, more active chains accumulate in the medium, resulting in an increase of monomer consumption, the so called autoacceleration [37].

The **glass effect** takes place in processes conducted under the glass temperature of the polymer. At higher conversion values, the viscosity affects even smaller molecules, such as the monomers [37]. Thus, the propagation rate is affected and the conversion decelerates until complete "freezing" of the species mobility, preventing conversion from reaching full monomer consumption [38].

The **cage effect** is related to the unstable nature of the initiator in its primary radical form. Upon decomposition, the recent generated radicals molecules are close proximity as well as surrounded by other molecules [38]. This creates a cage that the radicals must diffuse out of, so that reaction with monomer is possible. In the confinement stage, the primary radicals may react to other close molecule or self-terminate before being able to diffuse. These recombination reactions are specially prominent in commonly used initiators such as benzoyl peroxide (BPO), which is activated through thermal homolysis to generate benzoyloxy radicals. Figure (2.6) shows BPO decomposition as well as possible recombination reactions it can undergo due to the cage effect [29].

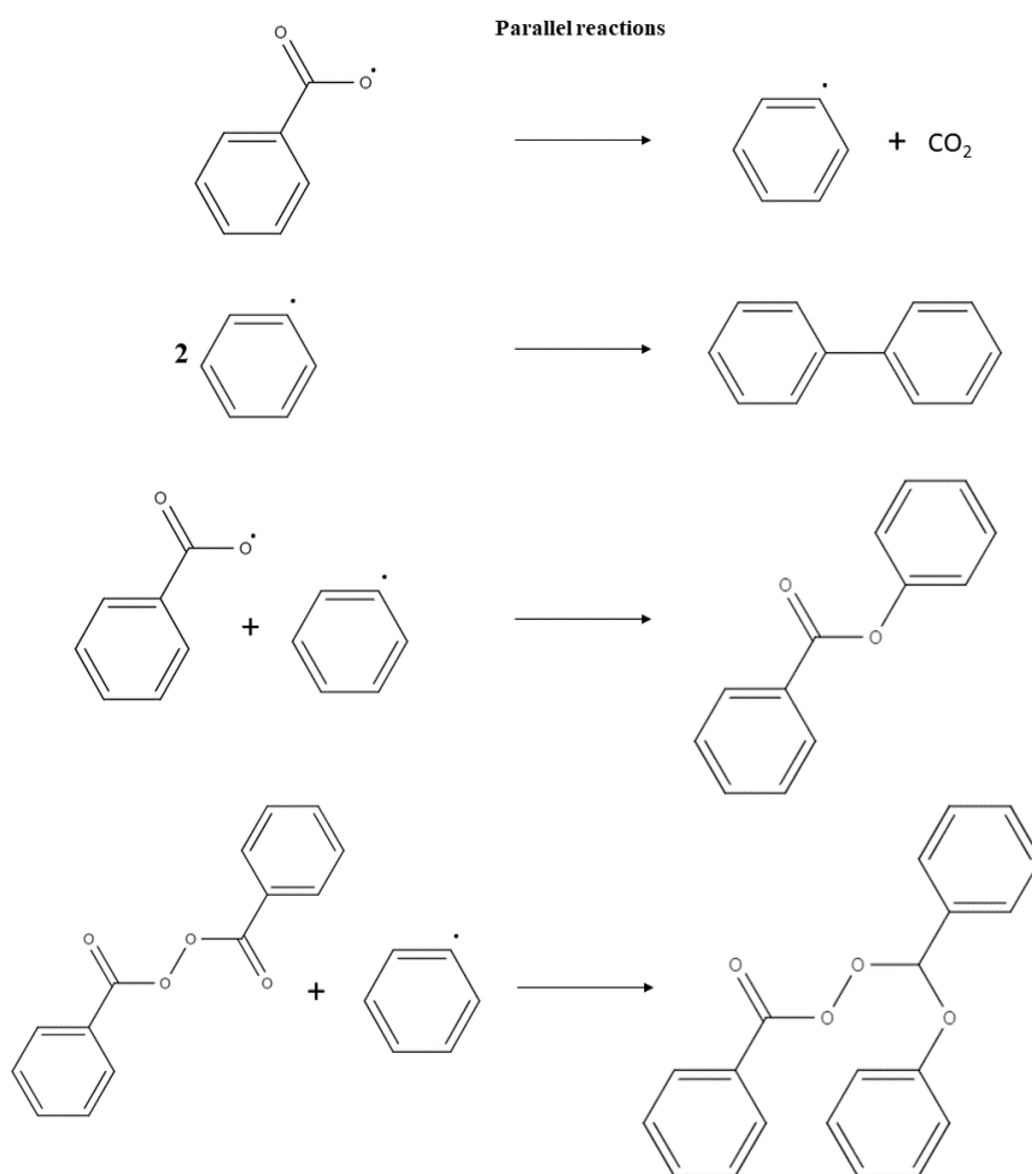
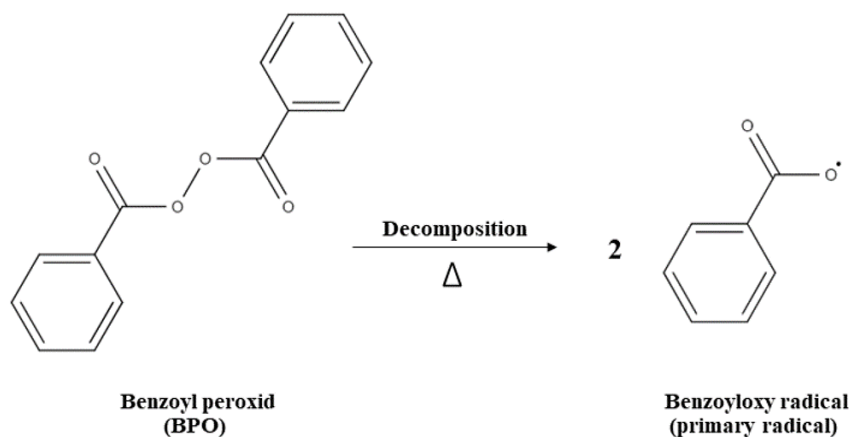


Figure 2.6: Benzoyl peroxide decomposition reaction and possible parallel reactions. Adapted from Su, 2013 [29].

To account for the lost primary radicals in kinetic modeling, an efficiency parameter has been established and it can be translated to the percentage of radicals that are able to leave the cage [21]. This effect is present even at lower conversions and are many times treated as constant in the literature. On the other hand, some authors state that as the polymerization advances considerably, the increase in viscosity hinders the radical probability of leaving the cage, resulting in a sudden decrease of the efficiency factor [20, 22, 39].

All these effects have been a challenge and, although different modeling techniques can be found in the literature, there is still much to be investigated [35, 40].

#### 2.1.4 Polymerization techniques

Polymerization can be implemented in different ways according to the desired properties of the final material and the physical properties of the involved species. These different techniques can be grouped in two major categories: **homogeneous**, when the polymerization happens in a single phase and **heterogeneous**, when more than one phase is involved [38]. Although many different polymerization techniques exist, only three are addressed in this document, as they are the most relevant for this research.

- **Bulk polymerization**

In bulk polymerization, the reaction medium is composed of monomer with a small portion of initiator, when needed. The mixture is maintained in constant agitation and heated to the temperature that triggers the initiation [29]. If the polymer is soluble in the monomer, as for poly(methyl methacrylate) and poly(vinyl acetate), it is considered an homogeneous polymerization. When the opposite happens, a second phase is formed with reaction advance, meaning it is an heterogeneous polymerization.

The limitations of bulk polymerization lies in the heterogeneity of the heat distribution. It is generated from the high viscosity of the monomer solution that becomes even higher as the reaction progress due to the viscous effects [38]. Depending on the application, this may be extremely detrimental as the hot spots make the polymerization advance at different rates, giving the resulting material different characteristics in its parts, increasing tendencies to fracture. Besides, the conversion is usually considerable low, in other words, lost of material. An advantage of this technique is the low rate of contaminants [29] and it is used to manufacture poly(methyl methacrylate), low-density poly(ethylene) and poly(styrene), for example [41].

- **Solution polymerization**

The solution polymerization is characterized by the solubility of the involved species in a solvent. This solves the heat problem present in bulk polymerization, as the medium viscosity is considered basically constant. A downside of this technique is that the polymer separation at the end of the reaction can be expensive. It is usually used in large scale production of polymers such as poly(vinyl chloride) (PVC) [38].

- **Suspension polymerization**

In suspension polymerization, there are two phases, meaning it is a heterogeneous process. One of the phases is composed of a mixture of monomers and initiator, while the other phase is insoluble for the other species and acts as the suspending phase, usually water [42]. The proportion is such that when the system is put through agitation, the phase with monomers is dispersed in the reactor volume, forming droplets.

In some cases, a stabilizing agent is needed to act on the interface and reduce coalescence. This process generates spherical polymer particles, which size commonly ranges between 50 to 500  $\mu m$  [38]. The droplets are big enough to hold a considerable amount of radicals, therefore the kinetic mechanism can be approximated to that of the bulk polymerization at very small volumes [43].

This process solves the major problems found in both bulk and solution polymerizations, because the suspending phase enables an homogeneous distribution of heat and, at the same time, its insolubility simplifies later separation [42].

When monomers have partial solubility in the suspending phase, the kinetics may deviate from a bulk behavior depending on the proportion of the phases [43]. For example, a study performed by Kalfas & Ray [43] has shown that the suspension polymerization of vinyl acetate is not significantly affected for values of monomer-to-aqueous phase ratio above 0.25.

Having all these polymer definitions established, it will be possible to better review some concepts present in the next section.

## 2.2

### **Vascular embolization**

The possibility of accessing remote blood vessels through minimally invasive video-guided intervention have revolutionized modern medicine [44]. Considering that blood vessels can be used to access almost every part of the body, they are ideal to serve as routes for medical mediation, allowing substitution of complex open surgeries for alternative, simpler and safer

methods [8]. One of these methods is a radiological technique that aims to obstruct target vessels in order to decrease blood flow in a determined area. This procedure is called vascular embolization.

### 2.2.1

#### History and applications

The first found record of embolization attempt dates back to 1904 when Robert Dawbarn injected a mixture of melted paraffin and vaselin to reduce tumor blood flow [45]. 26 years later, Luessenhop & Velasquez conducted valuable studies on the maneuverability of catheters in intracranial arteries [46]. Catheters are plastic or rubber tube tools used to administrate fluids in specific parts of the body and, in vascular embolization specifically, they are used to deposit the embolization material, also called the embolization agent [14]. Figure (2.7) illustrates a specific catheter being steered [47].

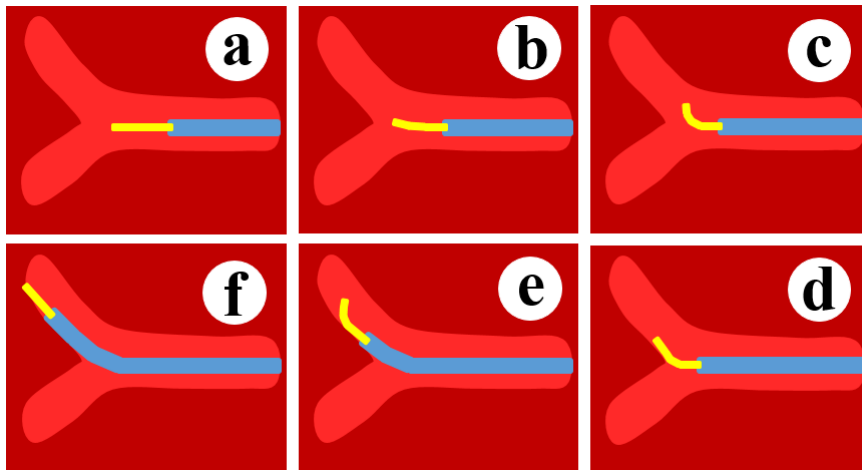


Figure 2.7: Illustration of a smart tip catheter being maneuvered to a target blood vessel. (a) Catheter placement; (b) Tip activation; (c) Bend adjustment; (d) Vessel selection; (e) Steer; (f) Tip deactivation; Adapted from Selvaraj & Takahata, 2020 [44].

In 1972, RÖSCH et al. attempted, without success, to manage acute gastrointestinal bleeding using vascular embolization technique. Their study have shown partial occlusion of the targeted vessels and argued one of the limitations of the technique were related to the embolic material used [48]. In embolization procedures performed in the 20th century, the most common embolic agents were made of autologous blood clot, muscle fragments or even stainless steel pellets [11]. Other applications of vascular embolization include treatment of arteriovenous fistula [49], pulmonary hemorrhage [50],

hemorrhage related to other medical procedures [51, 52, 53] and, more recently, tumors [54, 55, 56].

From the medical conditions where vascular embolization was applied between 1950 to 2015, 66 % were related to the treatment of uterine fibroids [14]. Figure (2.8) illustrates the procedure. This condition is described as a formation of benign tumors on the muscular layer of the uterus. The tumor mass is usually a mixture of collagen and other substances, resulting in a extracellular matrix [14]. The most common symptoms include heavy menstrual bleeding, anaemia, bowel and bladder dysfunction, urinary incontinence, infertility, recurrent miscarriage, pelvic and abdominal pain [57].

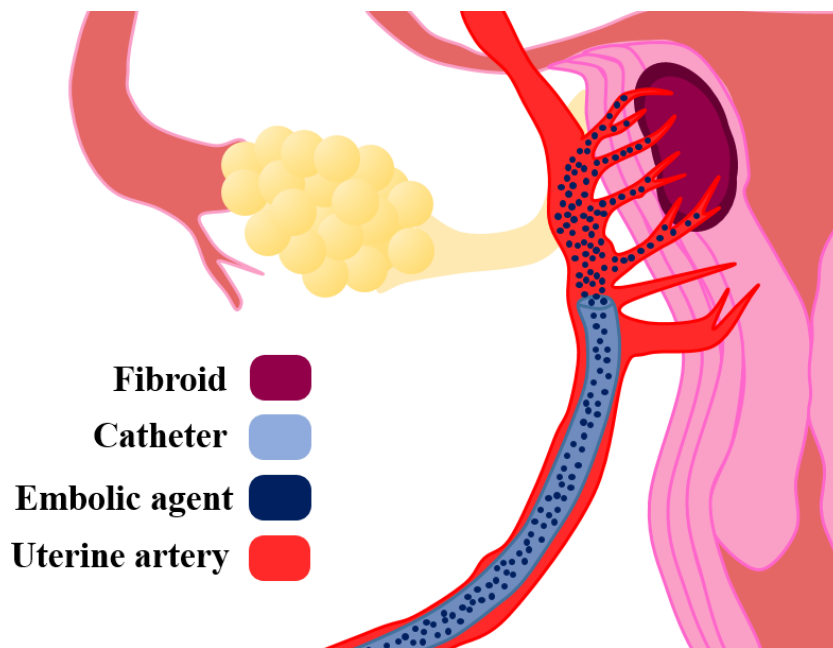


Figure 2.8: Illustration of vascular embolization procedure in the treatment of uterine fibroid. Adapted from Hu et al, 2019 [8].

A study performed by Lobel et al. in 2006 estimates 77 % of women in reproductive age develop uterine myoma in the United States, although 75 to 80 % of them are asymptomatic [58]. This statistic may vary according to region and socio-economic class as reported in 2013 by a Brazilian research conducted by Boclin & Faerstein [59].

The traditional and most used means of treatment of uterine fibroid are hysterectomy, surgery for complete removal of the uterus, and medication administration [14]. The first method is highly invasive and reports indicate a significant physical and psychological trauma post-procedure. The administration of medication, on the other hand, is focused on treatment of the symptoms and may present a series of side effects.

In summary, as it is still related to considerable morbidity and debilitation in quality of life, more research on this topic is needed, not only in potential causes, but also in non-surgical treatments [60].

### 2.2.2

#### Embolic agents

As already mentioned, an important part of the vascular embolization procedure is the selection of the embolic agent. An ideal candidate should present the following characteristics: non-antigenicity, non-toxicity, biocompatibility, non-biodegradability (depending on the case). It should also be easy to deliver through a catheter, to obtain, to disinfect, to be seen in fluoroscopy and to attach to the wall of the vessel without extravasation or recanalization. Another important property is to be soft enough to allow eventual excision without damaging surrounding normal tissue, if needed [7, 61].

A fair amount of materials have been proposed in the literature and they can be grouped into three major classes: **mechanical occlusion devices**, **liquid/gel** or **particulates**. Each classification has its own series of different materials and technologies with individual peculiarities. Extensive reviews on each type of application can be found in the literature [8, 11, 62, 63].

Strong candidates for embolic agents are polymeric particles. One of the first that has been widely used in early days of the technique is the poly(vinyl alcohol) (PVA), as it presents most of desired characteristics related to the biological interactions. Besides, it offers permanent occlusion of the vessels, being able to be re-applied in the same area if needed and there is already a considerable amount of skillful professionals capable of executing the technique [11]. Unfortunately, PVA particulates obtained by traditional means do not present the ideal morphology, as irregular shapes tend to generate more aggressive tissue inflammation and, in the case of PVA, it can cause particles to cluster hindering control over material delivery through the catheter [9]. This led to the development of alternative and more expensive materials, such as tris-acryl gelatin, N-butyl cyanoacrylate and many others [10, 11].

PVA is not directly obtained through polymerization of vinyl alcohol (VA), due to its tautomeric properties which change the molecule to acetaldehyde, a more stable form at room and polymerization temperatures [12, 64].

The most common synthetic route to obtain PVA is through solution polymerization of vinyl acetate in methanol with subsequent treatment of the solution, such as alkaline hydrolysis, to change the ester functional group into alkaline hydrolysis (saponification reaction). The PVA forms a gel mass that is then ground in a mill and then goes through a neutralization process. The

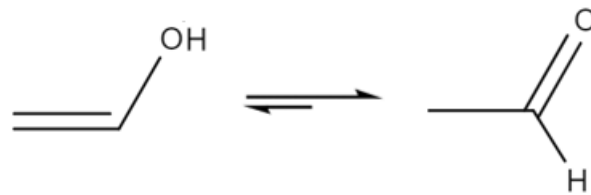


Figure 2.9: Vinyl alcohol tautomer equilibrium. Adapted from Cederstav & Novak, 1994 [61].

mixture is then washed with proper substances to remove traces of non reacted chemical species and the result is the PVA particulates [12, 14], as shown in Figure (2.10).

In 2007, Peixoto [65] has developed a process with potential scalability to produce PVA/PVAc spherical core-shell particles. The process consists on synthesizing spherical PVAc particles through suspension polymerization, followed by controlled hydrolysis, where conversion to PVA is limited to its surface, forming the shell. As a result, the appropriate shape is maintained, as well as the desired properties of PVA.

A considerable limitation of this process lies on the suspension polymerization step, because the glass temperature of PVAc (31 °C) is significantly lower than most polymerization temperatures [14]. Consequently, polymer spheres formed stay in a more viscous state, being more prone to cluster formation in subsequent treatments until their temperature decreases.

As a solution to this issue, Oliveira et al.[13] proposed the use of a copolymer, since its glass temperature can be adjusted by changing the monomer composition. In their research, they concluded a suspended phase composed of 30 m/m % methyl methacrylate and 70 m/m % vinyl acetate would provide enough increase of  $T_g$  to allow the spherical shape to be maintained at reaction temperatures. The different species structures are shown in Figure (2.11).

In 2019, Azevedo [14] has conducted a thorough experimental investigation of poly(vinyl acetate-co-methyl methacrylate) (P(VAc-co-MMA)) suspension polymerization using BPO as initiator. He has studied the particle size distribution for different combinations of multiple techniques found in the literature. The author also studied the hydrolysis process of the resulting particles and their swelling properties in conditions similar to blood to evaluate their applicability on embolization procedures. This research has shown not only the high sensibility of the particle size distribution to reaction conditions, but also how considerably low the process conversion is. Therefore, much in

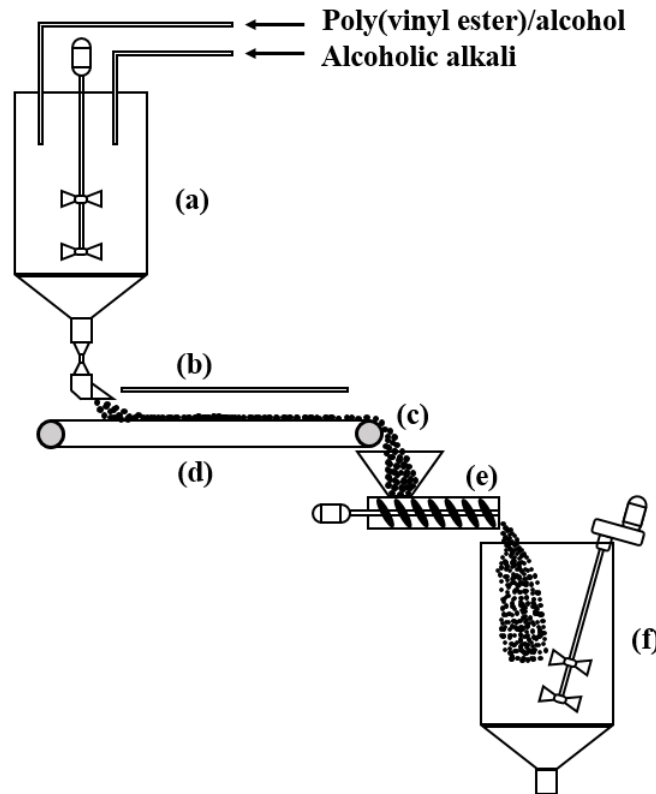


Figure 2.10: Illustration of belt saponification of poly(vinyl acetate) to generate poly(vinyl alcohol) particulates. (a) Mixing vessel; (b) Cover plate; (c) Discharge; (d) Conveyor belt; (e) Mill; (f) Washing vessel. Adapted from Hal-lensleben et al, 2015 [12]

this system has yet to be studied so optimal conditions are found, and a good starting point would be the kinetic modeling that could later be useful in future modeling of the particle size distribution.

### 2.3 Free radical polymerization modeling

Mathematical modeling is an important part of process development [66]. It allows to avoid expenses with a great quantity of experiments and can help understanding different mechanisms present in the system, while validating proposed theories. Modeling also plays an important role in manufacturing cycle and development of new products, as illustrated in Figure 2.12.

In free radical polymerization, there are three major modeling methodologies largely adopted in the literature [66]: **Monte Carlo**, in which the polymerization is carried out through stochastic development, meaning the process depends on probabilistic terms; **PREDICI**, a commercially available software specific for modeling and dynamic simulation of macromolecular processes; **Method of Moments**, a deterministic approach, where the average

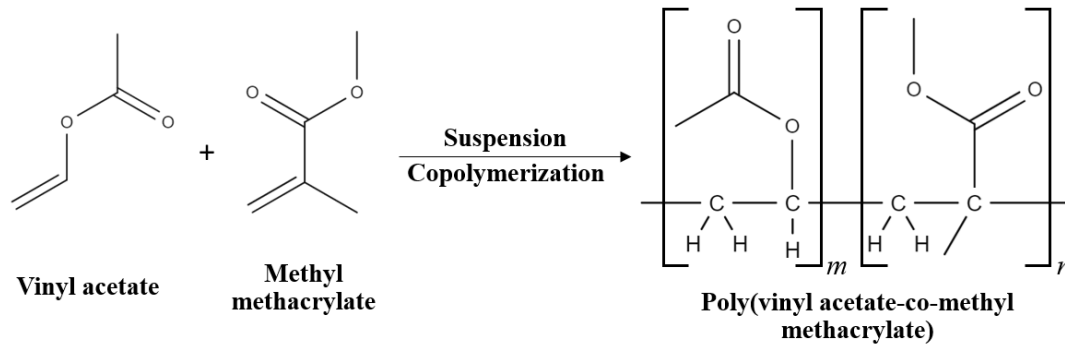


Figure 2.11: Monomers and polymer molecular structure used in the study performed by Oliveira et al, 2011 [13] and Azevedo, 2019 [14].

properties of the system are accounted. This last one was chosen for this research.

In the free radical polymerization, as shown before, each chain of a specific size is considered to be a different chemical species. Consequently, the differential system considering the variables as other simpler chemical processes would result in a impractical amount of equations to solve, even numerically. Therefore, the method of moments consists on a reparametrization of the variables related to polymeric chains, reducing the amount of equations to a solvable quantity [23]. The new variables must be established for both live and dead polymer chains separately, as shown in eq.(2-15) and (2-16).

$$\lambda_k = \sum_{i=1}^{\infty} i^k P_i^{\bullet} \quad (2-15)$$

$$\mu_k = \sum_{i=1}^{\infty} i^k D_i \quad (2-16)$$

The  $k$  index represents order of the moment and it is important as valuable information can be taken from them. Zeroth order moments represent the global amount of live and dead chains in the system. First order moments represent the quantity of incorporated monomers in the chains. The second order moments do not have a precise physical meaning, but they are related to the heterogeneity of molecular weights distribution [34]. Using these variables, it is possible to retrieve the average molecular weights, as shown in the following mathematical development.

$$M_n = MW_0 \frac{\sum_i i(P_i^{\bullet} + D_i)}{\sum_i (P_i^{\bullet} + D_i)} = MW_0 \left( \frac{\lambda_1 + \mu_1}{\lambda_0 + \mu_0} \right) \quad (2-17)$$

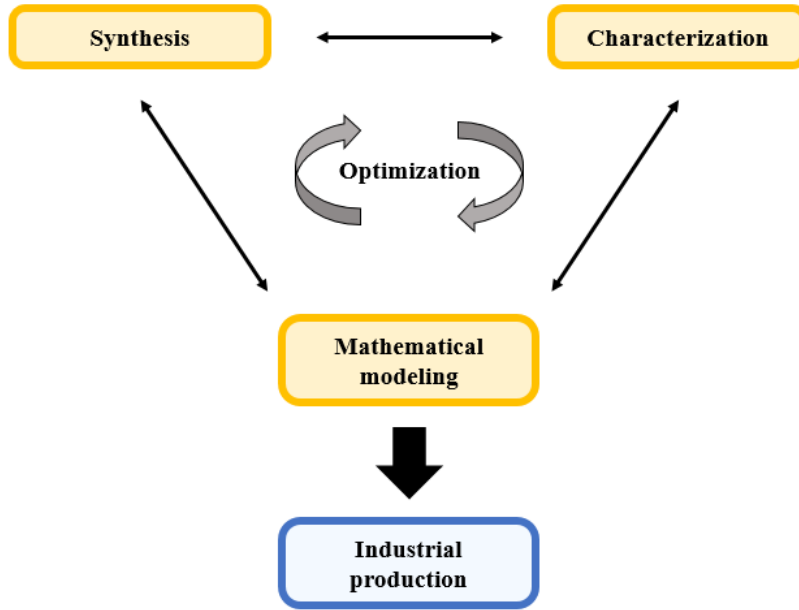


Figure 2.12: Commercialization cycle of new processes and products. Adapted from Al-Harhi [63].

$$M_w = MW_0 \frac{\sum_i i^2 (P_i^\bullet + D_i)}{\sum_i i (P_i^\bullet + D_i)} = MW_0 \left( \frac{\lambda_2 + \mu_2}{\lambda_1 + \mu_1} \right) \quad (2-18)$$

An important characteristic of these variables is that, due to the extreme reactive characteristics of live chains, the value of live moment variables is usually negligible when compared to dead ones of same order [23]. Applying this concept to eq.(2-17) and (2-18), the average molecular weights expression is simplified, as shown below.

$$M_n \approx MW_0 \left( \frac{\mu_1}{\mu_0} \right) \quad ; \quad M_w \approx MW_0 \left( \frac{\mu_2}{\mu_1} \right) \quad (2-19)$$

Material balance equations written from the method of moments only consider kinetic properties of the system. This is not enough in systems where the viscous properties have important influence, such the suspension copolymerization of P(VAc-co-MMA). As a solution to this limitation, Achilias & Kiparissides [21] proposed a model to account for the influence of diffusion properties of each species over the value of kinetic constants. To include the variation of the molecular diffusion coefficients of each species, they used the generalized free volume theory proposed by Vrentas & Duda [67, 68]. The following subsections explain how all these effects were mathematically included in the model developed on this study.

### 2.3.1

#### Free volume theory

The free volume theory, as the name indicates, evaluates the amount of space available in the medium for species to move. The total free volume is calculated from a weighted on the individual free volume of each component, as well as the mixture composition. Usually monomer, polymer, solvent and initiator are considered [67, 68]. In bulk and suspension polymerization techniques, no solvent term is needed, because the reaction happens in a monomer phase. In addition, the initiation fraction is usually minimal when compared to the other components, meaning its contribution to the free volume is negligible. Eq.(2-20) and (2-21) show the expressions obtained from these considerations.

$$V_f = \omega_m V_m^* V_{fm} + \omega_p V_p^* V_{fp} \quad (2-20)$$

where  $V_f$  is the total free volume,  $m$  denotes monomer,  $p$  indicates polymer,  $V_{fj}$ ,  $V_j^*$  and  $\omega_j$  are the free volume, the critical hole volume necessary for the molecule to jump to another position and the weight fraction of species  $j$ .

$$V_{fj} = \alpha_{j0} + \alpha_j(T - T_{gj}) \quad (2-21)$$

where  $T_{gj}$  is the glass transition temperature,  $\alpha_{j0}$  and  $\alpha_j$  are the thermal expansion coefficients below and above the  $T_{gj}$  for species  $j$ .

As indicated by the same authors, it is possible to calculate the variation of each component from the free volumes, as shown below for the initiator, monomer and polymer.

$$D_I = D_{I0} \exp\left(-\gamma_I \frac{\omega_m V_m^* \xi_{ip} / \xi_{mp} + \omega_p V_p^* \xi_{Ip}}{V_f}\right) \quad (2-22)$$

$$D_m = D_{m0} \exp\left(-\gamma_m \frac{\omega_m V_m^* + \omega_p V_p^* \xi_{mp}}{V_f}\right) \quad (2-23)$$

$$D_p = \left(\frac{D_{p0}}{M_w^2}\right) \exp\left(-\gamma_p \frac{\omega_m V_m^* / \xi_{mp} + \omega_p V_p^*}{V_f}\right) \quad (2-24)$$

where  $D_j$ , is the diffusion coefficient of species  $j$  in the mixture and its pre-exponential constant respectively.  $\gamma_j$  is the overlap factor, that accounts for species contact.  $\xi_{jp}$  is the ratio between the critical molar volume of the jumping unit of species  $j$  ( $V_j^* M W_j$ ) and the critical molar volume of the jumping unit of polymer ( $V_{Pj}$ ).

In eq.(3-142), it is important to notice the division by the squared weight-average molecular weight, which means the model is in accordance with the reptation model, which indicates long and linear polymer chains move in a reptile manner analogous to snakes, due to entanglement [69, 70].

$V_{Pj}$  can be approximated to the following general empirical expressions, according to the polymer  $T_g$  [22, 71].

$$\begin{cases} V_{pj} = 0.6224T_{gp} - 86.95, & T_{gp} \geq 295 \text{ K} \\ V_{pj} = 0.0925T_{gp} + 69.47, & T_{gp} \leq 295 \text{ K} \end{cases} \quad (2-25)$$

The pre-exponential factor for the monomer  $D_{m0}$ , also known as the monomer self diffusion coefficient, has its value tabled for different monomers.  $D_{I0}$  is unknown in most cases and, therefore, it is usually estimated.  $D_{p0}$ , on the other hand, considers extremely low polymer concentrations and can be calculated by substitution of eq.(2-26) (the Stokes-Einstein diffusion equation) in eq.(2-24)[20].

$$D_p = \frac{k_B T}{6\pi\eta_{mix}R_H} \quad (2-26)$$

where  $k_B$  is the Boltzmann constant,  $T$  is the temperature,  $\mu_{mix}$  is the dynamic viscosity of the mixture (in the homopolymerization case, the monomer) and  $R_h$  is the polymer hydrodynamic radius, calculated from the intrinsic viscosity of the polymer ( $[\eta]$ ) and its weight average molecular weight at infinite dilution, as shown below [72].

$$R_H = \left( \frac{3}{10\pi N_A} [\eta] M_w \right)^{1/3} \quad (2-27)$$

where  $N_A$  is the Avogadro number and  $[\eta]$  can be approximated as follows.

$$[\eta] = A_\eta (M_w)^{B_\eta} \quad (2-28)$$

where  $A_\eta$  and  $B_\eta$  are two constants that depend on the polymer [73].

The model in this form only represents the translational movement of particles, however the polymer chains must reorient themselves to be able to react. Therefore, segmental movement of the chains have to be accounted for. So, an extra term is added to the diffusion coefficient of polymer to calculate the effective diffusion coefficient ( $D_{pe}$ ).

$$D_{pe} = F_{seg} D_P \quad (2-29)$$

where  $F_{seg}$  is the reaction probability of two live polymer chains when their active centers are in close proximity and it can be calculated as follows [74].

$$F_{seg} = \frac{r_e^3[\pi r_e + 6(\sqrt{2})\alpha_{seg}r_B]}{16\pi r_B^4} \quad (2-30)$$

where  $r_e$ ,  $r_B$  and  $\alpha_{seg}$  are the Kuhn's segment length, the distance of the chain extremity from the sphere center and a parameter accounting segmental diffusion.

### 2.3.2 Diffusion-controlled reactions

Having established the method of evaluating the diffusion coefficients according to the medium composition, this subsection presents the model developed by Achilias & Kiparissides [21] to use these variables to determine diffusion influence over the free radical polymerization reaction in its different stages.

- **Cage effect:**

In the **initiation** reaction, the primary radicals are assumed to be formed within a sphere of radius  $r_{I1}$ . In addition, a larger concentric sphere of radius  $r_{I2}$  represents the volume from which radicals must traverse in order to react with a monomer molecule, as illustrated in Figure (2.13).

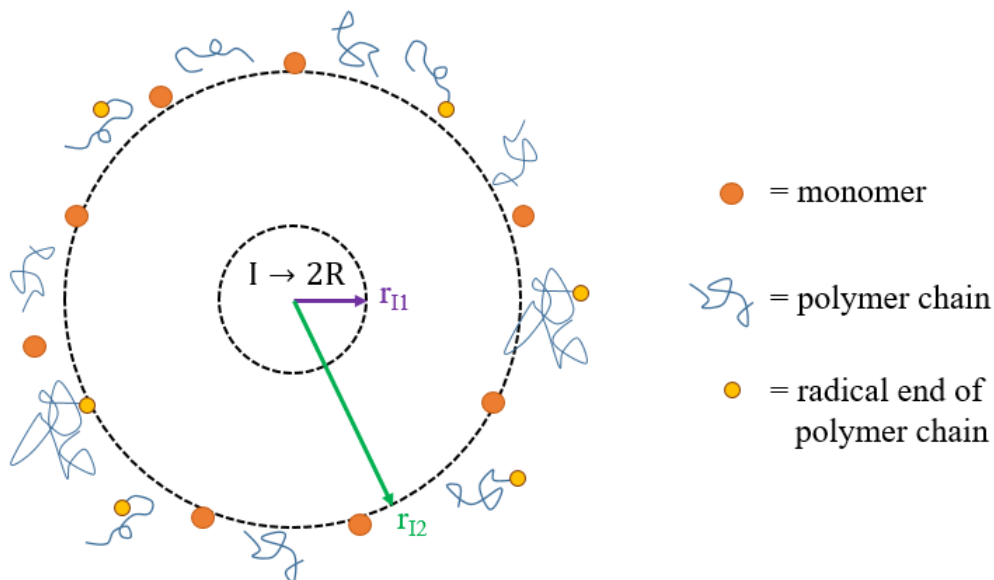


Figure 2.13: Cage effect geometry illustration. Adapted from Kiparissides [36].

If the mass-transfer process is considered to be at steady-state and one dimensional, the radial diffusion rate can be written as follows.

$$R'_I = -4\pi r^2 D_I \frac{dR}{dr} \quad (2-31)$$

Considering  $R_1$  is the concentration of primary radicals at  $r_{I1}$  and  $R_2$  is the concentration of the same species at  $r_{I2}$ , it is possible to integrate the previous expression.

$$R'_I \int_{r_{I1}}^{r_{I2}} \frac{1}{r^2} dr = -4\pi D_I \int_{R_1}^{R_2} dR \quad (2-32)$$

$$R'_I \left( \frac{1}{-r_{I2}} - \frac{1}{-r_{I1}} \right) = -4\pi D_I (R_2 - R_1) \quad (2-33)$$

Assuming  $r_{I1} \ll r_{I2}$ , the following expression can be retrieved for the initiator diffusion rate.

$$R'_I = 4r_{I1}\pi D_I (R_1 - R_2) \quad (2-34)$$

The chain initiation can be considered equal to  $R'_I$ , resulting in the following expression.

$$k_{i0} R_2 M V_I = 4r_{I1}\pi D_I (R_1 - R_2) \Rightarrow \frac{R_1}{R_2} = \left( 1 + \frac{k_{i0} M r_{I2}^3}{3r_{I1} D_I} \right) \quad (2-35)$$

where  $k_{i0}$  is the intrinsic kinetic constant of chain initiation and  $V_I$  is the effective volume of this reaction (larger sphere).

Considering the quasi-steady state approximation due to the extremely fast dynamics of free radical species and a bifunctional initiator, The concentration of primary radicals can be calculated from the expressions shown below.

$$\begin{cases} k_{i0} R_1 M = 2f_0 k_d I & \text{for lower conversions} \\ k_{i0} R_2 M = 2f k_d I & \text{for intermediate and higher conversions} \end{cases} \quad (2-36)$$

where  $f_0$  is the starting initiation efficiency. It is important to notice  $k_i$  is considered to be relatively unchanged, because the efficiency term already accounts for the cage effect.

Dividing the previous expressions and substituting them in eq.(2-35), it is possible to obtain the diffusion-controlled equation for the initiation.

$$\frac{1}{f} = \frac{1}{f_0} + k_{i0}M \frac{r_{I2}^3}{3r_{I1}D_I} \quad (2-37)$$

Notice that  $(k_{i0}M)^{-1}$  and  $\frac{r_2^3}{3r_1D_I}$  are equivalent to the characteristic times of the chain initiation reaction ( $\tau_{R_I}$ ) and the diffusion of primary radicals ( $\tau_{D_I}$ ), respectively. Thus, eq.(3-144) can be rewritten.

$$f = \frac{f_0}{1 + \tau_{D_I}/\tau_{R_I}} \quad (2-38)$$

As it can be seen, at lower conversions  $\tau_{D_I} \ll \tau_{R_I}$  and  $f \approx f_0$ . As reaction advances,  $\tau_{D_I} \gg \tau_{R_I}$ , which implies  $f < f_0$ . Therefore, this model accounts for the cage effect, as the medium becomes more viscous.

The intrinsic kinetic constant of the initiator ( $k_{i0}$ ) is not usually reported, so a common practice is to approximate this parameter to  $(\epsilon_{i0}k_{p0})$ , where  $\epsilon_{i0}$  is a proportionality constant.

- **Gel effect:**

The **termination** reactions are limited by the diffusion of the polymer chains. In their original work, Achilias & Kiparissides [20] follow a similar approach to the one in the cage effect. However, this methodology was later corrected [22, 75], as shown next.

The mass-transfer of an active chain diffusion towards another active chain in order to terminate ( $R'_t$ ), considering a one dimensional steady-state process, is expressed below.

$$R'_t = -4\pi r^2 D_p \frac{dC}{dr} \quad (2-39)$$

where  $D_p$  and  $C$  denote diffusion coefficient of the polymer chains and concentration respectively. This expression can be evaluated for the minimal distance for termination reaction to happen, also called termination radius ( $r_t$ ) and for  $r_b$ , distance where the concentration of chains is representative to that of the reaction medium. The geometry of the system is shown in Figure (2.14).

$R'_t$  can also be considered equal to the rate variation of molecules of polymer chains due to termination, as shown below.

$$R'_t = -k_{t0}C_b \frac{1}{N_A} \quad (2-40)$$

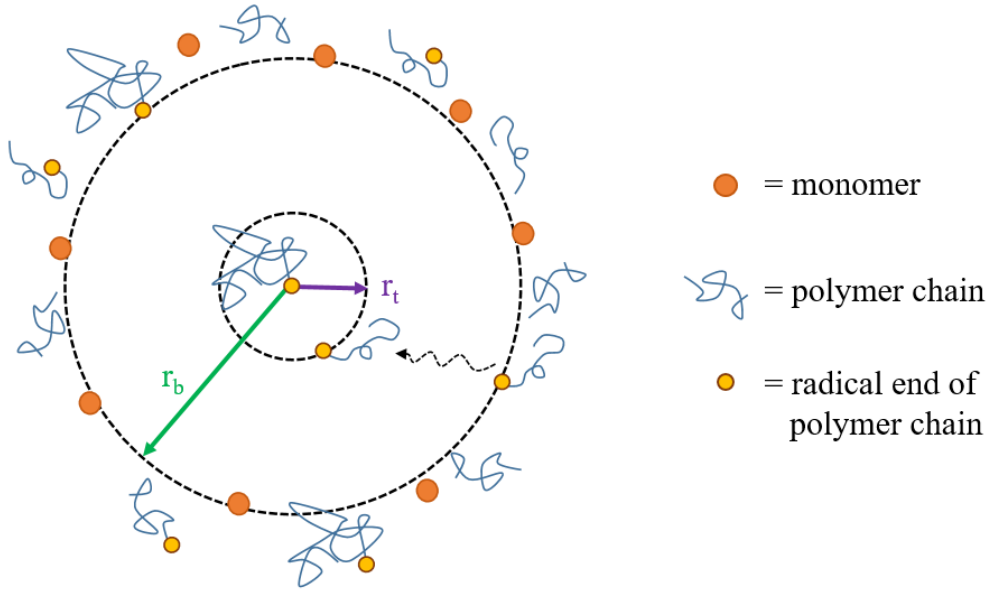


Figure 2.14: Gel effect geometry illustration. Adapted from Kiparissides [36].

where  $k_{t0}$  and  $C^b$  are the intrinsic termination kinetic constant and concentration at  $r_b$ , respectively.

Developing eq.(2-39) and (2-40) and considering  $r_b \gg r_t$ , it is possible to retrieve the following expression to account for the gel effect.

$$\frac{1}{k_t} = \frac{1}{k_{t0}} + \frac{1}{4\pi D_{pe} r_t N_A} \quad (2-41)$$

The termination reaction effective radius can be assessed from the following expression [21, 26].

$$r_t = \frac{\left[ \ln\left(\frac{1000\tau^3}{N_A \lambda_0 \pi^{3/2}}\right) \right]^{1/2}}{\tau} \quad (2-42)$$

$$\tau = \left( \frac{3}{2j_c \delta^2} \right)^{1/2} \quad (2-43)$$

where  $\lambda_0$  and  $\delta$  are the live moment of zeroth order and the average root-mean-square end-to-end distance of the polymer chain.  $j_c$ , on the other hand, is the entanglement spacing between chains and can be evaluated from eq.(2-44).

$$\frac{1}{j_c} = \frac{1}{j_{c0}} + \frac{2\phi_p}{X_{c0}} \quad (2-44)$$

where  $\phi_p$  is the volume fraction of polymer,  $X_{c0}$  is the critical degree of polymerization for the entanglement of polymer chains and  $j_{c0}$  is the critical value of  $j_c$  when it tends to zero conversion. This last term is not usually known, but can be approximated by considering  $r_t$  equal to  $R_H$  at initial

reaction conditions using the previous mathematical relations.

As reaction reaches a critical conversion where no chains are unable to move, this model indicates  $k_t$  tending to zero. Nevertheless, Russel et al [76] indicated that even in this condition there is still motion of the active site of the polymers through propagation growth. To account for this event, the authors proposed the following expressions.

$$k_{te} = k_t + k_{t,res} \quad (2-45)$$

$$k_{t,res} = Ak_p M \quad (2-46)$$

where  $k_{te}$  and  $k_{t,res}$  are the effective and residual termination kinetic constants.  $A$  is the proportionality rate constant and it can be calculated using eq.(2-47) according to Buback et al [77].

$$A = \pi \delta^3 j_c N_A \quad (2-47)$$

• **Glass effect:**

Monomer species control the diffusion influence over the propagation reaction. This happens because monomer molecules are smaller in size and, thus, affected by viscous effects at much higher conversions than polymer chains. The geometry of the problem is extremely similar to the one of the gel effect, as shown in Figure (2.15), but it accounts for the diffusion of monomer particles, resulting in eq.(2-48).

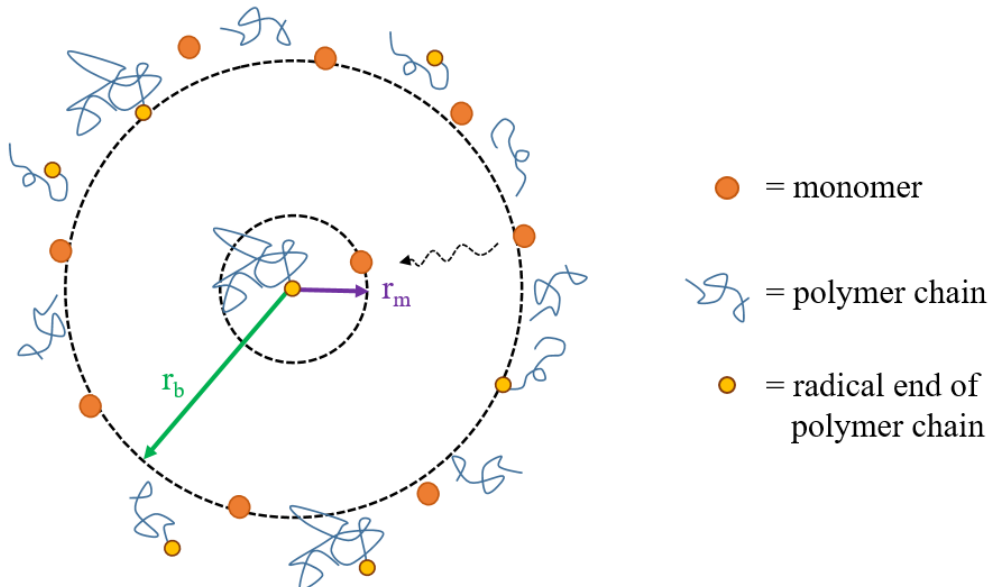


Figure 2.15: Glass effect geometry illustration. Adapted from Kiparissides [36].

$$\frac{1}{k_p} = \frac{1}{k_{p0}} + \frac{1}{4\pi D_m r_m N_A} \quad (2-48)$$

where  $k_{p0}$  is the intrinsic propagation kinetic constant and  $r_m$  is an effective radius assumed to be equivalent to the one of the termination reaction.

With all three effects in place, it is expected that  $k_t$ ,  $k_p$  and  $f$  follow a similar behavior expressed in Figures (2.16) and (2.17).

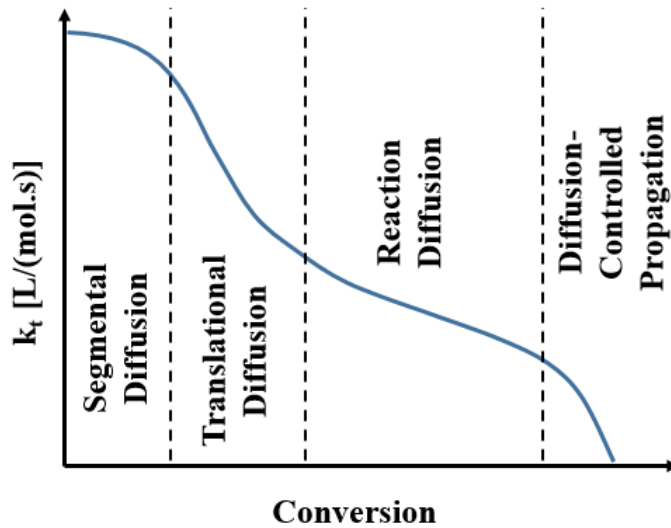


Figure 2.16: Example of expected behavior of  $k_t$  due to gel effect. Adapted from Achilias, 2007 [72].

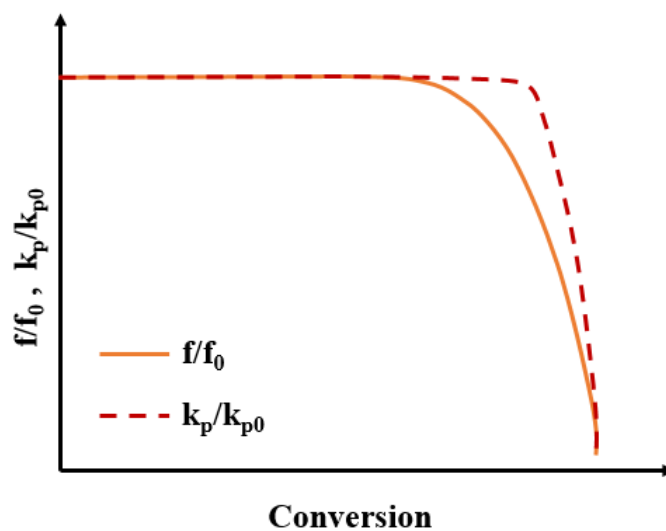


Figure 2.17: Example of expected behavior of  $f$  and  $k_p t$  due to cage and glass effects. Adapted from Achilias, 2007 [72].

## 2.4

### Parameter estimation

The diffusion of kinetic properties of the synthesis of polymer materials is many times not the main focus of researches. Besides, some constants are specific to the conditions of each system. Consequently, it is natural that not all necessary data is known. As a result, the estimation of parameters is a very efficient optimization tool to determine the values of the unknown model parameters.

#### 2.4.1

##### Estimation algorithm

In a parameter estimation problem, the results generated from the model are confronted with experimental data for different values of the unknown parameters [78]. According to the implemented algorithm, the values are then readjusted and reevaluated. This recurrence goes on until a specific condition is met, ending the estimation processes, as illustrated in Figure (2.18).

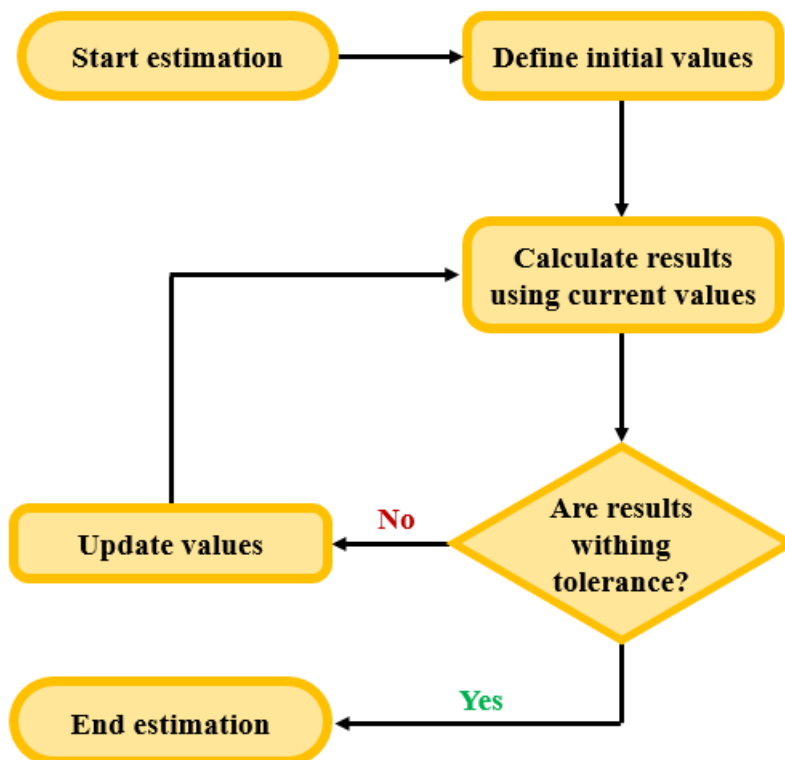


Figure 2.18: Simplified diagram of the parameter estimation process.

Even though there are many different estimation algorithms, the particle swarm optimization (PSO) is particularly interesting for being relatively easy

to implement and not being limited by local optimal search, because of its stochastic nature. The PSO was developed by Kennedy & Eberhart [79] and it was inspired by the behavior of bird flocking and fish schooling.

Although there is a considerable amount of variations for this algorithm [80], one of the simpler PSO versions was adopted in this research. It consists on a theoretical population, in which every individual, or particle, is given attributes of "position" (randomly assigned at the beginning from given intervals), "speed" (usually starts as zero) and "performance" (evaluation).

The position is equivalent to the parameters to be optimized while the performance attributes are composed of three elements: the evaluation of how "good" the current position is; the best individual evaluation with its coordinates; the best evaluation in the whole collective with its coordinates. From the performance attributes, the previous speed and a randomness factor, a new speed is calculated, the position is updated, the performances are reevaluated and so on, resulting in a swarm-like behavior, until they converge [79, 80].

The evaluation attributes are defined by an objective function ( $F_{obj}$ ) and the coordinates of position are the unknown parameters to be optimized. In the case of process modeling,  $F_{obj}$  is usually the error between the model prediction and the experimental data. The adopted expressions to update particles state are shown next.

$$V_i = \underbrace{\omega V_{i-1}}_{inercia} + C_1 \lambda \underbrace{(X_{\text{best ind}} - X_i)}_{\text{best individual direction}} + C_2 \mu \underbrace{(X_{\text{best global}} - X_i)}_{\text{best global direction}} \quad (2-49)$$

$$X_{i+1} = X_i + V_i \quad (2-50)$$

where  $V_i$  and  $X_i$  are the particle speed and position vectors at the  $i$ th iteration.  $\omega$  is the inertia weight and it decreases with each PSO iteration.  $C_1$  and  $C_2$  are acceleration coefficients of the individual and global best directions contribution. Finally,  $\lambda$  and  $\mu$  are random weights updated at each iteration to account for stochastic influence.

Figure 2.19 illustrates the speed update process of a single particle used for calculating the new position.

Lastly, the quantity of particles present in the population is of extreme importance, as more individuals imply more regions being investigated simultaneously, but it also means a longer processing time, because the model is executed once for every particle at each iteration, as indicated in Figure (2.20).

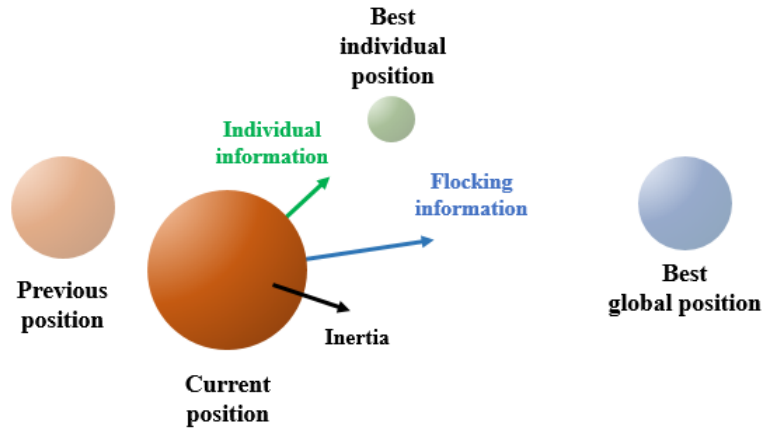


Figure 2.19: Illustration of PSO vector composition.

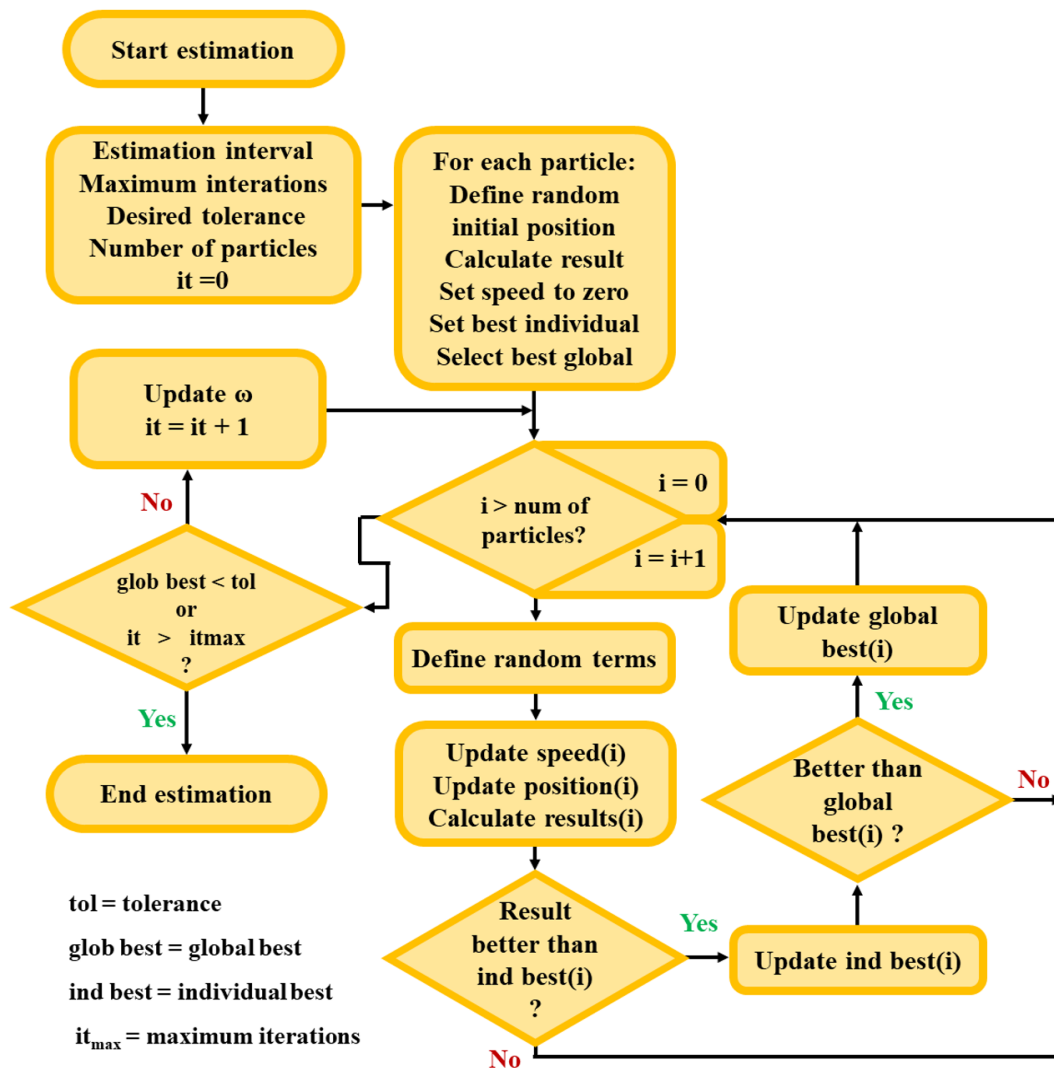


Figure 2.20: PSO implementation diagram.

### 2.4.2

#### Statistical evaluation

An essential part of parameter estimation is to evaluate the uncertainty of the optimal conditions found [81]. This can be achieved by calculating the parameters confidence region (CR) through statistical tools.

Assuming the experiments are well done, the parameters are in accordance to the normal distribution and the objective function returns an equivalent of the sum of squared residuals, the CR of the model can be approximated using the following expression [81].

$$f_{obj}(\alpha) \leq f_{obj}(\alpha_{opt}) \left( 1 + \frac{NP}{DF} F_{NP,DF}^{(1-\varphi)} \right) \quad (2-51)$$

$$DF = N - NP \quad (2-52)$$

$$NP = NE * NY \quad (2-53)$$

where  $\alpha$  is the vector of estimation parameters,  $\alpha_{opt}$  is the optimal parameters found in the estimation,  $NP$  is the total amount of estimated parameters,  $N$  is the number of experimental points,  $DF$  is the degree of freedom,  $NE$  is the number of experiments,  $NY$  is the number of dependent variables,  $1 - \varphi$  is the interval of confidence and  $F$  is the percent-point function of a Fisher distribution.

This method allows to generate a qualitative analysis of the CR through plot of all systems that are in conformity with the eq.(2-51). It also allows to approximate an interval limiting the value of each estimated parameter.

## 2.5

### Concluding remarks

Polymer materials have a considerable amount of classifications, as they present a variety of chemical and physical properties. In the medical field, they can be used in a procedure that allows treatment of uterine fibroid. This illness affect a wide range of demographics, specially women in reproductive age. The traditional treatments of uterine fibroids are invasive or focused on symptoms treatment and they are far from ideal.

With that being sad, the study of alternative treatments has lead to the development of the vascular embolization, a non-invasive video guided procedure that allows to cut the blood supply of the tumors by blocking vessels with embolic agents. From the different materials, spherical PVA particles have been proven to be effective, although they are not directly obtained through traditional polymerization techniques.

To produce the PVA micro spheres, a core-shell procedure has been proposed in the literature in which spherical PVAc is treated with controlled alkalyne hydrolysis only affecting its surface and, therefore, maintaining its morphology. As PVAc does not have an appropriate  $T_g$  to undergo suspension polymerization without particle clustering, the copolymerization of P(VAc-co-MMA) has been proposed so the resulting polymer  $T_g$  is appropriate.

Experimental studies have shown the morphology and reaction conversion of the material are highly sensible to the experimental conditions and the literature lacks modeling research of this specific system that would allow save expenses while searching for optimal conditions.

There are multiple reports of free radical polymerization modeling for different systems. Among them, the model proposed by Achilias & Kiparissides offer an interesting alternative, as it is based on diffusion-controlled reactions accounting for the cage-, gel- and glass-effects by relying on physical properties of the species involved in the process.

### 3 Model development

Modeling usually follow somewhat similar major steps. In copolymerization processes, for instance, it is expected that a model is first validated for the homopolymerization of its components, before being implemented for the desired system. Therefore, the implementation of P(VAc-co-MMA) was developed after the homopolymerizations of poly(vinyl acetate)(PVAc) and poly(methyl methacrylate)(PMMA). The general modeling process for the two types of system followed the same procedure and it is shown in Figure (3.1).

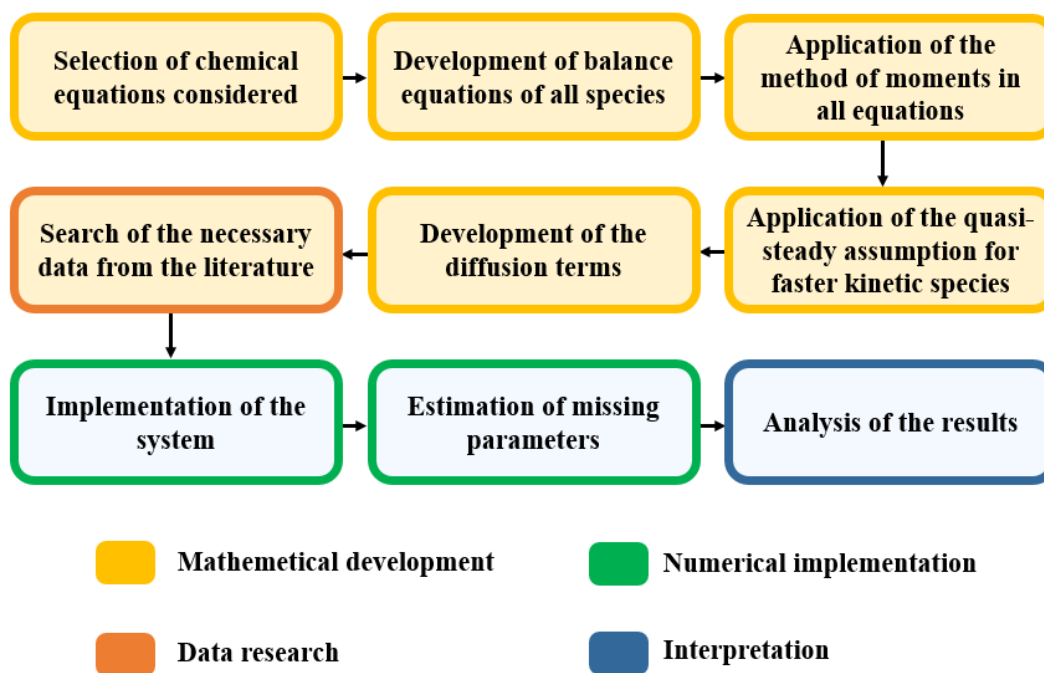


Figure 3.1: Flowchart of the model development process for all polymerization systems.

Despite their similarities, each system has its own particularities when it comes to mathematical development and theoretical considerations. For this reason, this chapter comprises the model development approach for each system, as well as the list of parameters collected from the literature.

### 3.1 Homopolymerizations

The polymerization models of poly(methyl methacrylate) and poly(vinyl acetate) were both implemented using the same structure, only differing on the value of variables like initial reaction conditions, kinetic constants and physical properties of the species. Therefore, this section is dedicated to the model development of the homopolymerizations.

Before presenting the chemical equations, it is important to establish the theoretical considerations taken for the suspension free-radical homopolymerizations.

Another important aspect is that transfer to polymer can happen in any repeating unit of the dead polymer chain. This indicates the possibility of ramification, but with at considerable lower rate than propagation. Thus, ramification was assumed to be so small that parameters like ramification frequency were not included in the model. Its relevance remained in the reincorporation of dead monomers.

As the chains are mostly linear, the ultimate unit model approach was adopted. Besides, as the reaction medium is mostly composed of monomer molecules, transfer to solvent was not taken into account and transfer to impurity was regarded as negligible.

Monomer transfer to suspending phase was considered negligible for the PVAc system, since monomer-to-aqueous phase ratio was above 0.25 [43]. The same was assumed for the PMMA system, because MMA solubility in water is even lower than VAc, meaning the monomer-to-aqueous ratio of 0.33 was also considered acceptable. Consequently, kinetics in the models were considered to be equivalent to that of a bulk polymerization with homogeneous heat distribution.

With the initial theoretical premises settled, the chemical system was formulated as shown in eq.(3-1) to (3-7).

- **Initiation:**



where  $I$ ,  $R^\bullet$ ,  $M$ ,  $P_1^\bullet$  are the concentrations of initiator, primary radicals, monomer and live chains of size one, respectively.

- **Propagation:**



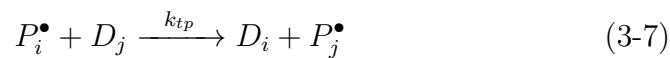
where  $P_i^\bullet$  denotes the concentration of live polymer chains of  $i$  repeating units.

- **Termination:**



where  $D_i$  indicates the concentration of dead polymer chains of  $i$  repeating units.

- **Transfer:**



### 3.1.1 Balance equations

To decrease the total amount of variables present in the mathematical expressions, the balance equations were implemented in terms of concentration instead of molar values. The development present in eq.(3-8) shows the equivalence between both systems, using a generic variable  $U$ .

$$\begin{aligned} \frac{1}{V} \frac{d(VU)}{dt} &= \frac{1}{V} \left( V \frac{d(U)}{dt} + U \frac{d(V)}{dt} \right) = \frac{d(U)}{dt} + \frac{U}{V} \frac{d(V)}{dt} \Rightarrow \\ &\Rightarrow \frac{dU}{dt} = \frac{1}{V} \frac{d(VU)}{dt} - \frac{U}{V} \frac{dV}{dt} \end{aligned} \quad (3-8)$$

From the chemical equations, the balances for the following species were written.

- **Initiator:**

$$\frac{1}{V} \frac{d(VI)}{dt} = -k_d I \quad (3-9)$$

- **Primary radicals:**

$$\frac{1}{V} \frac{d(VR^\bullet)}{dt} = 2fk_dI - k_iR^\bullet M \quad (3-10)$$

- **Monomer:**

$$\frac{1}{V} \frac{d(VM)}{dt} = -k_iR^\bullet M - k_pM \sum_{i=1}^{\infty} P_i^\bullet - k_{tm}M \sum_{i=1}^{\infty} P_i^\bullet \quad (3-11)$$

It is important to notice that the summation of  $P_i^\bullet$  allows to account for the contribution of polymer chains of every size.

To maintain physical consistency, the balance equations for polymeric chains must be grouped according to size, as it impacts in which reactions the chain is able to participate.

- **Live polymer chains:**

For ( $i = 1$ ):

$$\begin{aligned} \frac{1}{V} \frac{d(VP_1^\bullet)}{dt} = & k_iR^\bullet M - k_pMP_1^\bullet - k_{tm}MP_1^\bullet + k_{tm}M \sum_{j=1}^{\infty} P_j^\bullet \\ & - k_{tp}P_1^\bullet \sum_{j=1}^{\infty} jD_j + k_{tp}D_1 \sum_{j=1}^{\infty} P_j^\bullet - k_{td}P_1^\bullet \sum_{j=1}^{\infty} P_j^\bullet - k_{tc}P_1^\bullet \sum_{j=1}^{\infty} P_j^\bullet \end{aligned} \quad (3-12)$$

For ( $i \geq 2$ ):

$$\begin{aligned} \frac{1}{V} \frac{d(VP_i^\bullet)}{dt} = & -k_pMP_i^\bullet + k_pMP_{i-1}^\bullet - k_{tm}MP_i^\bullet - k_{tp}P_i^\bullet \sum_{j=1}^{\infty} jD_j \\ & + k_{tp}iD_i \sum_{j=1}^{\infty} P_j^\bullet - k_{td}P_i^\bullet \sum_{j=1}^{\infty} P_j^\bullet - k_{tc}P_i^\bullet \sum_{j=1}^{\infty} P_j^\bullet \end{aligned} \quad (3-13)$$

- **Dead polymer chains:**

For ( $i = 1$ ):

$$\frac{1}{V} \frac{d(VD_1)}{dt} = k_{tm}MP_1^\bullet + k_{tp}P_1^\bullet \sum_{j=1}^{\infty} jD_j - k_{tp}D_1 \sum_{j=1}^{\infty} P_j^\bullet + k_{td}P_1^\bullet \sum_{j=1}^{\infty} P_j^\bullet \quad (3-14)$$

For ( $i \geq 2$ ):

$$\begin{aligned} \frac{1}{V} \frac{d(VD_i)}{dt} = & k_{tm}MP_i^\bullet + k_{tp}P_i^\bullet \sum_{j=1}^{\infty} jD_j - k_{tp}iD_i \sum_{j=1}^{\infty} P_j^\bullet + k_{td}P_i^\bullet \sum_{j=1}^{\infty} P_j^\bullet \\ & + k_{tc} \frac{1}{2} \left( \sum_{j=1}^{i-1} P_j^\bullet P_{i-j}^\bullet \right) \end{aligned} \quad (3-15)$$

The total amount of differential equations approximates the number of possible polymeric chain sizes. As a result, it is impracticable to solve such massive system numerically. To overcome this limitation, the method of moments was implemented as shown next.

$$\lambda_k = \sum_{i=1}^{\infty} i^k P_i^\bullet \quad ; \quad \mu_k = \sum_{i=1}^{\infty} i^k D_i \quad (3-16)$$

The method of moment was applied to the balance system and the resulting equations are shown below. As the development for the live and dead moments is considerably long, only a simplified development is demonstrated. Besides, a series of mathematical equivalences that were needed can be found in Appendix A.

• **Monomer:**

$$\frac{1}{V} \frac{d(VM)}{dt} = -k_i R^\bullet M - k_p M \lambda_0 - k_{tm} M \lambda_0 \quad (3-17)$$

• **Live moments:**

$$\frac{1}{V} \frac{d(V\lambda_k)}{dt} = \frac{1}{V} \frac{d(V \sum_{i=1}^{\infty} i^k P_i^\bullet)}{dt} = \sum_{i=1}^{\infty} i^k \frac{1}{V} \frac{d(VP_i^\bullet)}{dt} \quad (3-18)$$

It is important to separate terms according to the index division shown in eq.(3-12) and (3-13).

$$\frac{1}{V} \frac{d(V\lambda_k)}{dt} = \frac{1}{V} \frac{d(VP_1^\bullet)}{dt} + \sum_{i=2}^{\infty} i^k \frac{1}{V} \frac{d(VP_i^\bullet)}{dt} \quad (3-19)$$

Replacing eq.(3-12) and (3-13), rearranging terms and developing the system for  $k = 0, 1$  and  $2$ , it is possible to retrieve eq.(3-20) to (3-22).

$$\frac{1}{V} \frac{d(V\lambda_0)}{dt} = k_i R^\bullet M - k_t \lambda_0^2 \quad (3-20)$$

$$\begin{aligned} \frac{1}{V} \frac{d(V\lambda_1)}{dt} = k_i R^\bullet M + k_p M \lambda_0 + k_{tm} M (\lambda_0 - \lambda_1) - k_t \lambda_1 \lambda_0 \\ + k_{tp} (\mu_2 \lambda_0 - \lambda_1 \mu_1) \end{aligned} \quad (3-21)$$

$$\begin{aligned} \frac{1}{V} \frac{d(V\lambda_2)}{dt} = k_i R^\bullet M + k_p M (2\lambda_1 + \lambda_0) + k_{tm} M (\lambda_0 - \lambda_2) \\ + k_{tp} (\mu_3 \lambda_0 - \lambda_2 \mu_1) - k_t \lambda_2 \lambda_0 \end{aligned} \quad (3-22)$$

• **Dead moments:**

$$\frac{1}{V} \frac{d(V\mu_k)}{dt} = \frac{1}{V} \frac{d(V \sum_{i=1}^{\infty} i^k D_i)}{dt} = \sum_{i=1}^{\infty} i^k \frac{1}{V} \frac{d(V D_i)}{dt} \quad (3-23)$$

It was necessary to separate terms according to the index division present in eq.(3-14) and (3-15).

$$\frac{1}{V} \frac{d(V\mu_k)}{dt} = \frac{1}{V} \frac{d(V D_1)}{dt} + \sum_{i=2}^{\infty} i^k \frac{1}{V} \frac{d(V D_i)}{dt} \quad (3-24)$$

To further equation development, eq.(3-14) and (3-15) were used and the terms were regrouped for  $k$  values of 0, 1 and 2, resulting in the following balances.

$$\frac{1}{V} \frac{d(V\mu_0)}{dt} = k_{tm} M \lambda_0 + \left( k_{td} + \frac{k_{tc}}{2} \right) \lambda_0^2 \quad (3-25)$$

$$\frac{1}{V} \frac{d(V\mu_1)}{dt} = k_{tm} M \lambda_1 + k_{tp} (\lambda_1 \mu_1 - \mu_2 \lambda_0) + k_t \lambda_0 \lambda_1 \quad (3-26)$$

$$\frac{1}{V} \frac{d(V\mu_2)}{dt} = k_{tm} M \lambda_2 + k_{tp} (\lambda_2 \mu_1 - \mu_3 \lambda_0) + k_t \lambda_0 \lambda_2 + k_{tc} \lambda_1^2 \quad (3-27)$$

The rate in which live polymers change is considerably higher than the rate of dead polymers variation, due to the unstable nature of free radical

species. Consequently, the use of differential equations from both species in the same system results in a convergence problem for the integrator method. This numerical limitation can be solved by adopting the quasi-steady-state approximation (QSSA) for all free radical molecules, since the rate of formation and consumption of free radicals are considerably high. Therefore, differential equations are considered to be equal to zero, resulting in algebraic expressions to calculate the concentration of these species. The following eq.(3-28) to (3-32) show the result of applying the QSSA on the considered system for the free radical species.

$$\frac{d(R^\bullet V)}{dt} = 0; \frac{d(\lambda_k V)}{dt} = 0, k = 0, 1, 2 \quad (3-28)$$

$$R^\bullet = \frac{2fk_d I}{k_i M} \quad (3-29)$$

$$\lambda_0 = \sqrt{\frac{2fk_d I}{k_t}} \quad (3-30)$$

$$\lambda_1 = \frac{2fk_d I + k_p M \lambda_0 + k_{tm} M \lambda_0 + k_{tp} \mu_2 \lambda_0}{k_{tm} M + k_{tp} \mu_1 + k_t \lambda_0} \quad (3-31)$$

$$\lambda_2 = \frac{2fk_d I + k_p M (2\lambda_1 + \lambda_0) + k_{tm} M \lambda_0 + k_{tp} \mu_3 \lambda_0}{k_{tm} M + k_{tp} \mu_1 + k_t \lambda_0} \quad (3-32)$$

As it can be seen, the resulting equation present moment variables of superior order. This is expected when transference to polymer reaction is considered and characterizes a closure problem. A common solution to approximate the third order moment value is shown in eq.(3-33) [82, 83].

$$\mu_3 = \frac{\mu_2}{\mu_0 \mu_1} (2\mu_0 \mu_2 - \mu_1^2) \quad (3-33)$$

The differential volume term was accounted considering the mass conservation principle that all monomer mass consumed is equivalent to all polymer mass generated. This allows to evaluate volume variation in terms of monomer variation when knowing the monomer specific mass ( $\rho_M$ ), the monomer molecular weight ( $MW_M$ ) and the polymer specific mass ( $\rho_P$ ), as shown in eq.(3-34)

to (3-39).

$$\frac{dV}{dt} = \frac{dV_{Monomers}}{dt} + \frac{dV_{Polymer}}{dt} \quad (3-34)$$

$$\frac{dV}{dt} = \frac{1}{\rho_M} \frac{dm_M}{dt} + \frac{1}{\rho_P} \frac{dm_P}{dt} \quad (3-35)$$

$$\frac{dV}{dt} = \frac{1}{\rho_M} \frac{dm_M}{dt} - \frac{1}{\rho_P} \frac{dm_M}{dt} = \left( \frac{1}{\rho_M} - \frac{1}{\rho_P} \right) \frac{dm_M}{dt} \quad (3-36)$$

$$\frac{dV}{dt} = \left( \frac{1}{\rho_M} - \frac{1}{\rho_P} \right) MW_M \frac{dN_M}{dt} \quad (3-37)$$

where  $m_i$  and  $N_i$  are the mass and molar quantity of species  $i$ , respectively.

$$\frac{dV}{dt} = \left( \frac{1}{\rho_M} - \frac{1}{\rho_P} \right) MW_M \frac{d(VM)}{dt} \quad (3-38)$$

$$\frac{dV}{dt} = \left( \frac{1}{\rho_M} - \frac{1}{\rho_P} \right) MW_M V \left( \frac{1}{V} \frac{d(VM)}{dt} \right) \quad (3-39)$$

Notice that the last term is equivalent to eq.(3-17)

### 3.1.2

#### Viscous effects

To account for the cage, gel and glass effects, the equations follow the updated model initially presented by Achilias & Kiparissides [21, 22]. The detailed equations used can be found in subsection 2.3.2.

Some parameters necessary for viscous effects calculations are related to the initial stages of the polymerization (when conversion is close to zero) and, unfortunately, their values do not seem to be reported in the literature. These parameters are  $D_{P0}$ ,  $R_{H,X \rightarrow 0}$  and  $j_{c0}$ .

To account for these variables, the simulation disregard viscous effects on the first reaction minute, where medium viscosity was considered to be unchanged.

In both homopolymerization of PVAc and PMMA systems, the only parameters not found in the literature were the adjustment parameter for the segmental diffusion ( $\alpha_{seg}$ ), the intrinsic viscosity factors ( $A_\eta$  and  $B_\eta$ ), the initial diffusion coefficient of the initiator ( $D_{I0}$ ) and the proportionality factor of the initiator kinetic constant ( $\epsilon_{i0}$ ). These last two constants appear in the same expression as a ratio ( $\epsilon_{i0}/D_{i0}$ ), so they were estimated as a single parameter.

### 3.2 Copolymerizations

Similarly to the homopolymerization modeling, some theoretical considerations were adopted for the copolymerization of p(VAc-co-MMA), resulting in a more simplified model. For the same reasons as in the homopolymerization, the initial considerations were the limitation of the transfer to polymer, implying no need to account for ramification frequency; no monomer diffusion to suspending phase and no chain transfer to impurity neither solvent.

A major consequence is created when adopting the ultimate unit model in the copolymerization system: live polymers now have two types, the ones which active unit has the VAc-like structure ( $P$  type) and the ones that have it in a MMA-like structure ( $Q$  type). All possible combinations with each type must be considered when writing the chemical equations, including the cross reactions (ones that involve both  $P$  and  $Q$  species).

To better express the different variables, the index  $1$  was used in a kinetic constants when it was related to the  $P$  type polymer chain. In contrast, the index  $2$  indicates relation to the  $Q$  type chains. For example,  $k_{tc11}$  is the kinetic constant of the termination by combination of a  $P$  type chain with another  $P$  type chain (equivalent to the homopolymerization process of VAc). A  $k_{tc12}$ , on the other hand, is related to the same process, but between a  $P$  type chain and  $Q$  type chain (cross reaction).

Like in the homopolymerization, the indexes in the  $P_{i,j}^\bullet$  and  $Q_{m,n}^\bullet$  variables indicate the quantity of each monomer present in the chain. For instance,  $Q_{5,8}^\bullet$  is the variable related to the concentration of active polymer chains with five mers coming from VAc monomers and eight coming from the MMA monomer from which one possesses the free radical.

Having the copolymerization nomenclature established, the following equations express all chemical reactions that were considered in the modeling for the initiation, propagation, termination and radical transfer to monomer and polymer.

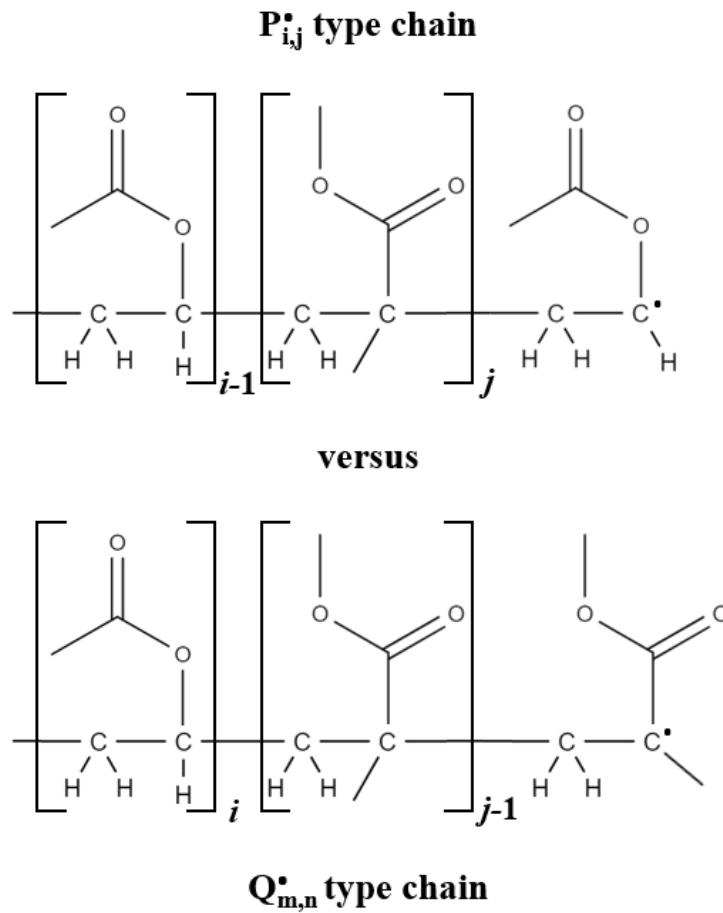
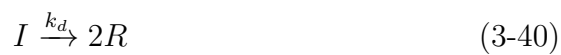


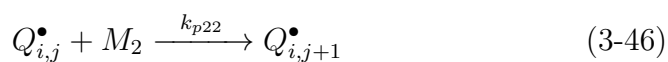
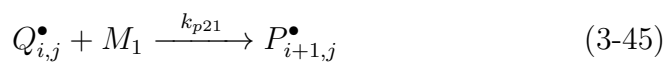
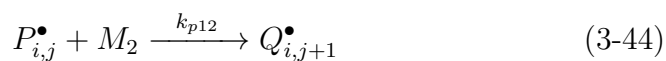
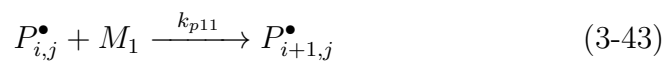
Figure 3.2: Representation of P and Q polymer chain types.

- **Initiation:**

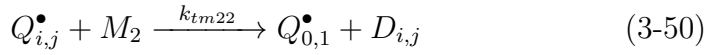
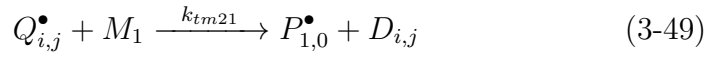
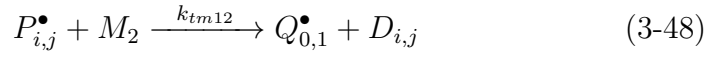
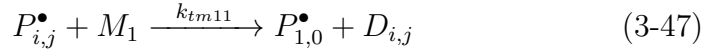


where  $M_1$  is the concentration of VAc monomers and  $M_2$  is the concentration of MMA monomers.

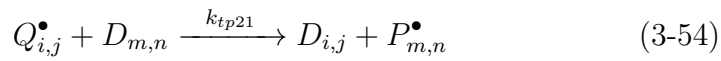
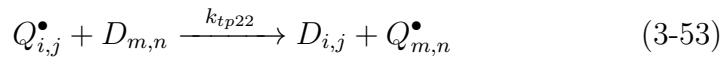
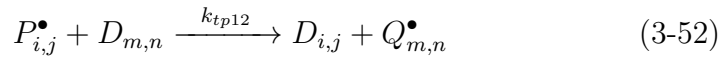
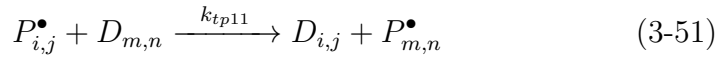
- **Propagation:**



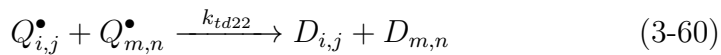
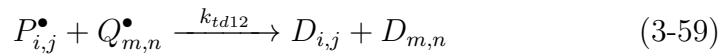
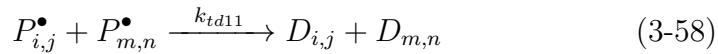
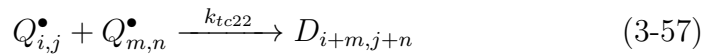
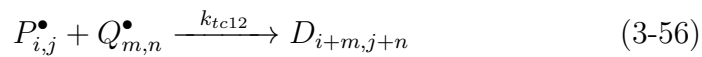
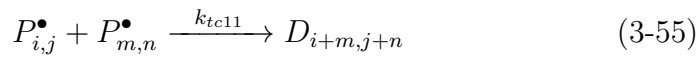
- Radical transfer to monomer:



- Radical transfer to polymer:



- Termination:



As it can be seen, the quantity of reactions taking place in the process rose considerably when compared to the homopolymerization.

### 3.2.1

#### Balance equations

To reduce the amount of variables present in the expressions, the concentration of each species is represented in terms of concentration instead of molar quantity. Eq.(3-61) to (3-64) express the balances written from the chemical equations for the initiator, the primary radicals and both monomers.

- **Initiator:**

$$\frac{1}{V} \frac{d(VI)}{dt} = -k_d I \quad (3-61)$$

- **Primary radicals:**

$$\frac{1}{V} \frac{d(VR^\bullet)}{dt} = 2fk_d I - k_{i1} R^\bullet M_1 - k_{i2} R^\bullet M_2 \quad (3-62)$$

- **Monomers:**

$$\begin{aligned} \frac{1}{V} \frac{d(VM_1)}{dt} = & -k_{i1} R^\bullet M_1 - k_{p11} M_1 \sum_{i=1}^{\infty} \sum_{j=0}^{\infty} P_{i,j}^\bullet - k_{p21} M_1 \sum_{i=0}^{\infty} \sum_{j=1}^{\infty} Q_{i,j}^\bullet \\ & - k_{tm11} M_1 \sum_{i=1}^{\infty} \sum_{j=0}^{\infty} P_{i,j}^\bullet - k_{tm21} M_1 \sum_{i=0}^{\infty} \sum_{j=1}^{\infty} Q_{i,j}^\bullet \end{aligned} \quad (3-63)$$

$$\begin{aligned} \frac{1}{V} \frac{d(VM_2)}{dt} = & -k_{i2} R^\bullet M_2 - k_{p12} M_2 \sum_{i=1}^{\infty} \sum_{j=0}^{\infty} P_{i,j}^\bullet - k_{p22} M_2 \sum_{i=0}^{\infty} \sum_{j=1}^{\infty} Q_{i,j}^\bullet \\ & - k_{tm12} M_2 \sum_{i=1}^{\infty} \sum_{j=0}^{\infty} P_{i,j}^\bullet - k_{tm22} M_2 \sum_{i=0}^{\infty} \sum_{j=1}^{\infty} Q_{i,j}^\bullet \end{aligned} \quad (3-64)$$

To be able to mathematically write the balance for the live and dead species without violating any theoretical concept, it is necessary to separate the different chain sizes ( $i$  and  $j$  indexes) into groups that have the same expression, as shown in eq.(3-65) to (3-78).

• Live polymer chains of P type:

For ( $i = 1$ ) and ( $j = 0$ ):

$$\begin{aligned}
 \frac{1}{V} \frac{d(VP_{1,0}^\bullet)}{dt} = & k_{i1}R^\bullet M_1 - k_{p11}P_{1,0}^\bullet M_1 - k_{p12}P_{1,0}^\bullet M_2 - k_{tm11}P_{1,0}^\bullet M_1 \\
 & - k_{tm12}P_{1,0}^\bullet M_2 + k_{tm11}M_1 \sum_{m=1}^{\infty} \sum_{n=0}^{\infty} P_{m,n}^\bullet + k_{tm21}M_1 \sum_{m=0}^{\infty} \sum_{n=1}^{\infty} Q_{m,n}^\bullet \\
 & - k_{tc11}P_{1,0}^\bullet \sum_{m=1}^{\infty} \sum_{n=0}^{\infty} P_{m,n}^\bullet - k_{tc12}P_{1,0}^\bullet \sum_{m=0}^{\infty} \sum_{n=1}^{\infty} Q_{m,n}^\bullet \\
 & - k_{td11}P_{1,0}^\bullet \sum_{m=1}^{\infty} \sum_{n=0}^{\infty} P_{m,n}^\bullet - k_{td12}P_{1,0}^\bullet \sum_{m=0}^{\infty} \sum_{n=1}^{\infty} Q_{m,n}^\bullet \\
 & + k_{tp11}D_{1,0} \sum_{m=1}^{\infty} \sum_{n=0}^{\infty} P_{m,n}^\bullet + k_{tp21}D_{1,0} \sum_{m=0}^{\infty} \sum_{n=1}^{\infty} Q_{m,n}^\bullet \\
 & - k_{tp11}P_{1,0}^\bullet \sum_{m=1}^{\infty} \sum_{n=0}^{\infty} mD_{m,n} - k_{tp12}P_{1,0}^\bullet \sum_{m=0}^{\infty} \sum_{n=1}^{\infty} nD_{m,n}
 \end{aligned} \tag{3-65}$$

For ( $i = 1$ ) and ( $j \geq 1$ ):

$$\begin{aligned}
 \frac{1}{V} \frac{d(VP_{1,j}^\bullet)}{dt} = & -k_{p11}M_1P_{1,j}^\bullet - k_{p12}M_2P_{1,j}^\bullet + k_{p21}M_1Q_{0,j}^\bullet - k_{tm11}M_1P_{1,j}^\bullet \\
 & - k_{tm12}M_2P_{1,j}^\bullet - k_{tc11}P_{1,j}^\bullet \sum_{m=1}^{\infty} \sum_{n=0}^{\infty} P_{m,n}^\bullet - k_{tc12}P_{1,j}^\bullet \sum_{m=0}^{\infty} \sum_{n=1}^{\infty} Q_{m,n}^\bullet \\
 & - k_{td11}P_{1,j}^\bullet \sum_{m=1}^{\infty} \sum_{n=0}^{\infty} P_{m,n}^\bullet - k_{td12}P_{1,j}^\bullet \sum_{m=0}^{\infty} \sum_{n=1}^{\infty} Q_{m,n}^\bullet \\
 & + k_{tp11}D_{1,j} \sum_{m=1}^{\infty} \sum_{n=0}^{\infty} P_{m,n}^\bullet + k_{tp21}D_{1,j} \sum_{m=0}^{\infty} \sum_{n=1}^{\infty} Q_{m,n}^\bullet \\
 & - k_{tp11}P_{1,j}^\bullet \sum_{m=1}^{\infty} \sum_{n=0}^{\infty} mD_{m,n} - k_{tp12}P_{1,j}^\bullet \sum_{m=0}^{\infty} \sum_{n=1}^{\infty} nD_{m,n}
 \end{aligned} \tag{3-66}$$

For ( $i \geq 2$ ) and ( $j \geq 0$ ):

$$\begin{aligned}
\frac{1}{V} \frac{d(VP_{i,j}^\bullet)}{dt} = & k_{p11}M_1(P_{i-1,j}^\bullet - P_{i,j}^\bullet) - k_{p12}M_2P_{i,j}^\bullet + k_{p21}M_1Q_{i-1,j}^\bullet \\
& - k_{tm11}M_1P_{i,j}^\bullet - k_{tm12}M_2P_{i,j}^\bullet - k_{tc11}P_{i,j}^\bullet \sum_{m=1}^{\infty} \sum_{n=0}^{\infty} P_{m,n}^\bullet \\
& - k_{tc12}P_{i,j}^\bullet \sum_{m=0}^{\infty} \sum_{n=1}^{\infty} Q_{m,n}^\bullet - k_{td11}P_{i,j}^\bullet \sum_{m=1}^{\infty} \sum_{n=0}^{\infty} P_{m,n}^\bullet \\
& - k_{td12}P_{i,j}^\bullet \sum_{m=0}^{\infty} \sum_{n=1}^{\infty} Q_{m,n}^\bullet + k_{tp11}iD_{i,j} \sum_{m=1}^{\infty} \sum_{n=0}^{\infty} P_{m,n}^\bullet \\
& - k_{tp11}P_{i,j}^\bullet \sum_{m=1}^{\infty} \sum_{n=0}^{\infty} mD_{m,n} - k_{tp12}P_{i,j}^\bullet \sum_{m=0}^{\infty} \sum_{n=1}^{\infty} nD_{m,n} \\
& + k_{tp21}iD_{i,j} \sum_{m=0}^{\infty} \sum_{n=1}^{\infty} Q_{m,n}^\bullet
\end{aligned} \tag{3-67}$$

• Live polymer chains of Q type:

For ( $i = 0$ ) and ( $j = 1$ ):

$$\begin{aligned}
\frac{1}{V} \frac{d(VQ_{0,1}^\bullet)}{dt} = & k_{i2}R^\bullet M_2 - k_{p22}Q_{0,1}^\bullet M_2 - k_{p21}Q_{0,1}^\bullet M_1 - k_{tm22}Q_{0,1}^\bullet M_2 \\
& - k_{tm21}Q_{0,1}^\bullet M_1 + k_{tm22}M_2 \sum_{m=0}^{\infty} \sum_{n=1}^{\infty} Q_{m,n}^\bullet + k_{tm12}M_2 \sum_{m=1}^{\infty} \sum_{n=0}^{\infty} P_{m,n}^\bullet \\
& - k_{tc22}Q_{0,1}^\bullet \sum_{m=0}^{\infty} \sum_{n=1}^{\infty} Q_{m,n}^\bullet - k_{tc12}Q_{0,1}^\bullet \sum_{m=1}^{\infty} \sum_{n=0}^{\infty} P_{m,n}^\bullet \\
& - k_{td22}Q_{0,1}^\bullet \sum_{m=0}^{\infty} \sum_{n=1}^{\infty} Q_{m,n}^\bullet - k_{td12}Q_{0,1}^\bullet \sum_{m=1}^{\infty} \sum_{n=0}^{\infty} P_{m,n}^\bullet \\
& + k_{tp22}D_{0,1} \sum_{m=0}^{\infty} \sum_{n=1}^{\infty} Q_{m,n}^\bullet + k_{tp12}D_{0,1} \sum_{m=1}^{\infty} \sum_{n=0}^{\infty} P_{m,n}^\bullet \\
& - k_{tp22}Q_{0,1}^\bullet \sum_{m=0}^{\infty} \sum_{n=1}^{\infty} nD_{m,n} - k_{tp21}Q_{0,1}^\bullet \sum_{m=1}^{\infty} \sum_{n=0}^{\infty} mD_{m,n}
\end{aligned} \tag{3-68}$$

For  $(i \geq 1)$  and  $(j = 1)$ :

$$\begin{aligned}
\frac{1}{V} \frac{d(VQ_{i,1}^\bullet)}{dt} = & -k_{p22}M_2Q_{i,1}^\bullet - k_{p21}M_1Q_{i,1}^\bullet + k_{p12}M_2P_{i,0}^\bullet - k_{tm22}M_2Q_{i,1}^\bullet \\
& - k_{tm21}M_1Q_{i,1}^\bullet - k_{tc22}Q_{i,1}^\bullet \sum_{m=0}^{\infty} \sum_{n=1}^{\infty} Q_{m,n}^\bullet - k_{tc12}Q_{i,1}^\bullet \sum_{m=1}^{\infty} \sum_{n=0}^{\infty} P_{m,n}^\bullet \\
& - k_{td22}Q_{i,1}^\bullet \sum_{m=0}^{\infty} \sum_{n=1}^{\infty} Q_{m,n}^\bullet - k_{td12}Q_{i,1}^\bullet \sum_{m=1}^{\infty} \sum_{n=0}^{\infty} P_{m,n}^\bullet \quad (3-69) \\
& + k_{tp22}D_{i,1} \sum_{m=0}^{\infty} \sum_{n=1}^{\infty} Q_{m,n}^\bullet + k_{tp12}D_{i,1} \sum_{m=1}^{\infty} \sum_{n=0}^{\infty} P_{m,n}^\bullet \\
& - k_{tp22}Q_{i,1}^\bullet \sum_{m=0}^{\infty} \sum_{n=1}^{\infty} nD_{m,n} - k_{tp21}Q_{i,1}^\bullet \sum_{m=1}^{\infty} \sum_{n=0}^{\infty} mD_{m,n}
\end{aligned}$$

For  $(i \geq 0)$  and  $(j \geq 2)$ :

$$\begin{aligned}
\frac{1}{V} \frac{d(VQ_{i,j}^\bullet)}{dt} = & k_{p22}M_2(Q_{i,j-1}^\bullet - Q_{i,j}^\bullet) - k_{p21}M_1Q_{i,j}^\bullet + k_{p12}M_2P_{i,j-1}^\bullet \\
& - k_{tm22}M_2Q_{i,j}^\bullet - k_{tm21}M_1Q_{i,j}^\bullet - k_{tc22}Q_{i,j}^\bullet \sum_{m=0}^{\infty} \sum_{n=1}^{\infty} Q_{m,n}^\bullet \\
& - k_{tc12}Q_{i,j}^\bullet \sum_{m=1}^{\infty} \sum_{n=0}^{\infty} P_{m,n}^\bullet - k_{td22}Q_{i,j}^\bullet \sum_{m=0}^{\infty} \sum_{n=1}^{\infty} Q_{m,n}^\bullet \quad (3-70) \\
& - k_{td12}Q_{i,j}^\bullet \sum_{m=1}^{\infty} \sum_{n=0}^{\infty} P_{m,n}^\bullet + k_{tp22}jD_{i,j} \sum_{m=0}^{\infty} \sum_{n=1}^{\infty} Q_{m,n}^\bullet \\
& - k_{tp22}Q_{i,j}^\bullet \sum_{m=0}^{\infty} \sum_{n=1}^{\infty} nD_{m,n} - k_{tp21}Q_{i,j}^\bullet \sum_{m=1}^{\infty} \sum_{n=0}^{\infty} mD_{m,n} \\
& + k_{tp12}jD_{i,j} \sum_{m=1}^{\infty} \sum_{n=0}^{\infty} P_{m,n}^\bullet
\end{aligned}$$

• **Dead polymer chains:**

For  $(i = 1)$  and  $(j = 0)$ :

$$\begin{aligned}
\frac{1}{V} \frac{d(VD_{1,0})}{dt} = & k_{tm11}M_1P_{1,0}^\bullet + k_{tm12}M_2P_{1,0}^\bullet + k_{td12}P_{1,0}^\bullet \sum_{m=0}^{\infty} \sum_{n=1}^{\infty} Q_{m,n}^\bullet \\
& + k_{td11}P_{1,0}^\bullet \sum_{m=1}^{\infty} \sum_{n=0}^{\infty} P_{m,n}^\bullet + k_{tp11}P_{1,0}^\bullet \sum_{m=1}^{\infty} \sum_{n=0}^{\infty} mD_{m,n} \quad (3-71) \\
& - k_{tp11}D_{1,0} \sum_{m=1}^{\infty} \sum_{n=0}^{\infty} P_{m,n}^\bullet + k_{tp12}P_{1,0}^\bullet \sum_{m=0}^{\infty} \sum_{n=1}^{\infty} nD_{m,n} \\
& - k_{tp21}D_{1,0} \sum_{m=0}^{\infty} \sum_{n=1}^{\infty} Q_{m,n}^\bullet
\end{aligned}$$

For ( $i = 0$ ) and ( $j = 1$ ):

$$\begin{aligned}
\frac{1}{V} \frac{d(VD_{0,1})}{dt} &= k_{tm22}M_2Q_{0,1}^\bullet + k_{tm21}M_1Q_{0,1}^\bullet + k_{td12}Q_{0,1}^\bullet \sum_{m=1}^{\infty} \sum_{n=0}^{\infty} P_{m,n}^\bullet \\
&\quad + k_{td22}Q_{0,1}^\bullet \sum_{m=0}^{\infty} \sum_{n=1}^{\infty} Q_{m,n}^\bullet + k_{tp22}Q_{0,1}^\bullet \sum_{m=0}^{\infty} \sum_{n=1}^{\infty} nD_{m,n} \\
&\quad - k_{tp22}D_{0,1} \sum_{m=0}^{\infty} \sum_{n=1}^{\infty} Q_{m,n}^\bullet + k_{tp21}Q_{0,1}^\bullet \sum_{m=1}^{\infty} \sum_{n=0}^{\infty} mD_{m,n} \\
&\quad - k_{tp12}D_{0,1} \sum_{m=1}^{\infty} \sum_{n=0}^{\infty} P_{m,n}^\bullet
\end{aligned} \tag{3-72}$$

For ( $i = 1$ ) and ( $j = 1$ ):

$$\begin{aligned}
\frac{1}{V} \frac{d(VD_{1,1})}{dt} &= k_{tm11}M_1P_{1,1}^\bullet + k_{tm12}M_2P_{1,1}^\bullet + k_{tm21}M_1Q_{1,1}^\bullet \\
&\quad + k_{tm22}M_2Q_{1,1}^\bullet + k_{tc12}P_{1,0}^\bullet Q_{0,1}^\bullet + k_{td12}P_{1,1}^\bullet \sum_{m=0}^{\infty} \sum_{n=1}^{\infty} Q_{m,n}^\bullet \\
&\quad + k_{td12}Q_{1,1}^\bullet \sum_{m=1}^{\infty} \sum_{n=0}^{\infty} P_{m,n}^\bullet + k_{td11}P_{1,1}^\bullet \sum_{m=1}^{\infty} \sum_{n=0}^{\infty} P_{m,n}^\bullet \\
&\quad + k_{td22}Q_{1,1}^\bullet \sum_{m=0}^{\infty} \sum_{n=1}^{\infty} Q_{m,n}^\bullet + k_{tp11}P_{1,1}^\bullet \sum_{m=1}^{\infty} \sum_{n=0}^{\infty} mD_{m,n} \\
&\quad - k_{tp11}D_{1,1} \sum_{m=1}^{\infty} \sum_{n=0}^{\infty} P_{m,n}^\bullet + k_{tp12}P_{1,1}^\bullet \sum_{m=0}^{\infty} \sum_{n=1}^{\infty} nD_{m,n} \\
&\quad - k_{tp12}D_{1,1} \sum_{m=1}^{\infty} \sum_{n=0}^{\infty} P_{m,n}^\bullet + k_{tp21}Q_{1,1}^\bullet \sum_{m=1}^{\infty} \sum_{n=0}^{\infty} mD_{m,n} \\
&\quad - k_{tp21}D_{1,1} \sum_{m=0}^{\infty} \sum_{n=1}^{\infty} Q_{m,n}^\bullet + k_{tp22}Q_{1,1}^\bullet \sum_{m=0}^{\infty} \sum_{n=1}^{\infty} nD_{m,n} \\
&\quad - k_{tp22}D_{1,1} \sum_{m=0}^{\infty} \sum_{n=1}^{\infty} Q_{m,n}^\bullet
\end{aligned} \tag{3-73}$$

For  $(i = 1)$  and  $(j \geq 2)$ :

$$\begin{aligned}
\frac{1}{V} \frac{d(VD_{1,j})}{dt} &= k_{tm11}M_1P_{1,j}^\bullet + k_{tm12}M_2P_{1,j}^\bullet + k_{tm21}M_1Q_{1,j}^\bullet \\
&+ k_{tm22}M_2Q_{1,j}^\bullet + k_{tc22} \sum_{n=1}^{j-1} Q_{0,n}^\bullet Q_{1,j-n}^\bullet + k_{tc12} \sum_{n=1}^{j-1} P_{1,j-n}^\bullet Q_{0,n}^\bullet \\
&+ k_{td12}P_{1,j}^\bullet \sum_{m=0}^{\infty} \sum_{n=1}^{\infty} Q_{m,n}^\bullet + k_{td12}Q_{1,j}^\bullet \sum_{m=1}^{\infty} \sum_{n=0}^{\infty} P_{m,n}^\bullet \\
&+ k_{td11}P_{1,j}^\bullet \sum_{m=1}^{\infty} \sum_{n=0}^{\infty} P_{m,n}^\bullet + k_{td22}Q_{1,j}^\bullet \sum_{m=0}^{\infty} \sum_{n=1}^{\infty} Q_{m,n}^\bullet \\
&+ k_{tc12}P_{1,0}^\bullet Q_{0,j}^\bullet + k_{tp11}P_{1,j}^\bullet \sum_{m=1}^{\infty} \sum_{n=0}^{\infty} mD_{m,n} \\
&- k_{tp11}D_{1,j} \sum_{m=1}^{\infty} \sum_{n=0}^{\infty} P_{m,n}^\bullet + k_{tp12}P_{1,j}^\bullet \sum_{m=0}^{\infty} \sum_{n=1}^{\infty} nD_{m,n} \\
&- k_{tp12}jD_{1,j} \sum_{m=1}^{\infty} \sum_{n=0}^{\infty} P_{m,n}^\bullet + k_{tp21}Q_{1,j}^\bullet \sum_{m=1}^{\infty} \sum_{n=0}^{\infty} mD_{m,n} \\
&- k_{tp21}D_{1,j} \sum_{m=0}^{\infty} \sum_{n=1}^{\infty} Q_{m,n}^\bullet + k_{tp22}Q_{1,j}^\bullet \sum_{m=0}^{\infty} \sum_{n=1}^{\infty} nD_{m,n} \\
&- k_{tp22}jD_{1,j} \sum_{m=0}^{\infty} \sum_{n=1}^{\infty} Q_{m,n}^\bullet
\end{aligned} \tag{3-74}$$

For  $(i \geq 2)$  and  $(j = 1)$ :

$$\begin{aligned}
\frac{1}{V} \frac{d(VD_{i,1})}{dt} &= k_{tm11}M_1P_{i,1}^\bullet + k_{tm12}M_2P_{i,1}^\bullet + k_{tm21}M_1Q_{i,1}^\bullet \\
&+ k_{tm22}M_2Q_{i,1}^\bullet + k_{tc11} \sum_{m=1}^{i-1} P_{m,0}^\bullet P_{i-m,1}^\bullet + k_{tc12} \sum_{m=1}^{i-1} P_{m,0}^\bullet Q_{i-m,1}^\bullet \\
&+ k_{td12}P_{i,1}^\bullet \sum_{m=0}^{\infty} \sum_{n=1}^{\infty} Q_{m,n}^\bullet + k_{td12}Q_{i,1}^\bullet \sum_{m=1}^{\infty} \sum_{n=0}^{\infty} P_{m,n}^\bullet \\
&+ k_{td11}P_{i,1}^\bullet \sum_{m=1}^{\infty} \sum_{n=0}^{\infty} P_{m,n}^\bullet + k_{td22}Q_{i,1}^\bullet \sum_{m=0}^{\infty} \sum_{n=1}^{\infty} Q_{m,n}^\bullet \\
&+ k_{tc12}P_{i,0}^\bullet Q_{0,1}^\bullet + k_{tp11}P_{i,1}^\bullet \sum_{m=1}^{\infty} \sum_{n=0}^{\infty} mD_{m,n} \\
&- k_{tp11}iD_{i,1} \sum_{m=1}^{\infty} \sum_{n=0}^{\infty} P_{m,n}^\bullet + k_{tp12}P_{i,1}^\bullet \sum_{m=0}^{\infty} \sum_{n=1}^{\infty} nD_{m,n} \\
&- k_{tp12}D_{i,1} \sum_{m=1}^{\infty} \sum_{n=0}^{\infty} P_{m,n}^\bullet + k_{tp21}Q_{i,1}^\bullet \sum_{m=1}^{\infty} \sum_{n=0}^{\infty} mD_{m,n} \\
&- k_{tp21}iD_{i,1} \sum_{m=0}^{\infty} \sum_{n=1}^{\infty} Q_{m,n}^\bullet + k_{tp22}Q_{i,1}^\bullet \sum_{m=0}^{\infty} \sum_{n=1}^{\infty} nD_{m,n} \\
&- k_{tp22}D_{i,1} \sum_{m=0}^{\infty} \sum_{n=1}^{\infty} Q_{m,n}^\bullet
\end{aligned} \tag{3-75}$$

For the three remaining index groups, the terms expressing termination by combination can have two different mathematical expressions depending on  $i$  and  $j$  assuming odd or even numbers. The difference was assumed to be small, considering the amount of terms involved, and the expressions with format usually seen in the literature were selected to be used in the model, as shown in eq.(3-76) to (3-78).

For ( $i \geq 2$ ) and ( $j = 0$ ):

$$\begin{aligned} \frac{1}{V} \frac{d(VD_{i,0})}{dt} = & k_{tm11}M_1P_{i,0}^\bullet + k_{tm12}M_2P_{i,0}^\bullet + k_{tc11}\frac{1}{2} \left( \sum_{m=1}^{i-1} P_{m,0}^\bullet P_{i-m,0}^\bullet \right) \\ & + k_{td12}P_{i,0}^\bullet \sum_{m=0}^{\infty} \sum_{n=1}^{\infty} Q_{m,n}^\bullet + k_{td11}P_{i,0}^\bullet \sum_{m=1}^{\infty} \sum_{n=0}^{\infty} P_{m,n}^\bullet \\ & + k_{tp11}P_{i,0}^\bullet \sum_{m=1}^{\infty} \sum_{n=0}^{\infty} mD_{m,n} - k_{tp11}iD_{i,0} \sum_{m=1}^{\infty} \sum_{n=0}^{\infty} P_{m,n}^\bullet \\ & + k_{tp12}P_{i,0}^\bullet \sum_{m=0}^{\infty} \sum_{n=1}^{\infty} nD_{m,n} - k_{tp21}iD_{i,0} \sum_{m=0}^{\infty} \sum_{n=1}^{\infty} Q_{m,n}^\bullet \end{aligned} \quad (3-76)$$

For ( $i = 0$ ) and ( $j \geq 2$ ):

$$\begin{aligned} \frac{1}{V} \frac{d(VD_{0,j})}{dt} = & k_{tm22}M_2Q_{0,j}^\bullet + k_{tm21}M_1Q_{0,j}^\bullet + k_{tc22}\frac{1}{2} \left( \sum_{n=1}^{j-1} Q_{0,n}^\bullet Q_{0,j-n}^\bullet \right) \\ & + k_{td12}Q_{0,j}^\bullet \sum_{m=1}^{\infty} \sum_{n=0}^{\infty} P_{m,n}^\bullet + k_{td22}Q_{0,j}^\bullet \sum_{m=0}^{\infty} \sum_{n=1}^{\infty} Q_{m,n}^\bullet \\ & + k_{tp22}Q_{0,j}^\bullet \sum_{m=0}^{\infty} \sum_{n=1}^{\infty} nD_{m,n} - k_{tp22}jD_{0,j} \sum_{m=0}^{\infty} \sum_{n=1}^{\infty} Q_{m,n}^\bullet \\ & + k_{tp21}Q_{0,j}^\bullet \sum_{m=1}^{\infty} \sum_{n=0}^{\infty} mD_{m,n} - k_{tp12}jD_{0,j} \sum_{m=1}^{\infty} \sum_{n=0}^{\infty} P_{m,n}^\bullet \end{aligned} \quad (3-77)$$

For ( $i \geq 2$ ) and ( $j \geq 2$ ):

$$\begin{aligned}
\frac{1}{V} \frac{d(VD_{i,j})}{dt} = & k_{tm11} M_1 P_{i,j}^\bullet + k_{tm12} M_2 P_{i,j}^\bullet + k_{tm21} M_1 Q_{i,j}^\bullet \\
& + k_{tc11} \left( \sum_{m=1}^{i-1} P_{m,0}^\bullet P_{i-m,j}^\bullet + \frac{1}{2} \left( \sum_{m=1}^{i-1} \sum_{n=1}^{j-1} P_{m,n}^\bullet P_{i-m,j-n}^\bullet \right) \right) \\
& + k_{tc22} \left( \sum_{n=1}^{j-1} Q_{0,n}^\bullet Q_{i,j-n}^\bullet + \frac{1}{2} \left( \sum_{m=1}^{i-1} \sum_{n=1}^{j-1} Q_{m,n}^\bullet Q_{i-m,j-n}^\bullet \right) \right) \\
& + k_{td12} P_{i,j}^\bullet \sum_{m=0}^{\infty} \sum_{n=1}^{\infty} Q_{m,n}^\bullet + k_{td12} Q_{i,j}^\bullet \sum_{m=1}^{\infty} \sum_{n=0}^{\infty} P_{m,n}^\bullet \\
& + k_{td11} P_{i,j}^\bullet \sum_{m=1}^{\infty} \sum_{n=0}^{\infty} P_{m,n}^\bullet + k_{td22} Q_{i,j}^\bullet \sum_{m=0}^{\infty} \sum_{n=1}^{\infty} Q_{m,n}^\bullet \\
& + k_{tc12} \sum_{m=1}^{i-1} \sum_{n=0}^{j-1} P_{m,n}^\bullet Q_{i-m,j-n}^\bullet + k_{tc12} \sum_{n=1}^{j-1} Q_{0,n}^\bullet P_{i,j-n}^\bullet \\
& + k_{tm22} M_2 Q_{i,j}^\bullet + k_{tc12} P_{i,0}^\bullet Q_{0,j}^\bullet + k_{tp11} P_{i,j}^\bullet \sum_{m=1}^{\infty} \sum_{n=0}^{\infty} m D_{m,n} \\
& - k_{tp11} i D_{i,j} \sum_{m=1}^{\infty} \sum_{n=0}^{\infty} P_{m,n}^\bullet + k_{tp12} P_{i,j}^\bullet \sum_{m=0}^{\infty} \sum_{n=1}^{\infty} n D_{m,n} \\
& - k_{tp12} j D_{i,j} \sum_{m=1}^{\infty} \sum_{n=0}^{\infty} P_{m,n}^\bullet + k_{tp21} Q_{i,j}^\bullet \sum_{m=1}^{\infty} \sum_{n=0}^{\infty} m D_{m,n} \\
& - k_{tp21} i D_{i,j} \sum_{m=0}^{\infty} \sum_{n=1}^{\infty} Q_{m,n}^\bullet + k_{tp22} Q_{i,j}^\bullet \sum_{m=0}^{\infty} \sum_{n=1}^{\infty} n D_{m,n} \\
& - k_{tp22} j D_{i,j} \sum_{m=0}^{\infty} \sum_{n=1}^{\infty} Q_{m,n}^\bullet
\end{aligned} \tag{3-78}$$

As two types of active polymer chains are present, an extra moment variable is needed in comparison to the homopolymerization. The variables related to the live moments of type  $P$  and  $Q$  are  $\gamma$  and  $\pi$  respectively, while  $\mu$  accounts for dead chains. Besides, two indexes ( $k$  and  $w$ ) were used to consider all variations, where their sum indicates the moment order.

$$\gamma_{k,w} = \sum_i^{\infty} \sum_j^{\infty} i^k j^w P_{i,j}^\bullet \quad \text{for all valid combinations of } i \text{ and } j \tag{3-79}$$

$$\pi_{k,w} = \sum_i^{\infty} \sum_j^{\infty} i^k j^w Q_{i,j}^\bullet \quad \text{for all valid combinations of } i \text{ and } j \tag{3-80}$$

$$\mu_{k,w} = \sum_i^{\infty} \sum_j^{\infty} i^k j^w D_{i,j} \quad \text{for all valid combinations of } i \text{ and } j \tag{3-81}$$

As indicated in eq.(3-79) to (3-81), not all combinations of  $i$  and  $j$  are valid, because setting the double summations to start at zero for both  $i$  and  $j$  would include species like  $P_{0,j}^\bullet$  and  $Q_{i,0}^\bullet$  which contradicts the chain type definition, meaning it is theoretically incorrect. The valid combination for each moment can be found in Appendix B.

The monomer balance including moment can be written by direct substitution of the live polymer parts in eq.(3-63) and (3-64), as they are equivalent to zeroth order moment expressions.

• **Monomers:**

$$\begin{aligned} \frac{1}{V} \frac{d(VM_1)}{dt} = & -k_{i1}R^\bullet M_1 - k_{p11}M_1\gamma_{0,0} - k_{p21}M_1\pi_{0,0} \\ & -k_{tm11}M_1\gamma_{0,0} - k_{tm21}M_1\pi_{0,0} \end{aligned} \quad (3-82)$$

$$\begin{aligned} \frac{1}{V} \frac{d(VM_2)}{dt} = & -k_{i2}R^\bullet M_2 - k_{p12}M_2\gamma_{0,0} - k_{p22}M_2\pi_{0,0} \\ & -k_{tm12}M_2\gamma_{0,0} - k_{tm22}M_2\pi_{0,0} \end{aligned} \quad (3-83)$$

The development of the method of moments of the live and dead chains for the copolymerization is considerably extensive as it includes twenty four different variables to account for the zeroth, first and second orders. Additionally, the starting point of each balance depends not only on valid  $i$  and  $j$  combination for each moment, but also on the intervals of these variables in which the different expressions can be used. Therefore, for each type of moment, the general differential moment expression is shown, followed by the balance equation already developed, as presented in eq.(3-84) to (3-104).

• **Live moments ( $\gamma$ ):**

$$\frac{1}{V} \frac{d(V\gamma_{k,w})}{dt} = \frac{1}{V} \frac{d(V \sum_i^\infty \sum_j^\infty i^k j^w P_{i,j}^\bullet)}{dt} = \sum_i^\infty \sum_j^\infty i^k j^w \frac{1}{V} \frac{d(V P_{i,j}^\bullet)}{dt} \quad (3-84)$$

for all valid combinations of  $i$  and  $j$

- **Zeroth order** ( $\gamma$ ):

$$\begin{aligned} \frac{1}{V} \frac{d(V\gamma_{0,0})}{dt} = & k_{i1} R^\bullet M_1 + k_{tm21} M_1 \pi_{0,0} - k_{p12} M_2 \gamma_{0,0} - k_{tm12} M_2 \gamma_{0,0} \\ & - k_{tc11} \gamma_{0,0}^2 - k_{tc12} \pi_{0,0} \gamma_{0,0} + k_{p21} M_1 \pi_{0,0} - k_{td11} \gamma_{0,0}^2 - k_{td12} \pi_{0,0} \gamma_{0,0} \\ & - k_{tp12} \gamma_{0,0} \mu_{0,1} + k_{tp21} \mu_{1,0} \pi_{0,0} \end{aligned} \quad (3-85)$$

- **First order** ( $\gamma$ ):

$$\begin{aligned} \frac{1}{V} \frac{d(V\gamma_{1,0})}{dt} = & k_{i1} R^\bullet M_1 + k_{tm21} M_1 \pi_{0,0} + k_{p11} M_1 \gamma_{0,0} - k_{p12} M_2 \gamma_{1,0} \\ & + k_{tm11} M_1 (\gamma_{0,0} - \gamma_{1,0}) - k_{tm12} M_2 \gamma_{1,0} - k_{tc11} \gamma_{0,0} \gamma_{1,0} - k_{tc12} \pi_{0,0} \gamma_{1,0} \\ & - k_{td11} \gamma_{0,0} \gamma_{1,0} - k_{td12} \pi_{0,0} \gamma_{1,0} + k_{p21} M_1 (\pi_{0,0} + \pi_{1,0}) + k_{tp11} \mu_{2,0} \gamma_{0,0} \\ & - k_{tp11} \gamma_{1,0} \mu_{1,0} - k_{tp12} \gamma_{1,0} \mu_{0,1} + k_{tp21} \mu_{2,0} \pi_{0,0} \end{aligned} \quad (3-86)$$

$$\begin{aligned} \frac{1}{V} \frac{d(V\gamma_{0,1})}{dt} = & -k_{p12} M_2 \gamma_{0,1} + k_{p21} M_1 \pi_{0,1} - k_{tm11} M_1 \gamma_{0,1} - k_{tm12} M_2 \gamma_{0,1} \\ & - k_{tc11} \gamma_{0,0} \gamma_{0,1} - k_{tc12} \pi_{0,0} \gamma_{0,1} - k_{td11} \gamma_{0,0} \gamma_{0,1} - k_{td12} \pi_{0,0} \gamma_{0,1} \\ & + k_{tp11} \mu_{1,1} \gamma_{0,0} - k_{tp11} \gamma_{0,1} \mu_{1,0} - k_{tp12} \gamma_{0,1} \mu_{0,1} + k_{tp21} \mu_{1,1} \pi_{0,0} \end{aligned} \quad (3-87)$$

- **Second order** ( $\gamma$ ):

$$\begin{aligned} \frac{1}{V} \frac{d(V\gamma_{2,0})}{dt} = & k_{i1} R^\bullet M_1 + k_{tm11} M_1 \gamma_{0,0} + k_{tm21} M_1 \pi_{0,0} - k_{p12} M_2 \gamma_{2,0} \\ & + k_{p11} M_1 (2\gamma_{1,0} + \gamma_{0,0}) - k_{tm11} M_1 \gamma_{2,0} - k_{tm12} M_2 \gamma_{2,0} - k_{tc11} \gamma_{0,0} \gamma_{2,0} \\ & - k_{tc12} \pi_{0,0} \gamma_{2,0} - k_{td11} \gamma_{0,0} \gamma_{2,0} + k_{p21} M_1 (\pi_{0,0} + 2\pi_{1,0} + \pi_{2,0}) \\ & - k_{td12} \pi_{0,0} \gamma_{2,0} + k_{tp11} \mu_{3,0} \gamma_{0,0} - k_{tp11} \gamma_{2,0} \mu_{1,0} \\ & - k_{tp12} \gamma_{2,0} \mu_{0,1} + k_{tp21} \mu_{3,0} \pi_{0,0} \end{aligned} \quad (3-88)$$

$$\begin{aligned} \frac{1}{V} \frac{d(V\gamma_{0,2})}{dt} = & -k_{p12} M_2 \gamma_{0,2} + k_{p21} M_1 \pi_{0,2} - k_{tm11} M_1 \gamma_{0,2} - k_{tc11} \gamma_{0,0} \gamma_{0,2} \\ & - k_{tc12} \pi_{0,0} \gamma_{0,2} - k_{td11} \gamma_{0,0} \gamma_{0,2} - k_{tm12} M_2 \gamma_{0,2} - k_{td12} \pi_{0,0} \gamma_{0,2} \\ & + k_{tp11} \mu_{1,2} \gamma_{0,0} - k_{tp11} \gamma_{0,2} \mu_{1,0} - k_{tp12} \gamma_{0,2} \mu_{0,1} + k_{tp21} \mu_{1,2} \pi_{0,0} \end{aligned} \quad (3-89)$$

$$\begin{aligned}
\frac{1}{V} \frac{d(V\gamma_{1,1})}{dt} = & k_{p11}M_1\gamma_{0,1} - k_{p12}M_2\gamma_{1,1} + k_{p21}M_1(\pi_{1,1} + \pi_{0,1}) \\
& - k_{tm11}M_1\gamma_{1,1} - k_{tm12}M_2\gamma_{1,1} - k_{tc11}\gamma_{0,0}\gamma_{1,1} - k_{tc12}\pi_{0,0}\gamma_{1,1} \\
& - k_{td11}\gamma_{0,0}\gamma_{1,1} - k_{td12}\pi_{0,0}\gamma_{1,1} + k_{tp11}\mu_{2,1}\gamma_{0,0} - k_{tp11}\gamma_{1,1}\mu_{1,0} \\
& - k_{tp12}\gamma_{1,1}\mu_{0,1} + k_{tp21}\mu_{2,1}\pi_{0,0}
\end{aligned} \tag{3-90}$$

• **Live moments** ( $\pi$ ):

$$\frac{1}{V} \frac{d(V\pi_{k,w})}{dt} = \frac{1}{V} \frac{d(V \sum_i^\infty \sum_j^\infty i^k j^w Q_{i,j}^\bullet)}{dt} = \sum_i^\infty \sum_j^\infty i^k j^w \frac{1}{V} \frac{d(VQ_{i,j}^\bullet)}{dt} \tag{3-91}$$

for all valid combinations of  $i$  and  $j$

- **Zeroth order** ( $\pi$ ):

$$\begin{aligned}
\frac{1}{V} \frac{d(V\pi_{0,0})}{dt} = & k_{i2}R^\bullet M_2 + k_{tm12}\gamma_{0,0}M_2 - k_{p21}M_1\pi_{0,0} - k_{tm21}M_1\pi_{0,0} \\
& - k_{tc22}\pi_{0,0}^2 - k_{tc12}\gamma_{0,0}\pi_{0,0} - k_{td22}\pi_{0,0}^2 - k_{td12}\gamma_{0,0}\pi_{0,0} + k_{p12}M_2\gamma_{0,0} \\
& - k_{tp21}\pi_{0,0}\mu_{1,0} + k_{tp12}\mu_{0,1}\gamma_{0,0}
\end{aligned} \tag{3-92}$$

- **First order** ( $\pi$ ):

$$\begin{aligned}
\frac{1}{V} \frac{d(V\pi_{1,0})}{dt} = & -k_{p21}M_1\pi_{1,0} + k_{p12}M_2\gamma_{1,0} - k_{tm22}M_2\pi_{1,0} - k_{tm21}M_1\pi_{1,0} \\
& - k_{tc12}\gamma_{0,0}\pi_{1,0} - k_{td22}\pi_{0,0}\pi_{1,0} - k_{td12}\gamma_{0,0}\pi_{1,0} - k_{tc22}\pi_{0,0}\pi_{1,0} \\
& + k_{tp22}\mu_{1,1}\pi_{0,0} - k_{tp22}\pi_{1,0}\mu_{0,1} - k_{tp21}\pi_{1,0}\mu_{1,0} + k_{tp12}\mu_{1,1}\gamma_{0,0}
\end{aligned} \tag{3-93}$$

$$\begin{aligned}
\frac{1}{V} \frac{d(V\pi_{0,1})}{dt} = & k_{i2}R^\bullet M_2 + k_{p22}M_2\pi_{0,0} - k_{p21}M_1\pi_{0,1} - k_{tm21}M_1\pi_{0,1} \\
& + k_{tm22}M_2(\pi_{0,0} - \pi_{0,1}) + k_{tm12}M_2\gamma_{0,0} - k_{tc22}\pi_{0,0}\pi_{0,1} - k_{tc12}\gamma_{0,0}\pi_{0,1} \\
& - k_{td22}\pi_{0,0}\pi_{0,1} - k_{td12}\gamma_{0,0}\pi_{0,1} + k_{p12}M_2(\gamma_{0,1} + \gamma_{0,0}) + k_{tp22}\mu_{0,2}\pi_{0,0} \\
& - k_{tp22}\pi_{0,1}\mu_{0,1} - k_{tp21}\pi_{0,1}\mu_{1,0} + k_{tp12}\mu_{0,2}\gamma_{0,0}
\end{aligned} \tag{3-94}$$

- **Second order** ( $\pi$ ):

$$\begin{aligned} \frac{1}{V} \frac{d(V\pi_{2,0})}{dt} = & -k_{p21}M_1\pi_{2,0} + k_{p12}M_2\gamma_{2,0} - k_{tm22}M_2\pi_{2,0} - k_{tm21}M_1\pi_{2,0} \\ & -k_{tc22}\pi_{0,0}\pi_{2,0} - k_{tc12}\gamma_{0,0}\pi_{2,0} - k_{td22}\pi_{0,0}\pi_{2,0} - k_{td12}\gamma_{0,0}\pi_{2,0} \\ & + k_{tp22}\mu_{2,1}\pi_{0,0} - k_{tp22}\pi_{2,0}\mu_{0,1} - k_{tp21}\pi_{2,0}\mu_{1,0} + k_{tp12}\mu_{2,1}\gamma_{0,0} \end{aligned} \quad (3-95)$$

$$\begin{aligned} \frac{1}{V} \frac{d(V\pi_{0,2})}{dt} = & k_{i2}R^\bullet M_2 + k_{tm12}M_2\gamma_{0,0} - k_{p21}M_1\pi_{0,2} - k_{tm21}M_1\pi_{0,2} \\ & + k_{p12}M_2(\gamma_{0,2} + 2\gamma_{0,1} + \gamma_{0,0}) - k_{tc22}\pi_{0,0}\pi_{0,2} - k_{tc12}\gamma_{0,0}\pi_{0,2} \\ & + k_{p22}M_2(2\pi_{0,1} + \pi_{0,0}) + k_{tm22}M_2(\pi_{0,0} - \pi_{0,2}) \\ & - k_{td22}\pi_{0,0}\pi_{0,2} - k_{td12}\gamma_{0,0}\pi_{0,2} + k_{tp22}\mu_{0,3}\pi_{0,0} \\ & - k_{tp22}\pi_{0,2}\mu_{0,1} - k_{tp21}\pi_{0,2}\mu_{1,0} + k_{tp12}\mu_{0,3}\gamma_{0,0} \end{aligned} \quad (3-96)$$

$$\begin{aligned} \frac{1}{V} \frac{d(V\pi_{1,1})}{dt} = & k_{p22}M_2\pi_{1,0} - k_{p21}M_1\pi_{1,1} + k_{p12}M_2(\gamma_{1,1} + \gamma_{1,0}) \\ & - k_{tm22}M_2\pi_{1,1} - k_{tm21}M_1\pi_{1,1} - k_{tc22}\pi_{0,0}\pi_{1,1} - k_{tc12}\gamma_{0,0}\pi_{1,1} \\ & - k_{td22}\pi_{0,0}\pi_{1,1} - k_{td12}\gamma_{0,0}\pi_{1,1} + k_{tp22}\mu_{1,2}\pi_{0,0} - k_{tp22}\pi_{1,1}\mu_{0,1} \\ & - k_{tp21}\pi_{1,1}\mu_{1,0} + k_{tp12}\mu_{1,2}\gamma_{0,0} \end{aligned} \quad (3-97)$$

• **Dead moments** ( $\mu$ ):

$$\frac{1}{V} \frac{d(V\mu_{k,w})}{dt} = \frac{1}{V} \frac{d(V \sum_i^\infty \sum_j^\infty i^k j^w D_{i,j})}{dt} = \sum_i^\infty \sum_j^\infty i^k j^w \frac{1}{V} \frac{d(V D_{i,j})}{dt} \quad (3-98)$$

for all valid combinations of  $i$  and  $j$

- **Zereth order** ( $\mu$ ):

$$\begin{aligned} \frac{1}{V} \frac{d(V\mu_{0,0})}{dt} = & k_{tm22}M_2\pi_{0,0} + k_{tm21}M_1\pi_{0,0} + 2k_{td12}\gamma_{0,0}\pi_{0,0} + k_{td22}\pi_{0,0}^2 \\ & + k_{tm11}M_1\gamma_{0,0} + k_{tm12}M_2\gamma_{0,0} + k_{td11}\gamma_{0,0}^2 + k_{tc12}\gamma_{0,0}\pi_{0,0} \\ & + \frac{1}{2}k_{tc11}\gamma_{0,0}^2 + \frac{1}{2}k_{tc22}\pi_{0,0}^2 - k_{tp12}\gamma_{0,0}\mu_{0,1} + k_{tp21}\mu_{1,0}\pi_{0,0} \\ & + k_{tp22}\mu_{0,1}\pi_{0,0} - k_{tp22}\pi_{0,0}\mu_{0,1} + k_{tp11}\mu_{1,0}\gamma_{0,0} \\ & - k_{tp11}\gamma_{0,0}\mu_{1,0} + k_{tp12}\mu_{0,1}\gamma_{0,0} - k_{tp21}\pi_{0,0}\mu_{1,0} \end{aligned} \quad (3-99)$$

- **First order** ( $\mu$ ):

$$\begin{aligned}
\frac{1}{V} \frac{d(V\mu_{1,0})}{dt} &= k_{tm11}M_1\gamma_{1,0} + k_{tm12}M_2\gamma_{1,0} + k_{td12}(\pi_{0,0}\gamma_{1,0} + \gamma_{0,0}\pi_{1,0}) \\
&+ k_{td11}\gamma_{0,0}\gamma_{1,0} + k_{tm21}M_1\pi_{1,0} + k_{tm22}M_2\pi_{1,0} + k_{td22}\pi_{0,0}\pi_{1,0} \\
&+ k_{tc12}(\gamma_{0,0}\pi_{1,0} + \gamma_{1,0}\pi_{0,0}) + k_{tc11}\gamma_{1,0}\gamma_{0,0} + k_{tc22}\pi_{1,0}\pi_{0,0} \\
&- k_{tp12}\gamma_{0,0}\mu_{1,1} + k_{tp21}\mu_{1,0}\pi_{1,0} + k_{tp22}\mu_{0,1}\pi_{1,0} \\
&- k_{tp22}\pi_{0,0}\mu_{1,1} + k_{tp11}\mu_{1,0}\gamma_{1,0} - k_{tp11}\gamma_{0,0}\mu_{2,0} \\
&+ k_{tp12}\mu_{0,1}\gamma_{1,0} - k_{tp21}\pi_{0,0}\mu_{2,0}
\end{aligned} \tag{3-100}$$

$$\begin{aligned}
\frac{1}{V} \frac{d(V\mu_{0,1})}{dt} &= k_{tm22}M_2\pi_{0,1} + k_{tm21}M_1\pi_{0,1} + k_{td12}(\gamma_{0,0}\pi_{0,1} + \pi_{0,0}\gamma_{0,1}) \\
&+ k_{td22}\pi_{0,0}\pi_{0,1} + k_{tm11}M_1\gamma_{0,1} + k_{tm12}M_2\gamma_{0,1} + k_{td11}\gamma_{0,0}\gamma_{0,1} \\
&+ k_{tc12}(\pi_{0,1}\gamma_{0,0} + \pi_{0,0}\gamma_{0,1}) + k_{tc22}\pi_{0,1}\pi_{0,0} + k_{tc11}\gamma_{0,0}\gamma_{0,1} \\
&- k_{tp12}\gamma_{0,0}\mu_{0,2} + k_{tp21}\mu_{1,0}\pi_{0,1} + k_{tp22}\mu_{0,1}\pi_{0,1} \\
&- k_{tp22}\pi_{0,0}\mu_{0,2} + k_{tp11}\mu_{1,0}\gamma_{0,1} - k_{tp11}\gamma_{0,0}\mu_{1,1} \\
&+ k_{tp12}\mu_{0,1}\gamma_{0,1} - k_{tp21}\pi_{0,0}\mu_{1,1}
\end{aligned} \tag{3-101}$$

- **Second order** ( $\mu$ ):

$$\begin{aligned}
\frac{1}{V} \frac{d(V\mu_{2,0})}{dt} &= k_{tm11}M_1\gamma_{2,0} + k_{tm12}M_2\gamma_{2,0} + k_{td12}(\pi_{0,0}\gamma_{2,0} + \gamma_{0,0}\pi_{2,0}) \\
&+ k_{td11}\gamma_{0,0}\gamma_{2,0} + k_{tm21}M_1\pi_{2,0} + k_{tm22}M_2\pi_{2,0} + k_{td22}\pi_{0,0}\pi_{2,0} \\
&+ k_{tc11}(\gamma_{1,0}^2 + \gamma_{0,0}\gamma_{2,0}) + k_{tc12}(\pi_{2,0}\gamma_{0,0} + \gamma_{2,0}\pi_{0,0} + 2\pi_{1,0}\gamma_{1,0}) \\
&+ k_{tc22}(\pi_{2,0}\pi_{0,0} + \pi_{1,0}^2) - k_{tp12}\gamma_{0,0}\mu_{2,1} + k_{tp21}\mu_{1,0}\pi_{2,0} \\
&+ k_{tp22}\mu_{0,1}\pi_{2,0} - k_{tp22}\pi_{0,0}\mu_{2,1} + k_{tp11}\mu_{1,0}\gamma_{2,0} \\
&- k_{tp11}\gamma_{0,0}\mu_{3,0} + k_{tp12}\mu_{0,1}\gamma_{2,0} - k_{tp21}\pi_{0,0}\mu_{3,0}
\end{aligned} \tag{3-102}$$

$$\begin{aligned}
\frac{1}{V} \frac{d(V\mu_{0,2})}{dt} = & k_{tm22}M_2\pi_{0,2} + k_{tm21}M_1\pi_{0,2} + k_{td12}(\gamma_{0,0}\pi_{0,2} + \pi_{0,0}\gamma_{0,2}) \\
& + k_{td22}\pi_{0,0}\pi_{0,2} + k_{tm12}M_2\gamma_{0,2} + k_{tm11}M_1\gamma_{0,2} + k_{td11}\gamma_{0,0}\gamma_{0,2} \\
& + k_{tc22}(\pi_{0,2}\pi_{0,0} + \pi_{0,1}^2) + k_{tc12}(\gamma_{0,0}\pi_{0,2} + 2\gamma_{0,1}\pi_{0,1} + \gamma_{0,2}\pi_{0,0}) \\
& + k_{tc11}(\gamma_{0,2}\gamma_{0,0} + \gamma_{0,1}^2) - k_{tp12}\gamma_{0,0}\mu_{0,3} + k_{tp21}\mu_{1,0}\pi_{0,2} \\
& + k_{tp22}\mu_{0,1}\pi_{0,2} - k_{tp22}\pi_{0,0}\mu_{0,3} + k_{tp11}\mu_{1,0}\gamma_{0,2} \\
& - k_{tp11}\gamma_{0,0}\mu_{1,2} + k_{tp12}\mu_{0,1}\gamma_{0,2} - k_{tp21}\pi_{0,0}\mu_{1,2}
\end{aligned} \quad (3-103)$$

$$\begin{aligned}
\frac{1}{V} \frac{d(V\mu_{1,1})}{dt} = & k_{tm11}M_1\gamma_{1,1} + k_{tm12}M_2\gamma_{1,1} + k_{td12}(\pi_{0,0}\gamma_{1,1} + \gamma_{0,0}\pi_{1,1}) \\
& + k_{td22}\pi_{0,0}\pi_{1,1} + k_{tm22}M_2\pi_{1,1} + k_{td11}\gamma_{0,0}\gamma_{1,1} + k_{tm21}M_1\pi_{1,1} \\
& + k_{tc11}(\gamma_{1,1}\gamma_{0,0} + \gamma_{0,1}\gamma_{1,0}) + k_{tc22}(\pi_{1,1}\pi_{0,0} + \pi_{1,0}\pi_{0,1}) \\
& + k_{tc12}(\pi_{1,1}\gamma_{0,0} + \pi_{1,0}\gamma_{0,1} + \pi_{0,1}\gamma_{1,0} + \gamma_{1,1}\pi_{0,0}) \\
& - k_{tp12}\gamma_{0,0}\mu_{1,2} + k_{tp21}\mu_{1,0}\pi_{1,1} + k_{tp22}\mu_{0,1}\pi_{1,1} \\
& - k_{tp22}\pi_{0,0}\mu_{1,2} + k_{tp11}\mu_{1,0}\gamma_{1,1} - k_{tp11}\gamma_{0,0}\mu_{2,1} \\
& + k_{tp12}\mu_{0,1}\gamma_{1,1} - k_{tp21}\pi_{0,0}\mu_{2,1}
\end{aligned} \quad (3-104)$$

The QSSA was then applied to all balances of free radical species (primary radicals and live moments). In the resulting expressions, the terms  $\gamma_{i,j}$  and  $\pi_{m,n}$ , where  $i = m$  and  $j = n$  presented mutual dependency, resulting in two variables and two equations system for each case. When all indexes are zero, the QSSA results in a second order system, which is not easily solved. A simplification method [84] was adapted for this system, where a  $K_s$  variable is introduced, as shown in eq.(3-106).

$$R^\bullet = \frac{2fk_dI}{k_{i1}M_1 + k_{i2}M_2} \quad (3-105)$$

$$K_s = \frac{(k_{p12} + k_{tm12})M_2 + k_{tp12}\mu_{01}}{(k_{p21} + k_{tm21})M_1 + k_{tp21}\mu_{10}} \quad (3-106)$$

$$\gamma_{0,0} = \sqrt{\frac{k_{i1}R^\bullet M_1 + k_{i2}R^\bullet M_2}{k_{t11} + 2k_{t12}K_s + k_{t22}K_s^2}} \quad (3-107)$$

$$\pi_{0,0} = K_s\gamma_{0,0} \quad (3-108)$$

All other systems are linear when considering only the common variables. An interesting observation is that all moments of same the type presented identical denominators, addressed as  $\gamma_{den}$  and  $\pi_{den}$ , and they possess the same general form, shown in eq.(3-109) and (3-110). This was used to express the develop and solution of each combination as shown next.

$$\gamma_{k,w} = \frac{\gamma_{k,w,terms} + k_{p21}M_1\pi_{k,w}}{\gamma_{den}} \quad (3-109)$$

$$\pi_{k,w} = \frac{\pi_{k,w,terms} + k_{p12}M_2\gamma_{k,w}}{\pi_{den}} \quad (3-110)$$

By replacing eq.(3-110) in eq.(3-109) and developing the expressions, it is possible to retrieve eq.(3-111).

$$\gamma_{k,w} = \frac{\gamma_{k,w,terms}\pi_{den} + k_{p21}M_1\pi_{k,w,terms}}{\gamma_{den}\pi_{den} - k_{p12}k_{p21}M_1M_2} \quad (3-111)$$

The value of these terms for each case is presented next.

$$\begin{aligned} \gamma_{den} = & k_{p12}M_2 + k_{tm11}M_1 + k_{tm12}M_2 + k_{tc11}\gamma_{0,0} + k_{tc12}\pi_{0,0} \\ & + k_{td11}\gamma_{0,0} + k_{td12}\pi_{0,0} + k_{tp11}\mu_{1,0} + k_{tp12}\mu_{0,1} \end{aligned} \quad (3-112)$$

$$\begin{aligned} \pi_{den} = & k_{p21}M_1 + k_{tm22}M_2 + k_{tm21}M_1 + k_{tc22}\pi_{0,0} + k_{tc12}\gamma_{0,0} \\ & + k_{td22}\pi_{0,0} + k_{td12}\gamma_{0,0} + k_{tp22}\mu_{0,1} + k_{tp21}\mu_{1,0} \end{aligned} \quad (3-113)$$

$$\begin{aligned} \gamma_{1,0,terms} = & k_{i1}R^\bullet M_1 + k_{tm21}M_1\pi_{0,0} + k_{p11}M_1\gamma_{0,0} + k_{tm11}M_1\gamma_{0,0} \\ & + k_{p21}M_1\pi_{0,0} + k_{tp11}\mu_{2,0}\gamma_{0,0} + k_{tp21}\mu_{2,0}\pi_{0,0} \end{aligned} \quad (3-114)$$

$$\pi_{1,0,terms} = k_{tp22}\mu_{1,1}\pi_{0,0} + k_{tp12}\mu_{1,1}\gamma_{0,0} \quad (3-115)$$

$$\gamma_{0,1,terms} = k_{tp11}\mu_{1,1}\gamma_{0,0} + k_{tp21}\mu_{1,1}\pi_{0,0} \quad (3-116)$$

$$\begin{aligned} \pi_{0,1,terms} = & k_{i2}R^\bullet M_2 + k_{p22}M_2\pi_{0,0} + k_{tm22}M_2\pi_{0,0} + k_{tm12}M_2\gamma_{0,0} \\ & + k_{p12}M_2\gamma_{0,0} + k_{tp22}\mu_{0,2}\pi_{0,0} + k_{tp12}\mu_{0,2}\gamma_{0,0} \end{aligned} \quad (3-117)$$

$$\begin{aligned} \gamma_{2,0,terms} = & k_{i1}R^\bullet M_1 + k_{tm11}M_1\gamma_{0,0} + k_{tm21}M_1\pi_{0,0} + k_{tp21}\mu_{3,0}\pi_{0,0} \\ & + k_{p21}M_1(\pi_{0,0} + 2\pi_{1,0}) + k_{tp11}\mu_{3,0}\gamma_{0,0} + k_{p11}M_1(2\gamma_{1,0} + \gamma_{0,0}) \end{aligned} \quad (3-118)$$

$$\pi_{2,0,terms} = k_{tp22}\mu_{2,1}\pi_{0,0} + k_{tp12}\mu_{2,1}\gamma_{0,0} \quad (3-119)$$

$$\gamma_{0,2,terms} = k_{tp11}\mu_{1,2}\gamma_{0,0} + k_{tp21}\mu_{1,2}\pi_{0,0} \quad (3-120)$$

$$\begin{aligned} \pi_{0,2,terms} = & k_{i2}R^\bullet M_2 + k_{tm12}M_2\gamma_{0,0} + k_{tp12}\mu_{0,3}\gamma_{0,0} + k_{tm22}M_2\pi_{0,0} \\ & + k_{p22}M_2(2\pi_{0,1} + \pi_{0,0}) + k_{tp22}\mu_{0,3}\pi_{0,0} + k_{p12}M_2(2\gamma_{0,1} + \gamma_{0,0}) \end{aligned} \quad (3-121)$$

$$\gamma_{1,1,terms} = k_{p11}M_1\gamma_{0,1} + k_{p21}M_1\pi_{0,1} + k_{tp11}\mu_{2,1}\gamma_{0,0} + k_{tp21}\mu_{2,1}\pi_{0,0} \quad (3-122)$$

$$\pi_{1,1,terms} = k_{p22}M_2\pi_{1,0} + k_{p12}M_2\gamma_{1,0} + k_{tp22}\mu_{1,2}\pi_{0,0} + k_{tp12}\mu_{1,2}\gamma_{0,0} \quad (3-123)$$

The inclusion of transfer to polymer implies the appearance of third order moments. The solution shown in the literature for the closure problem of  $\mu_{3,0}$  and  $\mu_{0,3}$  is similar to the approach presented in the homopolymerization [36].

$$\mu_{3,0} = \frac{\mu_{2,0}}{\mu_{0,0}\mu_{1,0}}(2\mu_{0,0}\mu_{2,0} - \mu_{1,0}^2) \quad (3-124)$$

$$\mu_{0,3} = \frac{\mu_{0,2}}{\mu_{0,0}\mu_{0,1}}(2\mu_{0,0}\mu_{0,2} - \mu_{0,1}^2) \quad (3-125)$$

No specific relation was found in the literature for the  $\mu_{2,1}$  and  $\mu_{1,2}$  moments. Therefore, in this research expressions based on the structure of the previous ones are proposed.

$$\mu_{2,1} = \frac{\mu_{1,1}}{\mu_{0,0}\mu_{1,0}}(2\mu_{0,0}\mu_{1,1} - \mu_{1,0}^2) \quad (3-126)$$

$$\mu_{1,2} = \frac{\mu_{1,1}}{\mu_{0,0}\mu_{0,1}}(2\mu_{0,0}\mu_{1,1} - \mu_{0,1}^2) \quad (3-127)$$

The volume variation follows the same principles of mass conservation. In addition, the volume related to the monomers was considered to be equal to the individual contribution of each. In other words, potential variations in volume due to monomers interactions were assumed to be negligible. The mathematical development is shown in eq.(3-128) to (3-133).

$$\frac{dV}{dt} = \frac{dV_{Monomers}}{dt} + \frac{dV_{Polymer}}{dt} \quad (3-128)$$

$$\frac{dV_{Monomers}}{dt} = \frac{dV_{M_1}}{dt} + \frac{dV_{M_2}}{dt} = \frac{MW_{M_1}}{\rho_{M_1}} \frac{dN_{M_1}}{dt} + \frac{MW_{M_2}}{\rho_{M_2}} \frac{dN_{M_2}}{dt} \quad (3-129)$$

$$\frac{dV_{Polymer}}{dt} = \frac{1}{\rho_P} \frac{dm_P}{dt} = \frac{1}{\rho_P} \left( - \frac{dm_{M_1}}{dt} - \frac{dm_{M_2}}{dt} \right) \quad (3-130)$$

$$\frac{dV_{Polymer}}{dt} = - \frac{1}{\rho_P} \left( MW_{M_1} \frac{dN_{M_1}}{dt} + MW_{M_2} \frac{dN_{M_2}}{dt} \right) \quad (3-131)$$

$$\frac{dV}{dt} = \left( \frac{1}{\rho_{M_1}} - \frac{1}{\rho_P} \right) MW_{M_1} \frac{dN_{M_1}}{dt} + \left( \frac{1}{\rho_{M_2}} - \frac{1}{\rho_P} \right) MW_{M_2} \frac{dN_{M_2}}{dt} \quad (3-132)$$

$$\begin{aligned} \frac{dV}{dt} = & \left( \frac{1}{\rho_{M_1}} - \frac{1}{\rho_P} \right) MW_{M_1} V \left( \frac{1}{V} \frac{d(VM_1)}{dt} \right) \\ & + \left( \frac{1}{\rho_{M_2}} - \frac{1}{\rho_P} \right) MW_{M_2} V \left( \frac{1}{V} \frac{d(VM_2)}{dt} \right) \end{aligned} \quad (3-133)$$

### 3.2.2

#### Viscous effects

As presented by Keramopoulos & Kiparissides [22], although some adaptations were needed, the basic principles used in the homopolymerization model were applied to the copolymerization, so viscous effects could be accounted for. Therefore, this subsection is devoted to these differences.

- **Free volume theory:** In the copolymerization, the free volume must include both monomers and the polymer.

$$V_f = \omega_{m1} V_{m1}^* V_{fm1} + \omega_{m2} V_{m2}^* V_{fm2} + \omega_p V_p^* V_{fp} \quad (3-134)$$

where the  $m1$  and  $m2$  indexes indicate variables related to VAc and MMA, respectively.

The individual free volume of each monomer is calculated from the thermal expansion coefficients and the glass transition temperature in the same manner. The polymer, on the other hand, also depends on its molar composition [22].

$$\alpha_p = F_{n1} \alpha_{p1} + F_{n2} \alpha_{p2} \quad (3-135)$$

where the index  $p1$  and  $p2$  refer to properties of PVAc and PMMA respectively.  $F_{n1}$  and  $F_{n2}$  are the incorporated molar fraction for VAc and MMA. This logic was applied for the thermal expansion coefficients for both above and below  $T_g$  and also for the critical hole volume necessary for the molecule to jump to another position ( $V_p^*$ ).

The approximation of the glass temperature of the copolymer was obtained through the model proposed by Suzuki & Mathot [71].

$$T_{gp} = F_{n1} T_{gp1} + F_{n2} T_{gp2} + \left( \frac{R_T}{100} \right) \left( T_{gp12} - \frac{T_{gp1} + T_{gp2}}{2} \right) \quad (3-136)$$

where  $R_T$  (run number) is the average quantity of both  $M_1$  and  $M_2$  sequences occurring in the chain per 100 monomer units and can be estimated as shown below.

$$R_T = \frac{F_{n1}F_{n2}}{1 + (1 + 4F_{n1}F_{n2}(r_1r_2 - 1))^{1/2}} \quad (3-137)$$

where  $r_1$  and  $r_2$  are the reactivity ratios, characteristic from the propagation kinetic constants.

$$r_1 = \frac{k_{p11}}{k_{p12}} \quad ; \quad r_2 = \frac{k_{p22}}{k_{p21}} \quad (3-138)$$

$T_{gp12}$  is defined as the glass temperature of the strictly alternating copolymer. It can be calculated by considering  $F_{n1} = F_{n2} = 0.5$ , replacing these values in eq.(3-136) and (3-137) and solving the system of equations for  $T_{gp12}$ .

With the free volume calculated, it is possible to calculate the variation in diffusion coefficient for each species as shown in eq.(3-139) to (3-142) [22].

$$D_I = D_{I0} \exp\left(-\gamma_I \frac{\omega_{m1}V_{m1}^*\xi_{ip}/\xi_{m1p} + \omega_{m2}V_{m2}^*\xi_{ip}/\xi_{m2p} + \omega_p V_p^* \xi_{Ip}}{V_f}\right) \quad (3-139)$$

$$D_{m1} = D_{m10} \exp\left(-\gamma_{m1} \frac{\omega_{m1}V_{m1}^* + \omega_{m2}V_{m2}^*\xi_{m1p}/\xi_{m2p} + \omega_p V_p^* \xi_{m1p}}{V_f}\right) \quad (3-140)$$

$$D_{m2} = D_{m20} \exp\left(-\gamma_{m2} \frac{\omega_{m1}V_{m1}^*\xi_{m2p}/\xi_{m1p} + \omega_{m2}V_{m2}^* + \omega_p V_p^* \xi_{m2p}}{V_f}\right) \quad (3-141)$$

$$D_p = \left(\frac{D_{p0}}{M_w^2}\right) \exp\left(-\gamma_p \frac{\omega_{m1}V_{m1}^*/\xi_{m1p} + \omega_{m2}V_{m2}^*/\xi_{m2p} + \omega_p V_p^*}{V_f}\right) \quad (3-142)$$

One can notice that differently from the model proposed by Keramopoulos & Kiparissides, 2002 [22],  $\gamma_m$  was treated as different for each monomer and were assumed to be close to the homopolymerization.

The viscosity of the mixture is necessary in the Einstein-Stokes equation used in the evaluation of  $D_{p0}$ . At the beginning of the reaction, when the

suspended phase is mostly monomer mixture,  $\eta_{mix}$  can be approximated as indicated below [85].

$$\ln(\eta_{mix}) = x_1 \ln(\eta_1) + x_2 \ln(\eta_2) + x_1 x_2 G_{12} \quad (3-143)$$

where  $x_i$  is the molar fraction of monomer  $i$  in the mixture and  $G_{12}$  is the parameter of binary interaction between monomer 1 and 2.

For the internal viscosity of the polymer, it was considered to be mostly constant and, therefore, its factors ( $A_\eta$  and  $B_\eta$ ) were estimated along the adjustment parameter for the segmental diffusion ( $\alpha_{seg}$ ).

The Kuhn's segment ( $r_e$ ) of the copolymer was calculated from the homopolymer values and the molar composition as shown in eq.(3-135).

• **Cage effect:** To account the change of viscosity on the initiation reaction, the following expression that follows the development in the homopolymerization was used.

$$\frac{1}{f} = \frac{1}{f_0} + (k_{i10}M_1 + k_{i20}M_2) \frac{r_{I2}^3}{3r_{I1}D_I} \quad (3-144)$$

The ratio of initial diffusion coefficient for the initiator ( $D_{i0}$ ) and the initiator proportionality constants were assumed to be the same as the homopolymerizations.

• **Gel effect:** As the free volume already accounts for the contribution of all present components, the gel effect was calculated in the same way of the homopolymerizations.

$$\frac{1}{k_{tii}} = \frac{1}{k_{tii0}} + \frac{1}{4\pi D_{pe} r_{ti} N_A} \quad (3-145)$$

where  $i = 1$  indicates  $P$  chains related reactions or PVAc parameters and  $i = 2$  indicates  $Q$  chains related reactions or PMMA parameters.

The effective termination radius for the termination reaction  $r_{ti}$  was calculated from the same equations, but the term related to the zeroth order moment changes according to which reaction it refers.

$$r_{ti} = \frac{\left[ \ln \left( \frac{1000\tau_i^3}{N_A \lambda_{0,0} \pi^{3/2}} \right) \right]^{1/2}}{\tau_i} \quad (3-146)$$

$$\tau_i = \left( \frac{3}{2j_{ci}\delta_i^2} \right)^{1/2} \quad (3-147)$$

$$\frac{1}{j_{ci}} = \frac{1}{j_{ci0}} + \frac{2\phi_p}{X_{ci0}} \quad (3-148)$$

$$\begin{cases} \lambda_{0,0} = \gamma_{0,0} & \text{for } i = 1 \\ \lambda_{0,0} = \pi_{0,0} & \text{for } i = 2 \end{cases} \quad (3-149)$$

The values of  $\delta_i$ ,  $j_{ci0}$  and  $X_{ci0}$  were assumed to be equal to the ones in the homopolymerizations. The same can be said about the residual termination.

$$k_{tei} = k_{tii} + k_{tii,res} \quad (3-150)$$

$$k_{tii,res} = Ak_{pii}M_i \quad (3-151)$$

$$A = \pi\delta_i^3 j_{ci} N_A \quad (3-152)$$

The following relation was applied to account for cross termination.

$$\phi_t = \frac{k_{t12}}{2(k_{t11}k_{t22})^{1/2}} \quad (3-153)$$

where  $\phi_t$  is the cross termination parameter.

• **Glass effect:**

For the same reason as in the gel effect, the propagation kinetic constants were treated individually as shown in eq.(3-154)

$$\frac{1}{k_{pii}} = \frac{1}{k_{pii0}} + \frac{1}{4\pi D_{mi}r_{mi}N_A} \quad (3-154)$$

Considering the cross propagation kinetic constants can be directly calculated from the reactivity parameters as shown in eq.(3-138), the glass effect on these terms are already being accounted for.

## 3.3

## Model parameters

An extensive literature research was performed to find kinetic and physical parameters of both systems. The values and expressions used in the simulations are separated into two groups: kinetic parameters and species properties. It is important to notice subscription *1* is related to vinyl acetate, while *2* relates to methyl methacrylate.

Table 3.1: Kinetic parameters gathered from the literature.

Parameter	Value/Expression	Unit	Ref.
$k_d$	$1.7 \times 10^{14} \exp(-30000/(R^*T))$	$s^{-1}$	[86]
$k_{p110}$	$4.2 \times 10^9 \exp(-6300/(R^*T))$	$Lmol^{-1}min^{-1}$	[39]
$k_{tc110}$	$1.6 \times 10^{12} \exp(-2800/(R^*T))$	$Lmol^{-1}min^{-1}$	[39]
$k_{td110}$	0	-	[87]
$k_{tm110}$	$k_{p110} 4.42 \times 10^{-2} \exp(-11297/(RT))$	$Lmol^{-1}min^{-1}$	[88]
$k_{tp110}$	$9.912 \times 10^5 \exp(-6300/(R^*T))$	$Lmol^{-1}min^{-1}$	[87]
$k_{p220}$	$2.95 \times 10^7 \exp(-4353/(R^*T))$	$Lmol^{-1}min^{-1}$	[21]
$k_{tc220}$	0	-	[87]
$k_{td220}$	$5.88 \times 10^9 \exp(-701/(R^*T))$	$Lmol^{-1}min^{-1}$	[21]
$k_{tm220}$	$4.3 \times 10^{12} \exp(-71800/(RT))$	$cm^3mol^{-1}s^{-1}$	[88]
$k_{tp220}$	$4.425 \times 10^3 \exp(-4353/(R^*T))$	$Lmol^{-1}min^{-1}$	[87]
$r_{12}$	0.0261	[Dl]	[89]
$r_{21}$	24.025	[Dl]	[89]
$k_{tp120}$	$3.86 \times 10^7 \exp(-6300/(R^*T))$	$Lmol^{-1}min^{-1}$	[87]
$k_{tp210}$	$k_{p110} 4.42 \times 10^{-2} \exp(-11297/(R^*T))$	$Lmol^{-1}min^{-1}$	[87]
$\phi_1$	1	[Dl]	[87]
$\phi_2$	1	[Dl]	[87]

$R = 8.314 (J mol^{-1}K^{-1})$  ;  $R^* = 1.9872 (cal mol^{-1}K^{-1})$ ; Ref. denotes reference.

- **Species properties:**

The considered species are BPO, VAc, MMA, PVAc and PMMA. The copolymer properties are calculated from the last two, as mentioned in the previous section. The physicochemical properties of each of them can be found in Tables (3.2) to (3.6).

Table 3.2: Benzoyl peroxyde properties.

Parameter	Value	Unit	Ref.
$MW_I$	242.2	$gmol^{-1}$	[90]
$V_I^*$	0.822	$cm^3g^{-1}$	[91]
$\rho_I$	1.334	$gL^{-1}$	[92]
$M_{jI}$	101.12	$gmol^{-1}$	[91]
$\gamma_I$	1	[Dl]	[91]

No relation with BPO density as function of temperature was found, so its difference was assumed to be negligible.

Table 3.3: Vinyl acetate properties.

Parameter	Value/Expression	Unit	Ref.
$\rho_{m1}$	$0.9584 - 1.3276 \times 10^{-3}(T - 293.15)$	$gmL^{-1}$	[93]
$MW_1$	86.02	$gmol^{-1}$	[94]
$V_{m1}^*$	0.840	$cm^3g^{-1}$	[87]
$M_{j1}$	$= MW_1$	$gmol^{-1}$	-
$\alpha_{m10}$	0.070	[Dl]	[27]
$\alpha_{m1}$	$5.1 \times 10^{-4}$	$K^{-1}$	[27]
$T_{gm1}$	109	$K$	[27]
$\gamma_{m1}$	0.6	[Dl]	[87]
$D_{m10}$	0.000026	$cm^2s^{-1}$	[88]

Table 3.4: Methyl methacrylate properties.

Parameter	Value/Expression	Unit	Ref.
$\rho_{m2}$	$0.968 - 1.225 \times 10^{-3}(T - 293.15)$	$gmL^{-1}$	[20]
$MW_2$	100.13	$gmol^{-1}$	[20]
$V_{m2}^*$	0.868	$cm^3g^{-1}$	[87]
$M_{j2}$	$= MW_2$	$gmol^{-1}$	-
$\alpha_{m20}$	0.011	[ <i>DI</i> ]	[27]
$\alpha_{m2}$	$2.9 \times 10^{-4}$	$K^{-1}$	[27]
$T_{gm2}$	159.15	$K$	[27]
$\gamma_{m2}$	0.3	[ <i>DI</i> ]	[87]
$D_{m20}$	$4.96 \times 10^{-10}$	$dm^2min^{-1}$	[20]

Table 3.5: Poly(vinyl acetate) properties.

Parameter	Value/Expression	Unit	Ref.
$\rho_{p1}$	$1.211 - 8.496 \times 10^{-4}(T - 273.15)$	$gmL^{-1}$	[87]
$r_{e1}$	$1.6 \times 10^{-7}$	$cm$	[87]
$V_{p1}^*$	0.748	$cm^3g^{-1}$	[87]
$\alpha_{p10}$	0.025	[ <i>DI</i> ]	[27]
$\alpha_{p1}$	$5.0 \times 10^{-4}$	$K^{-1}$	[27]
$T_{gp1}$	305.19	$K$	[27]
$X_{c10}$	100	[ <i>DI</i> ]	[28]
$\delta_1$	$6.9 \times 10^{-8}$	$cm$	[95]
$G_{12}$	0.129	[ <i>DI</i> ]	[87]

Table 3.6: Poly(methyl methacrylate) properties.

Parameter	Value/Expression	Unit	Ref.
$\rho_{p2}$	$1.212 - 8.45 \times 10^{-4}(T - 273.15)$	$gmL^{-1}$	[20]
$r_{e2}$	$1.7 \times 10^{-7}$	$cm$	[87]
$V_{p2}^*$	0.788	$cm^3g^{-1}$	[87]
$\alpha_{p20}$	0.025	[ $DL$ ]	[27]
$\alpha_{p2}$	$3.0 \times 10^{-4}$	$K^{-1}$	[27]
$T_{gp2}$	388.15	$K$	[27]
$X_{c20}$	256	[ $DL$ ]	[28]
$\delta_2$	$6.9 \times 10^{-8}$	$cm$	[95]
$G_{21}$	$G_{12}$	[ $DL$ ]	-

As mentioned before, not all constants are available in the literature and some are highly dependent on the system. Thus, the particle swarm optimization algorithm was implemented to estimate the missing data. Table (3.7) lists all estimated parameters for each polymerization simulated.

Table 3.7: List of estimated variables in each polymerization system.

PMMA	$\alpha_{seg}$	$A_\eta$	$B_\eta$	$\gamma_p$	$f_0$	$\epsilon_{i20}/D_{i0}$
PVAc	$\alpha_{seg}$	$A_\eta$	$B_\eta$	$\gamma_p$	$\epsilon_{i10}/D_{i0}$	
P(VAc-co-MMA)	$\alpha_{seg}$	$A_\eta$	$B_\eta$	$\gamma_p$	$f_0$	$\beta_{tp12}$ $\beta_{tp21}$

As it can be seen, all estimated variables are related to viscous effects.  $\beta_{tp12}$  and  $\beta_{tp21}$  are terms that multiply the cross transfer to polymer constants of same index. They were added to have the possibility of adjusting the system, since not all authors consider this cross reaction [96]. The fraction parameters estimated in the homopolymerizations were used in the copolymerization.

All other parameters were estimated because, their value were not found in the literature or they are susceptible to change according to the reaction medium or conditions.

In relation to the BPO efficiency, for example, different values have been reported. Zhang & Ray [19] indicate a range between 0.5 and 0.6 for temperatures above 100 °C. Mayo et al [97] reported values of approximately 0.9 and 0.95 at 60 °C. Silva et al [40] considered  $f$  equal to 0.8 at 70 °C. Verros & Achilias [35] has performed a solution polymerization of vinyl acetate initialized by BPO, where they estimated an initiator efficiency of extremely lower value at 60 °C. They debate the present species may have influence over this parameter.

With all the uncertainty present in the literature in relation to the initiator efficiency of BPO, it was decided that this parameter would be estimated. The value found in the modeling of PMMA was used in the PVAc implementation.  $f_0$  was also reestimated in the copolymerization modeling in order to provide means of comparison to the first estimation.

### 3.4

#### Program structure

The model was implemented in **Python** and the main packages used were **NumPy**, for matrix operations; **SciPy**, for integration tools, **Matplotlib** for graph generation and **random** for stochastic variables. As three different systems are considered, three programs following the same major structure of four scripts were written.

- **Susp\_simu.py**

Responsible for the routine that receives one value for each unknown parameter, the available experimental data and a variable that indicates if plot is desired. It possesses all functions related to viscous effects, differential equation system, the initial conditions and all other parameters needed for the simulation. It returns the error value related to the experimental data.

- **Graphs\_plot.py**

Script called by `Susp_simu.py` to generate simulation and experimental data graphs.

- **Main.py**

Calls `Susp_simu.py` a single time for an specific set of values of the unknown variables, sending the plotting variable as true and also informing the experimental data. It displays experimental error.

- **PSO\_estimation.py**

Script that estimates the unknown parameters through error minimization using particle swarm optimization method. The objective function to be minimized is set using `Susp_simu.py`. In addition, to avoid problems on speed calculations related to the different scale size of each variable, estimation was performed in terms of logarithm instead of direct values.

The method chosen as stopping criteria for the PSO was the sum of particle speeds, because low sum values indicates particles are practically static and the system is not likely to improve further. The value of all variables used in this numerical method are shown in Table (3.8).

Table 3.8: List of PSO parameters used in the estimation process.

Number of particles	$\omega$	$C_1$	$C_2$	$*it_{max}$	tolerance
30	0.9	1	1	500	0.1

$*it_{max}$  is the maximum amount of PSO iterations before the program stops.

The acceleration coefficients were defined as the same, so no priority would be taken between the individual and global best influence. The inertia weight, on the other hand, was defined as slightly lower, in order to favor convergence.

In relation to the objective function, using the residual sum of squares was not appropriate to evaluate the model performance, because the order of magnitude between the evaluated experimental parameters (conversion, average molecular weights and composition). Since no experimental variance was available, eq.(3-155) was chosen empirically to solve this problem. It is important to notice there is presence of unit in the error terms.

$$Error = \sum_i \frac{(U_i^{predicted} - U_i^{experimental})^2}{U_i^{experimental}} \quad (3-155)$$

where  $U$  is a general variable to represent a given experimental data being analyzed.

### 3.5

#### Concluding remarks

From the considered chemical equations, it was possible to write the balance equations for both homopolymerizations and copolymerization systems. The amount of differential equations generated are impracticable for numerical resolutions, so the method of moments was applied and, after a long mathematical development, it resulted in a considerable reduction of the quantity of expressions.

As the reaction rate of free radical species is significantly higher than the other components, the QSSA was applied and the final balance system for the homopolymerization processes include 6 differential equations and 3 live moments expressions. The copolymerization balance, on the other hand, included 10 differential equations and 12 live moments expressions.

With the balances established, the viscous effects were included using a diffusion-controlled model already present in the literature. Having all needed expressions, the physicochemical parameters of each species were retrieved from different reports and the missing or uncertain parameters were selected for estimation using the particle swarm optimization algorithm.

## 4

### Experimental procedure of collected data

Even though all experimental data was collected from the literature, it is important to understand how the experiments were performed. Therefore, this chapter is devoted to a brief description of the experimental procedures that resulted in the data used in the modeling. It is important to mention that, in these studies, several conditions and characterizations were performed, but only the ones viewed as relevant to this research were specified. Besides, the analyzed experiments do not present any duplicate, meaning no experimental variance can be calculated.

#### 4.1

##### Poly(vinyl acetate)

The suspension homopolymerization of vinyl acetate was performed by Azevedo in more than one condition [14, 98], following a literature proportion recipe [65]. The considered conditions for the simulation are shown in Table (4.1).

Table 4.1: Experimental conditions for PVAc synthesis.

<b>Substance</b>	<b>Value</b>	<b>Unit</b>
VAc	200.0	g
BPO	2.0	g
PVA	0.2	g
Water	420.0	g
<b>Temperature</b>	80	°C
<b>Stirring speed</b>	500	rpm
<b>Reaction duration</b>	4	h

- **Experimental procedure**

To be able to contain the planned volume, a 1 L jacketed glass reactor was used. The reactor was sealed with a metallic lid supporting the reflux condenser (set at 10 °C), the termocouple and the stirring rod, as illustrated in Figure (4.1).

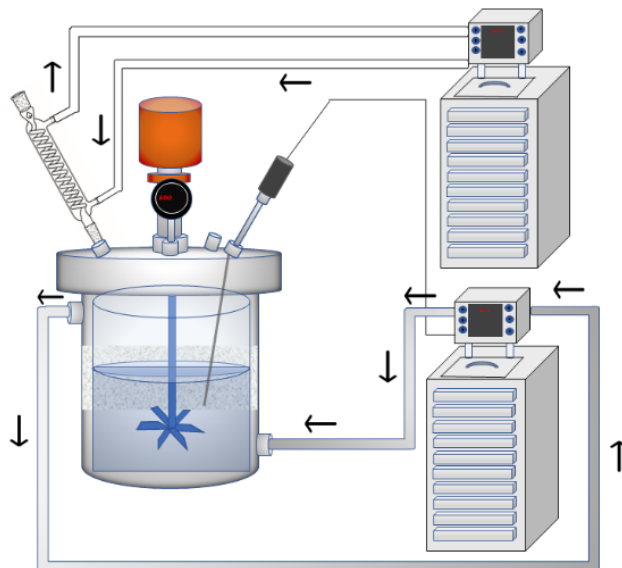


Figure 4.1: Illustration of the experimental structure used.

The reaction procedure started by preparing the suspending phase (distilled water) with dissolution of 0.05 m/m % of stabilizer agent (PVA). The solution was set to 500 rpm agitation and it was heated using a termobath of ethylene glycol (99.5 %). Upon reaching reaction temperature (80 °C), a previously prepared solution containing the monomer and initiator at desired quantities was added to the reactor. The system conditions were kept constant until 4 hours of reaction, when thermobath was set to room temperature and no more agitation was applied. The solution was then transferred to a beaker and stored in a refrigerator. After cooling, the polymer was separated from the liquid phases using suction filtration and put into a drying oven with air recirculation for 24 hours before being analyzed.

#### • Characterizations

During the course of the reaction, samples of approximately 3 mL were collected through one of the lid openings using a flask and line system. They were then neutralized with three drops of alcoholic solution of hydroquinone and dried under vacuum before being stored in a dry oven until possessing constant mass. Conversion was calculated through gravimetry, as presented in eq.(4-1).

$$X = \frac{m_i - m_p}{m_p \varphi} \quad (4-1)$$

where  $X$ ,  $m_i$ ,  $m_p$  and  $\varphi$  are the conversion, sample weight before drying, sample weight after drying and the relative amount of organic phase in the reaction.

The number- and weight-average molecular weights were only measured for the system after reaction ended by size exclusion chromatography using a 200  $\mu\text{L}$  tetrahydrofuran solution containing 1  $\text{mg.mL}^{-1}$  of polymer. The chromatograph was the Viscotek GPC Max VE 2001 (Malvern, United Kingdom), while the three chromatography columns used were Shodex (Tóquio, Japan). For detection, the system was plugged in a Viscotek VE 3580 refractometer detector and the system temperature was set to 40 °C. For calibration, polystyrene standards between  $5 \times 10^3$  and  $1 \times 10^6$   $\text{Da}$  were used.

The  $^1\text{H}$  Nuclear Magnetic Resonance ( $^1\text{H-NMR}$ ) spectroscopy was also applied to the final material in order to confirm the obtained structure. The equipment used was a Bruker AVIII-500 (Billerica, United States), at 500 MHz frequency and equipped with a 5 mm probe. The solvent containing the sample was deuterated chloroform.

## 4.2

### Poly(methyl methacrylate)

Although it was carried out in a smaller scale, the suspension homopolymerization of MMA, performed by Santos [99], followed relatively close proportions of the VAc reaction as it can be seen in Table (4.2).

Table 4.2: Experimental conditions for PMMA synthesis.

Substance	Value	Unit
MMA	75	g
BPO	0.525	g
PVA	1	$\text{g.L}^{-1}$
Water	225	g
<b>Temperature</b>	80	°C
<b>Stirring speed</b>	800	rpm
<b>Reaction duration</b>	1.5	h

#### • Experimental procedure

The homopolymerization of MMA was performed in a 0.5 L jacketed glass reactor with a glass lid possessing opening from where the termocouple, the stirring rod and the reflux system were connected to the reactor. Figure (4.1) also accurately represents the system in place.

First, the aqueous solution containing 1  $\text{g.L}^{-1}$  of stabilizer agent (PVA) was prepared and added to the reactor. Agitation was maintained and temperature was set to 80 °C. When reaction temperature was attained, a mixture of monomer and initiator previously prepared was transferred to the reactor.

At 90 min of reaction time, heating and agitation were turned off. At lower temperatures, the polymer was separated from liquid phases using vacuum filtration and was it transferred to the drying oven set at room temperature. After completely dried, the material was analyzed.

#### • Characterizations

During the reaction, solution samples of 5 g were collected through one of the openings of the lid using a pipette. The samples were put in an aluminium foil recipient containing an 1 %m/m solution of hydroquinone for neutralizing the solution. The recipient was then transferred to be cooled in the freezer for 10 minutes. Then, the material was put in the drying oven until constant weight.

The molecular weights were also measured through size exclusion chromatography only for the final material.

### 4.3

#### Poly(vinyl acetate-co-methyl methacrylate)

The suspension copolymerization of poly(vinyl acetate-co-methyl methacrylate) was performed by Azevedo in many different conditions [14]. These studies resulted in three publications focused on analysing differences in particle size distribution and on posterior alkalyne hydrolysis process [100, 101, 102].

As this research was carried out in the course of the same study of PVAc suspension polymerization, the exact same procedure was implemented, including the characterization methodology and the equipments used. The major differences are related to the conditions, as shown in Table (4.3).

Table 4.3: Experimental conditions for P(VAc-co-MMA) synthesis.

Substance	Value	Unit
VAc	140.0	g
MMA	60.0	g
BPO	2.0	g
PVA	0.2	g
Water	420	g
<b>Temperature</b>	80	°C
<b>Stirring speed</b>	500	rpm
<b>Reaction duration</b>	4	h

An important extra characterization step is the evaluation of the copolymer's composition. From the  $^1\text{H-NMR}$  spectrum it was possible not only to

identify the present structures, but also to quantify the molar fractions of incorporated monomers with considerable precision.

#### **4.4**

##### **Concluding remarks**

Experimental data of the homopolymerization of poly(vinyl acetate) and poly(methyl methacrylate), as well as the copolymerization of poly(vinyl acetate-co-methyl methacrylate), have been collected. The three experiments follow a very similar methodology and also possess reagents in comparable proportions.

All experiments presented conversion evolution over time, but the average molecular weights were assessed only for the material at the end of the reaction duration. As no duplicate data was informed, it was not possible to calculate the experimental variance for the conversion, although a precision range for the average molecular weights was given for the copolymerization.

## 5 Simulation Performances

As the title suggests, this chapter contains the results and discussion related to the simulation of the polymerizations of VAc, MMA, and P(VAc-co-MMA). The model was able to predict the experimental data with close proximity for the homopolymerizations. In the copolymerization, it also had a fairly good performance, with some details that will be further discussed.

### 5.1 Estimation process

Every estimation took a considerable amount of time to be executed, specially for the copolymerization, as presented in Table (5.1). This was expected, because a numerical integration is performed each time a particle position is updated and the total amount of balance equations to be solved in the homopolymerization is 6 with 5 or 6 estimated parameters, while in the copolymerization this quantity practically doubles (10 equations with 7 estimated parameters). Another factor that contributes to the extended execution duration of the copolymerization system, is the fact that for every execution the position of the particle and its  $F_{obj}$  were register for later statistical analysis.

Table 5.1: PSO execution time.

PVAc	PMMA	P(VAc-co-MMA)
3h 6 min	1h 34 min	7h 8 min

As the PSO execution time was considerably high for all polymerizations, the application of the Numba package was considered, since it accelerates python code execution. Unfortunately, it was not possible to implement it, due to its incompatibility with the integrator package (Scipy). Other alternatives to improve execution performance were considered such as parallel processing and cython programming. However, differently from the Numba package, the two alternatives require to rewrite a significant portion of the program, which is not a viable option for the moment.

It is possible to observe from Figures (5.1) to (5.3) how the best global error decreases rapidly at the beginning of the process to later stay almost constant. Such behavior can be interpreted as an initial general search when particles are scattered and start converging to the region with lowest errors, followed by a more "fine tuning" in this limited area before stopping. As expected, the decrease of the global best is followed by a slight increase in speed, meaning particles start moving towards the new best position. This is usually followed by a decrease of the speed. It is important to comment that the initial values for the estimated parameters are chosen randomly, which means the behavior observed may vary in each execution.

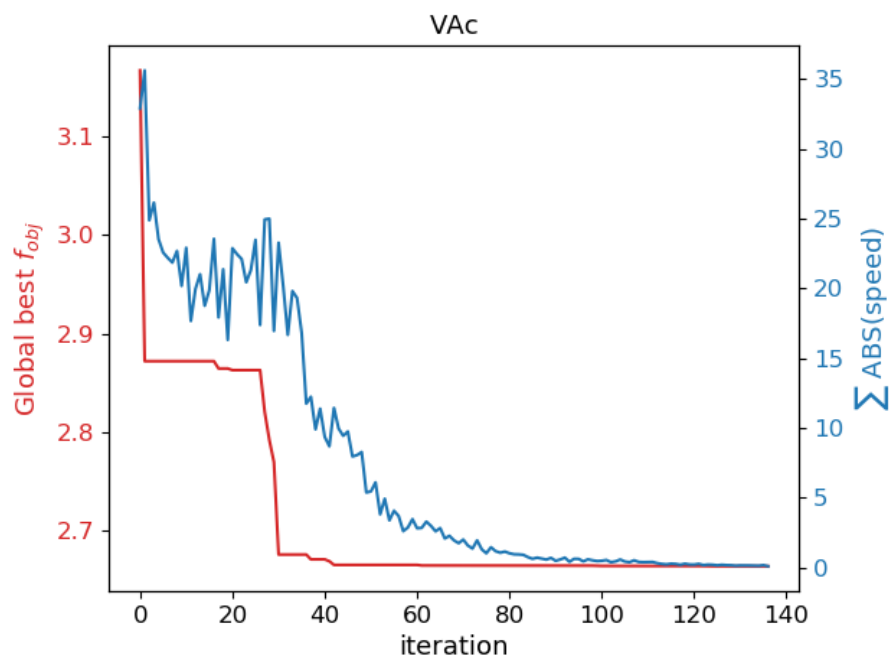


Figure 5.1: Vinyl acetate estimation progress at each iteration.

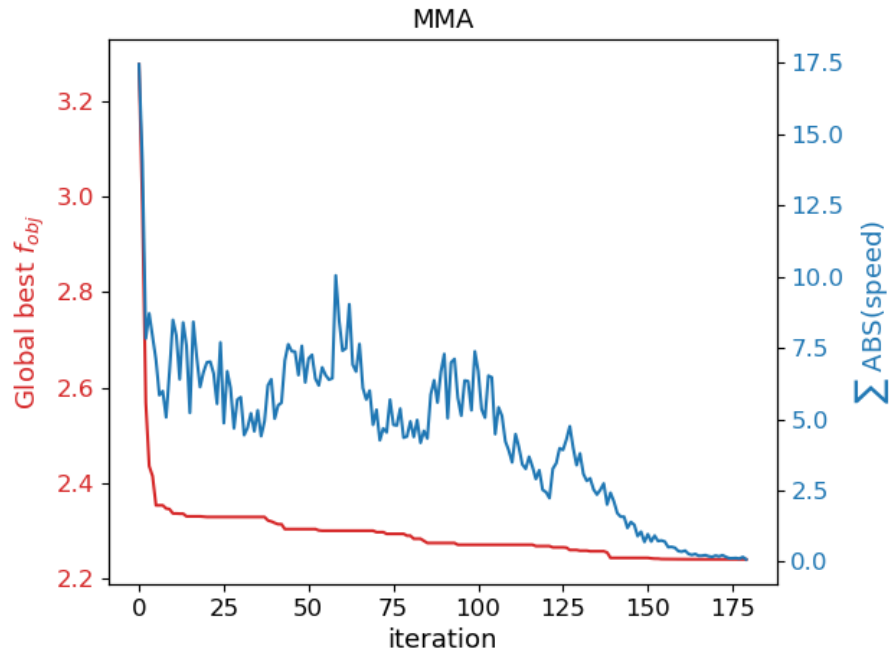


Figure 5.2: Methyl methacrylate estimation progress at each iteration.

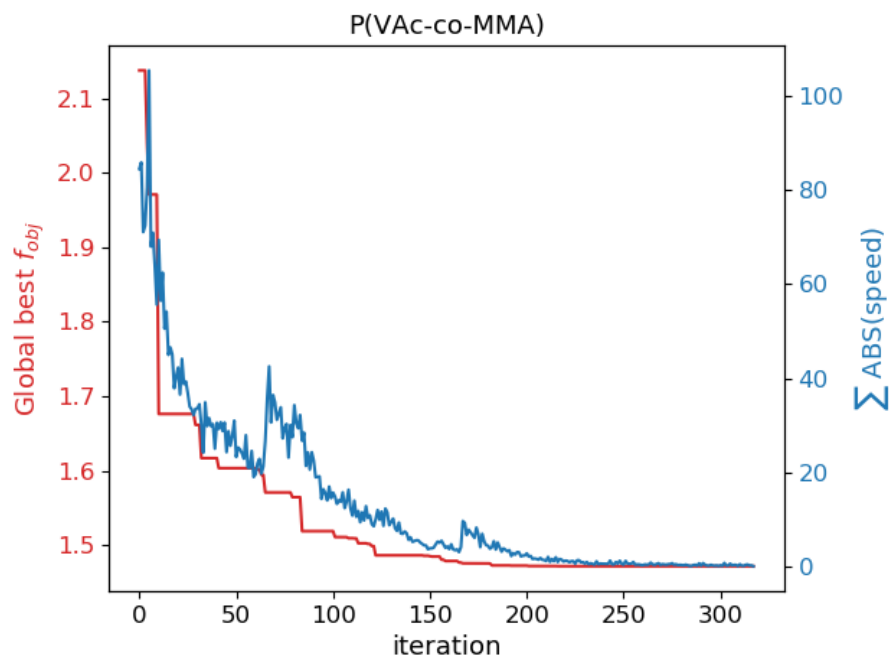


Figure 5.3: Poly(vinyl acetate-co-methyl methacrylate) estimation progress at each iteration.

Finally, the optimal parameter values found for each system are shown in Table (5.2).

Table 5.2: Results of the estimation for all three polymerizations.

Parameter	PVAc	PMMA	P(VAc-co-MMA)
$\alpha_{seg}$	3.99	$1.37 \times 10^{-1}$	$5.74 \times 10^{-2}$
$A_\eta$	$4.83 \times 10^{-4}$	$2.62 \times 10^{-4}$	$2.82 \times 10^{-4}$
$B_\eta$	$5.58 \times 10^{-1}$	$5.33 \times 10^{-1}$	$6.80 \times 10^{-1}$
$\gamma_p$	$2.11 \times 10^{-1}$	$7.30 \times 10^{-1}$	$4.34 \times 10^{-2}$
$\epsilon_{i10}/D_{i0}$	$9.99 \times 10^2$	$9.91 \times 10^{-1}$	-
$f_0$	-	$3.12 \times 10^{-1}$	$3.26 \times 10^{-1}$
$\beta_{tp12}$	-	-	$3.55 \times 10^{-3}$
$\beta_{tp21}$	-	-	$6.17 \times 10^1$

In the three estimations,  $\alpha_{seg}$  and  $\gamma_p$  change considerably, indicating the relation between the homopolymerization and copolymerization parameters is more complex than pondering according to medium composition when it comes to the gel effect. The fraction related to the glass effect also changes, as it is highly dependent on the initiator and the reaction medium. The parameter  $B_\eta$  presented a slightly higher value for the copolymer and the terms related to it have a considerable impact on the system, which was not expected, since the copolymer intrinsic viscosity was thought to present a behavior between the ones of the homopolymers. The estimation of the initial efficiency of the initiator resulted in very similar values in both homopolymerization of PMMA and copolymerization of P(VAc-co-MMA), which presents which is a positive indication on the estimation of this parameter.

## 5.2

### Polymerization prediction

Differently from 5.1, in this section, the polymerizations are treated separately, because each system has its peculiarities.

#### 5.2.1

##### Poly(vinyl acetate)

The model presented great capability for predicting the conversion, as it can be seen in Figure (5.4). Besides, the slight fluctuation observed in the experimental data is probably related to imprecision normally expected for this type of heterogeneous system, where sampling can be extremely difficult to be representative. Unfortunately, as no duplicate was performed to allow reevaluation of experimental variance.

The experimental data indicates a rapid increase in conversion and the model is capable of repeating this behavior. The gel effect seems to be strongly present from the beginning of the polymerization, which was not expected, as conversion is considerably low. This can be confirmed by observing the behavior of  $k_{t11}$  plot shown in Figure (5.5). This parameter decreases fast at the beginning, followed by a stabilization related to the translation diffusion and reaction diffusion shown previously in Figure (2.16). The reaction diffusion decrease represents stage of diffusion-controlled propagation. This behavior was expected to be a smoother, but it was considered coherent with the conversion plot, as it presented all expected stages and also good prediction capabilities. Additionally, this behavior could be related to a model inaccuracy, due to some parameters that presented different values in the literature.

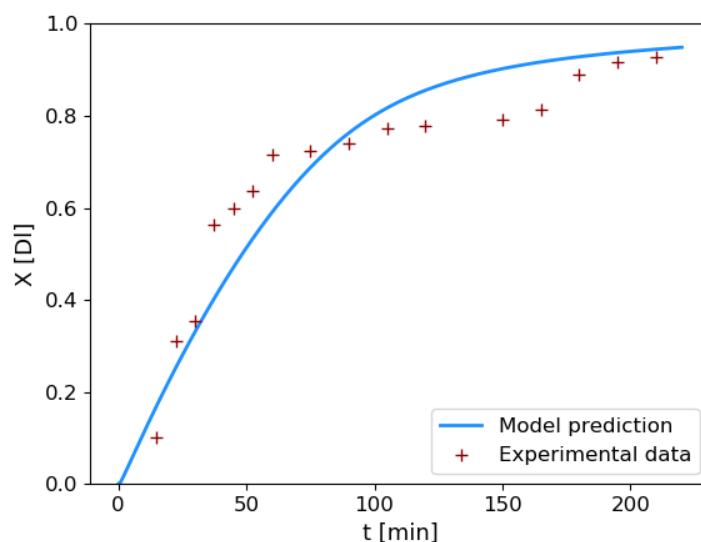


Figure 5.4: Conversion over time for the experimental data and model prediction of vinyl acetate homopolymerization.

From the conversion chart, it is also possible to observe the glass and cage effects, represented by the stabilization at higher conversions. As shown in Figure (5.6), these effects present the expected behavior, because the cage effect reduces the initiator efficiency before  $k_{p11}$  decrease due to glass effect.

The model also approximated fairly well the number- and weight-average molecular weights, as shown in Figure (5.7). In both cases, the predicted value stayed below the experimental data, but it was considered to be well representative, considering no imprecision range was given for further evaluation.

Figure (5.8) shows the evolution of  $M_n$  and  $M_w$  as reaction advances. All throughout the simulation,  $M_n$  stays smaller than  $M_w$ , which is expected.

A fast increase can be observed at the beginning of the process for both cases. However, for  $M_n$  variation stabilizes while  $M_w$  continue increasing, but in a considerably lower rate. This probably happens because of the gel effect, where chains do not terminate as fast as monomer is incorporated, increasing the amount of high molecular weight chains.

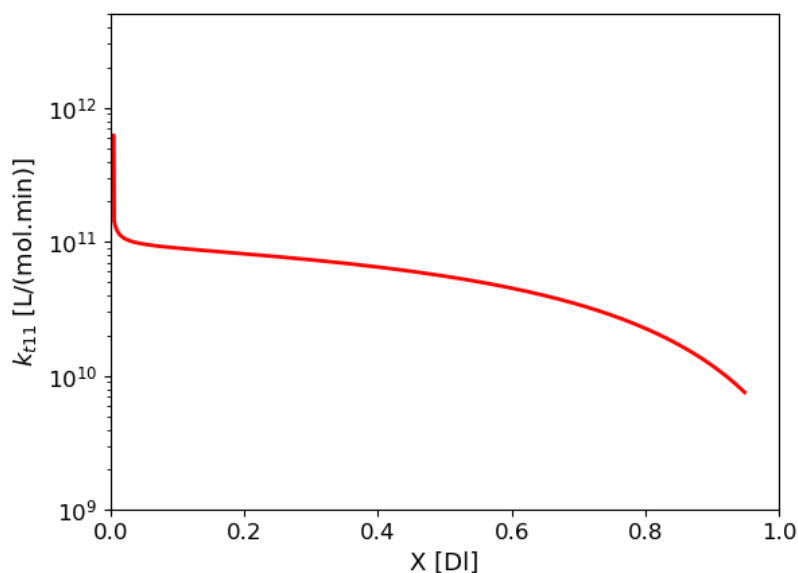


Figure 5.5: Gel effect present in the simulation of PVAc.

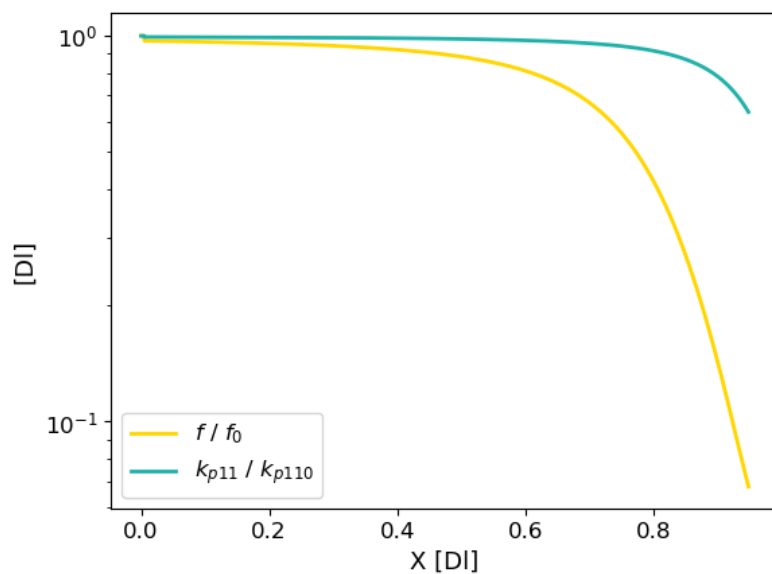


Figure 5.6: Cage and glass effects present in the simulation of PVAc.

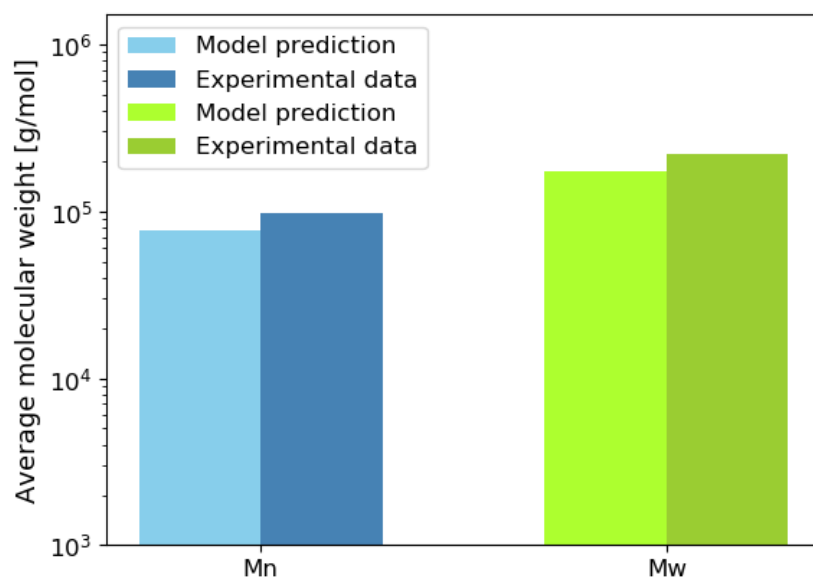


Figure 5.7: Final average molecular weights for the experimental data and model prediction in the homopolymerization of vinyl acetate.

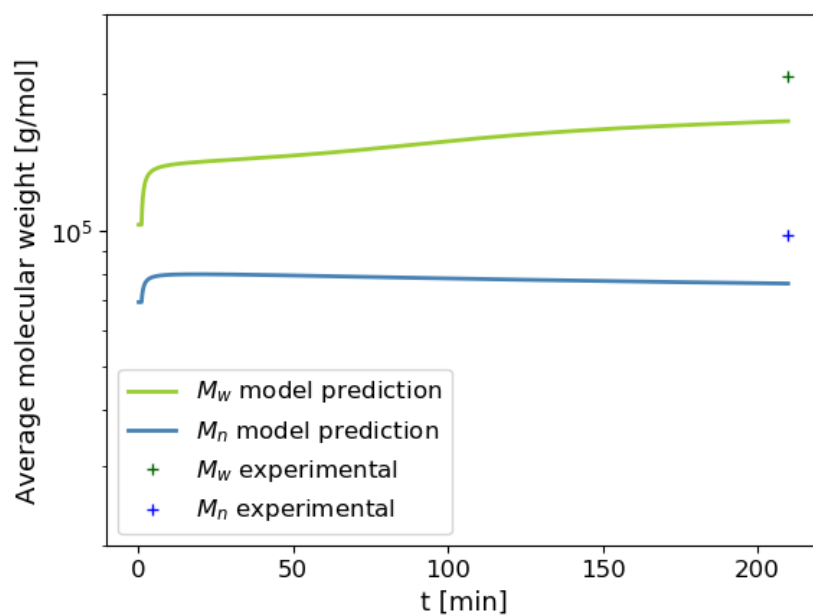


Figure 5.8: Average molecular weights evolution in the simulation of PVAc.

### 5.2.2 Poly(methyl methacrylate)

As observed in the experimental data, the synthesis of poly(methyl methacrylate) is susceptible to the viscous effects in a different pace than the PVAc process. Figure (5.9) shows the experimental data seems to have less fluctuations than the other homopolymerization, probably due to the difference in sampling methodology or simply in the kinetic behavior of each system. Consequently, the model was able to have better performance in the prediction of conversion.

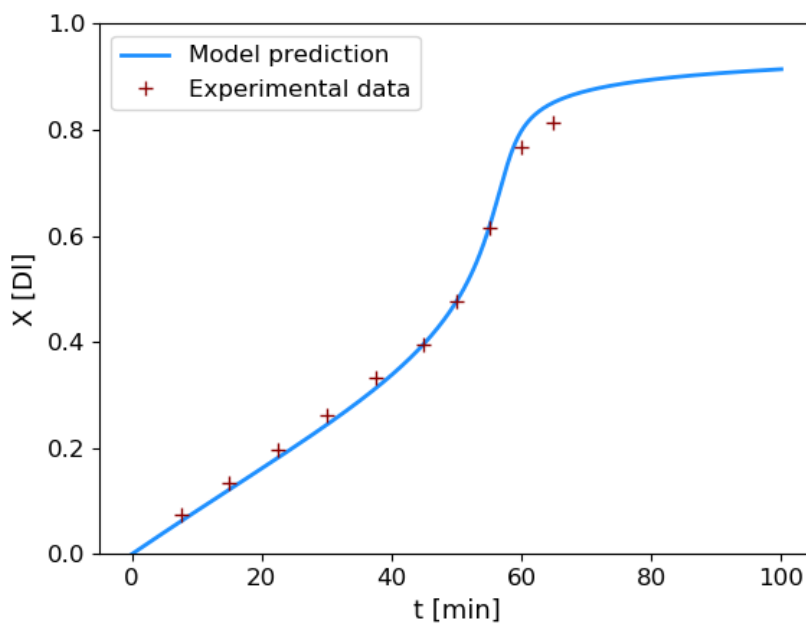


Figure 5.9: Conversion over time for the experimental data and model prediction of methyl methacrylate homopolymerization.

The gel effect happens at intermediate conversion where  $k_{t22}$  decreases significantly, as indicated in Figure (5.10), reflecting in the autoacceleration effect observed around 50 minutes. The following stabilization of the reaction happens due to the cage and glass effects that can be confirmed to be accounted by observation of Figure (5.11).

One may notice that a very small change can be observed in the behavior of  $k_{t22}$  after 0.75 conversion. It is the transition to the stage where chain motion is controlled by propagation, meaning  $k_{t,res}$  becomes important, following eq.(2-45) and (2-46).

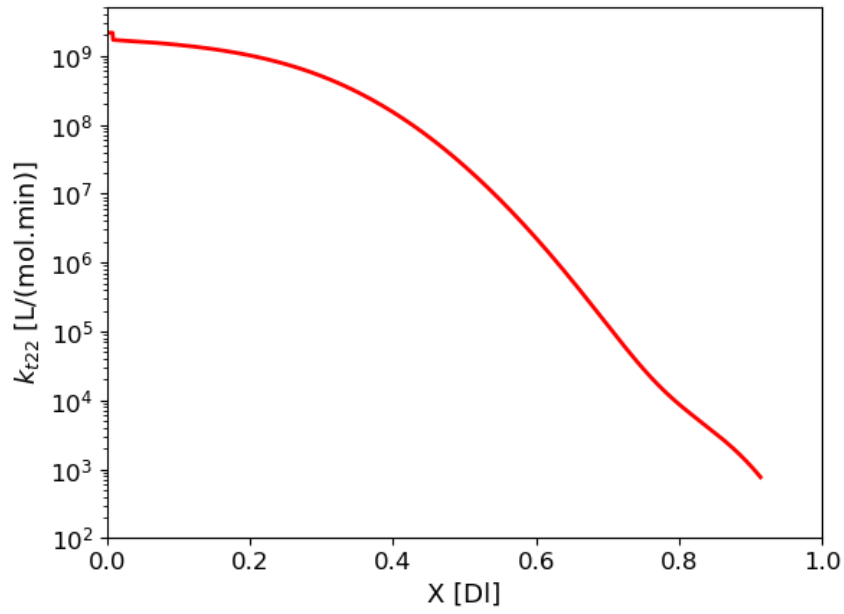


Figure 5.10: Gel effect in methyl methacrylate modeling.

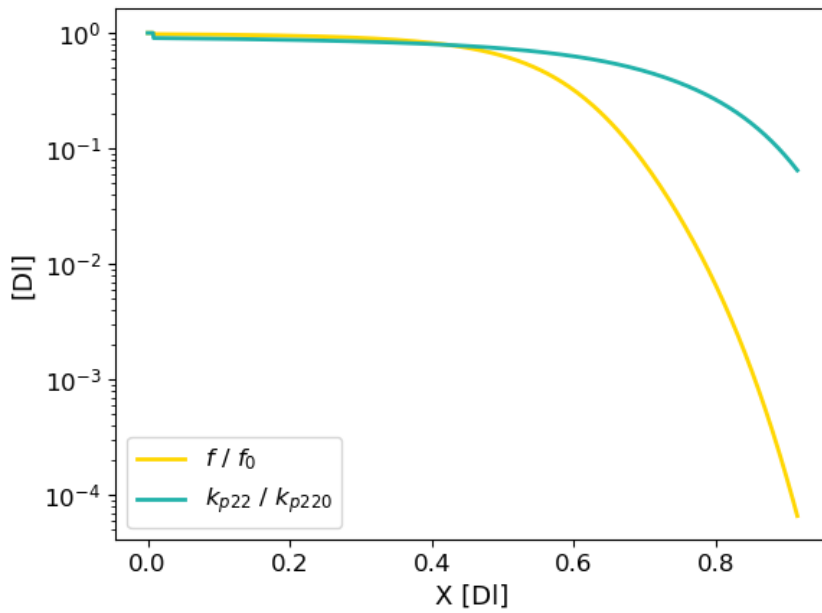


Figure 5.11: Cage and glass effects in methyl methacrylate modeling.

The behavior of the average molecular weights as well as the comparison to the experimental data at the end of the reaction are shown in Figures (5.12) and (5.13).

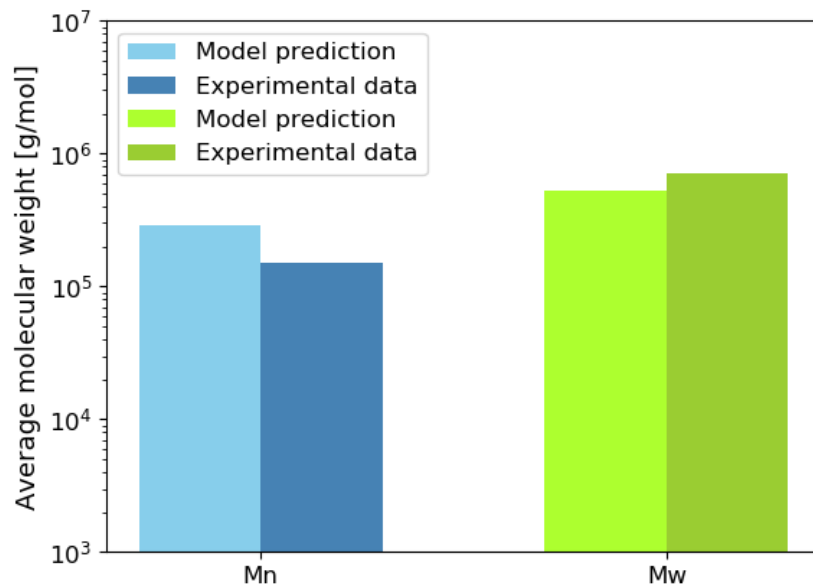


Figure 5.12: Final average molecular weights for the experimental data and model prediction in the homopolymerization of methyl methacrylate.

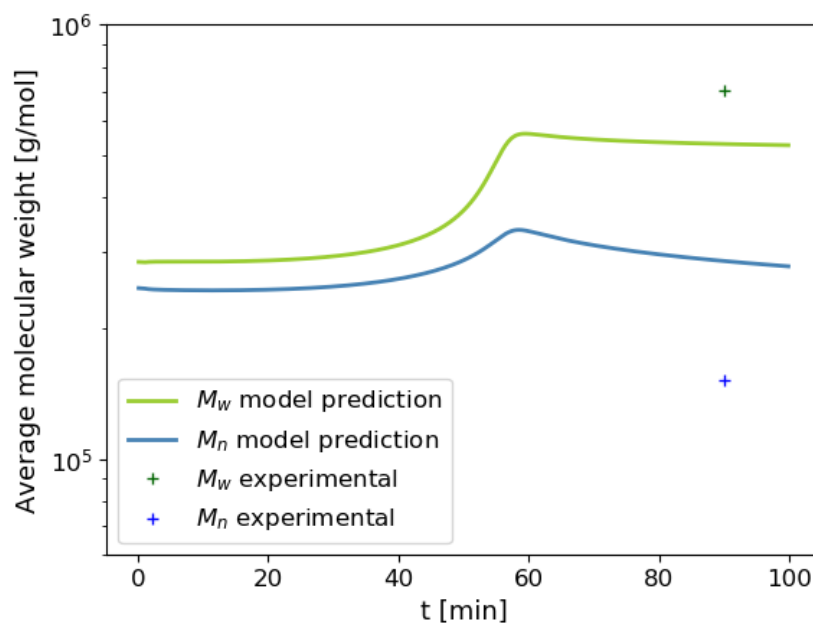


Figure 5.13: Average molecular weights evolution in the simulation of PMMA.

Although the average molecular weight predictions seems to be not so good than the ones in VAc simulation, the experimental data may not have high accuracy. Santos [99] explained in his thesis that during the measurement of the molecular weights, other analyzed products caused the clogging of the filter in the equipment, changing the previously constant pressure of the system. Consequently, the resulting values are not as precise as desired. Despite this inaccuracy, one can see the general order of magnitude of the model remained close to the experimental data, therefore it was considered to be successful. From Figure (5.12), it is possible to notice a sudden increase in both weight- and number-average molecular weights around fifty minutes, when the gel effect is considerable, as it can be seen in Figures (5.9) and (5.10). This increase stops around sixty minutes, when the glass effect starts happening, as shown in Figure (5.11), meaning the average molecular weights behavior are coherent with the viscous effects.

### 5.2.3

#### **Poly(vinyl acetate-co-methyl methacrylate)**

Before presenting and discussing the simulation final results for the copolymerization system, it is important to explain a specific part of the development that lead to the analysis of the experimental data for the conversion.

At initial testing simulations of the copolymerization model, the PSO did not seem to be able to adjust conversion and composition at the same time. This performance was odd, since these parameters are considerably related and the reaction followed the faster consumption of MMA in relation to VAc as it was expected from the literature [14]. Considering the copolymer composition measurement was performed by  $^1\text{H-NMR}$ , an extremely precise technique, and the initial monomer masses were also measured with precision, the limitation in the PSO could be related to conversion data imprecision being more important than expected.

As already mentioned, Azevedo [14] reported the sampling method adopted consisted on recovering the material using a flask line system. Unfortunately, it means there is no guarantee the samples were retrieved from the same spot in the reactor, which increases possible experimental inaccuracy. Besides, the suspension polymerization is a heterogeneous technique and, consequently, as reaction advances, these differences in location become more important.

To confirm the suspected inaccuracy and quantitatively approximate the measurement precision range, the following mathematical development was

conducted.

MMA molar fraction and the total mass consumed in the reaction can be calculated as shown in eq.(5-1) and (5-2).

$$F_{n2} = \frac{n_{2,cons}}{n_{1,cons} + n_{2,cons}} \quad (5-1)$$

$$m_{cons} = n_{1,cons}MW_1 + n_{2,cons}MW_2 \quad (5-2)$$

where  $n$  is quantity in moles,  $1$  denotes VAc,  $2$  expresses MMA and  $cons$  indicates quantity consumed in the reaction.

By isolating  $n_{1,cons}$  in the first expression, replacing it in the second and rearranging terms, it is possible to obtain eq.(5-3).

$$n_{2,cons} = \frac{m_{cons}}{MW_2 + \frac{1-F_{n2}}{F_{n2}}MW_1} \quad (5-3)$$

The polymer composition was evaluated only for the material at the end of the reaction, so the following data is referring to this experimental moment.

Considering the measured global conversion was of 53.7 % and the total initial mass was 200.0 g,  $m_{cons}$  can be approximated to 107.4 g. From the  $^1\text{H-NMR}$ , MMA molar fraction was measured to be around 61.40 %, meaning the consumed molar quantity of MMA can be calculated from eq.(5-3) resulting in 0.697 mol which is equivalent to approximately 69.75 g of total MMA consumed.

As shown in Table (4.3), the initial mass of MMA used in the process was 60.0 g, meaning there is an extra 9.75 g accounted that can be translated as an approximated inaccuracy of at least 16.25 % in relation to the initial mass. This could explain the PSO difficulty on adjusting composition and conversion at the same time. Besides, it is not possible to generate the experimental variance matrix, meaning a quantitative confidence region for the estimated parameters could not be reached.

Although the presented experimental error indicates the system is not exactly in accordance to the well-done experiment hypothesis, the statistical evaluation using the Fisher parameter, as shown in eq.(2-51), was implemented to illustrate the estimation behavior and give a qualitative analysis of the model's confidence region. The charts of multiple values of model parameter combinations can be found in Appendix C, while Table (5.3) shows the

confidence limits for each estimated parameter if the well-done experiment assumption could be adopted. Keeping all this in mind, it is now possible to analyze the copolymerization results. The confidence region plots present in Appendix C indicate the parametric regions observed are not much populated, implying the confidence region is probably bigger than the one observed. This behavior could be explained by the low amount of particles in the PSO algorithm and by the tuning parameters chosen, that lead to a faster convergence, since a slower convergence would mean a more complete analysis of the region. Unfortunately, for hardware limitations and execution time, the system was not reevaluated with different parameters.

Table 5.3: Confidence region of the estimated parameters in the copolymerization considering the well-done experiment hypothesis.

Parameter	Minimum	Optimum	Maximum
$\alpha_{seg}$	$2.72 \times 10^{-2}$	$5.74 \times 10^{-2}$	$9.56 \times 10^{-2}$
$A_{\eta}$	$1.57 \times 10^{-4}$	$2.82 \times 10^{-4}$	$3.49 \times 10^{-4}$
$B_{\eta}$	$6.65 \times 10^{-1}$	$6.80 \times 10^{-1}$	$7.36 \times 10^{-1}$
$\gamma_p$	$1.01 \times 10^{-2}$	$4.34 \times 10^{-2}$	$1.0 \times 10^0$
$f_0$	$3.25 \times 10^{-1}$	$3.26 \times 10^{-1}$	$3.78 \times 10^{-1}$
$\beta_{tp12}$	$1.09 \times 10^{-3}$	$3.55 \times 10^{-3}$	$1.35 \times 10^{-2}$
$\beta_{tp21}$	$4.11 \times 10^1$	$6.17 \times 10^1$	$8.50 \times 10^1$

Figure (5.14) expresses the model prediction and experimental data for the conversion of poly(vinyl acetate-co-methyl methacrylate). Notice the error bar is the approximated experimental imprecision calculated above.

As it can be seen, the model prediction is significantly close to the experimental data. As reaction advances, the latter indicates a sigmoid behavior where cage and glass effects would supposedly happen at extremely low conversion values. The model, on the other hand, indicates the gel effect would only have just started happening around the time the reaction was stopped. This indicates the extent of the conversion imprecision could include the three last points, but not the others. This could be considered coherent, because of the heterogeneous characteristics of the process. Additionally, it is important

to observe that the behavior of the systems is, again, much more complex than the a simple pondering of the homopolymerization systems.

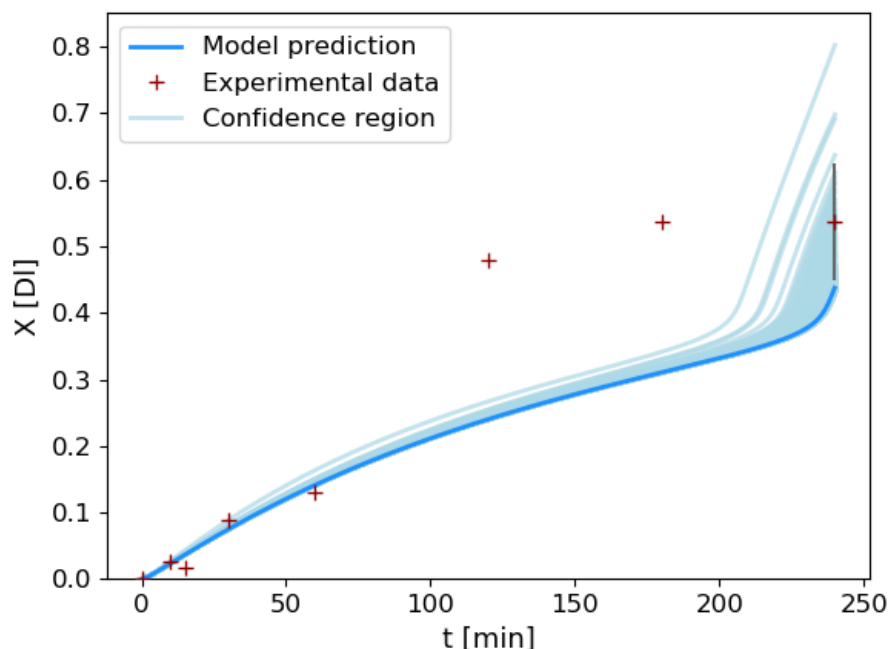


Figure 5.14: Conversion over time for the experimental data and model prediction of poly(vinyl acetate-co-methyl methacrylate copolymerization).

The optimal estimation is extremely close to the lower end of the approximated error bar. This makes sense, since that lower region allows composition to be close to the  $^1\text{H-NMR}$  analysis.

The behavior of the model confidence region could be explained by two reasons. Firstly, the estimated parameters are mostly related to the viscous effects which happen at higher conversion values, meaning they would not affect the initial stages of the polymerization without significantly affect the composition and molecular weights that are accounted in the estimation.

Secondly, the lack of precise data after the fifth point could be generating the observed enlargement of the confidence region, since the viscous effects themselves are more sensitive at these conversion levels. Notice the qualitative confidence region is almost all aligned with the approximated experimental inaccuracy.

An important aspect that influence the accuracy of the model and deserves to be recognized is the variability of parameters present in the literature, such as the kinetic constants, specially when it comes to the copolymerization. As the amount of experimental data is was already limited,

it was not possible to estimate these parameters, so the most prevalent ones were selected.

To verify the hypothesis about the model indicating the gel effect has barely started around 240 minutes, the conversion, the kinetic constants and the initiator efficiency were evaluated for higher reaction time (325 minutes) and the extrapolated region was indicated by a vertical line, resulting in Figures (5.15) to (5.18).

It is possible to notice indeed the presence of the gel effect followed by the glass effect in the extrapolated region in Figure (5.15). One can notice the sudden increase starts stabilizing for higher conversion values, indicating the presence of the glass effect. Additionally, the conversion rate is lower than both homopolymerizations for both model and experimental data, which reinforces the non-linearity between the polymerization behavior and the composition variation.

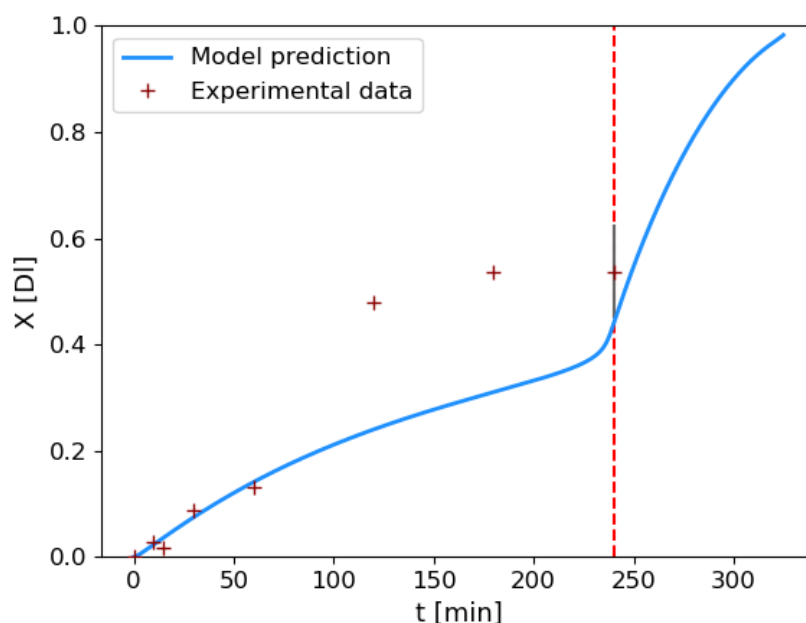


Figure 5.15: Conversion over time for the copolymerization. The vertical red line indicates the start of the extrapolated region.

Figure (5.16) shows the decrease of each termination constant. The parameter  $k_{t11}$  suffers a considerable decrease from the beginning of the reaction, which is coherent with the expected consumption of MMA, because of its higher reactivity. The reduction related to the PVA termination kinetic constants, on the other hand, happen sooner than expected. It is possible to observe a more significant decrease of the termination kinetic constants in the

extrapolated region which is reflected in the sudden increase observed in the conversion.

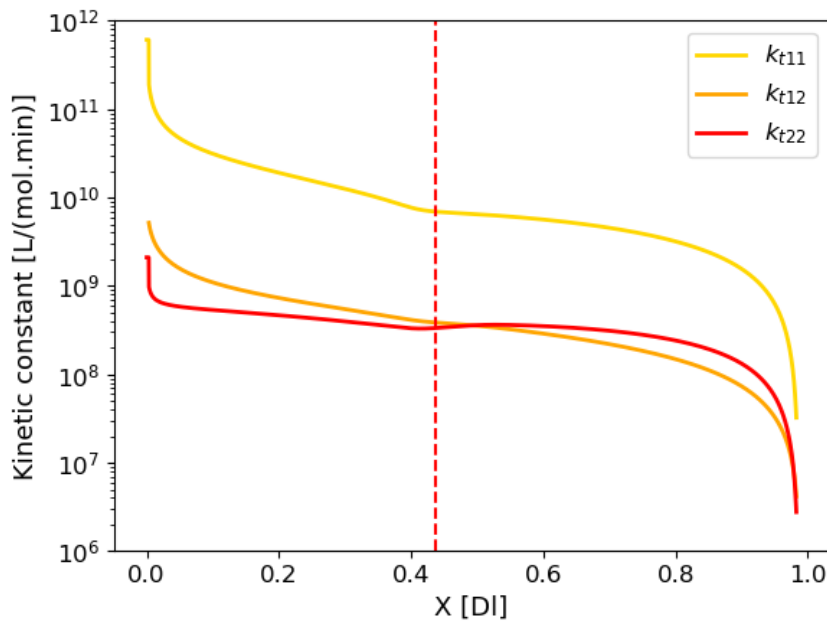


Figure 5.16: Gel effect in P(VAc-co-MMA) modeling. The vertical red line indicates the start of the extrapolated region.

Figure (5.17) indicates the presence of glass effect only for extremely high conversions and for the  $k_{p21}$  and  $k_{p22}$  parameters. This behavior is comprehensible, since there is no experimental data in this region to better adjust the glass effect. Even though the decrease in the propagation constants is relatively low, it reflects in the stabilization observe in the conversion chart.

The initiator efficiency stays constant until around 80 % conversion where it starts decreasing rapidly due to cage effect, as it can be observed in Figure (5.18). This effect also contributes to the stabilization observed at higher conversion values.

In relation to all viscous effects, it was possible to observe how challenging modeling these effects can be, specially when it comes to copolymerization systems.

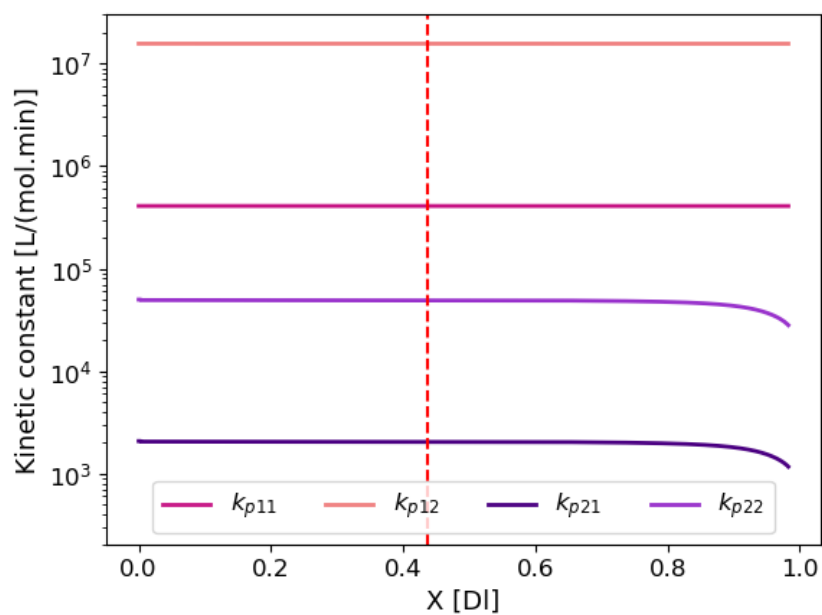


Figure 5.17: Cage effect in P(VAc-co-MMA) modeling. The vertical red line indicates the start of the extrapolated region.

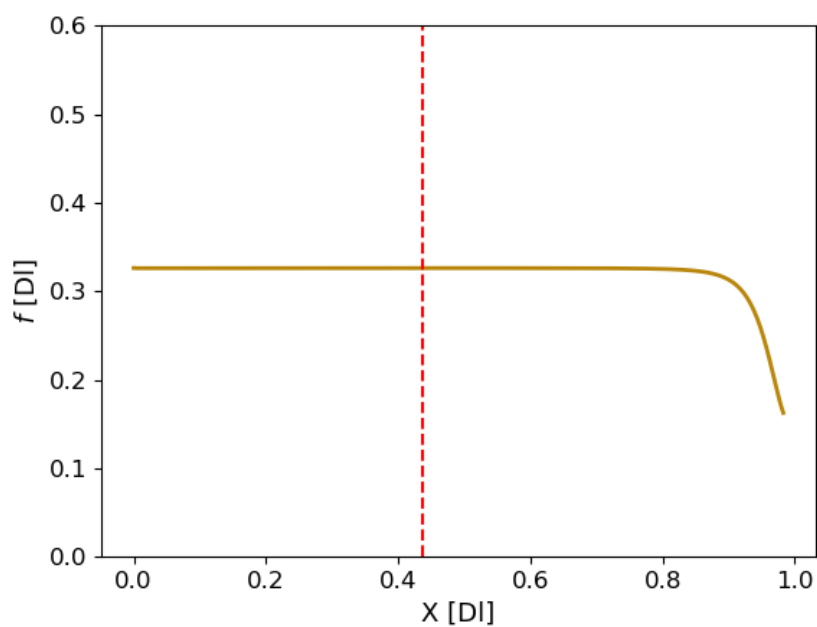


Figure 5.18: Glass effect in P(VAc-co-MMA) modeling. The vertical red line indicates the start of the extrapolated region.

As indicated in Figure (5.19), the composition prediction is extremely close to the experimental measurement.

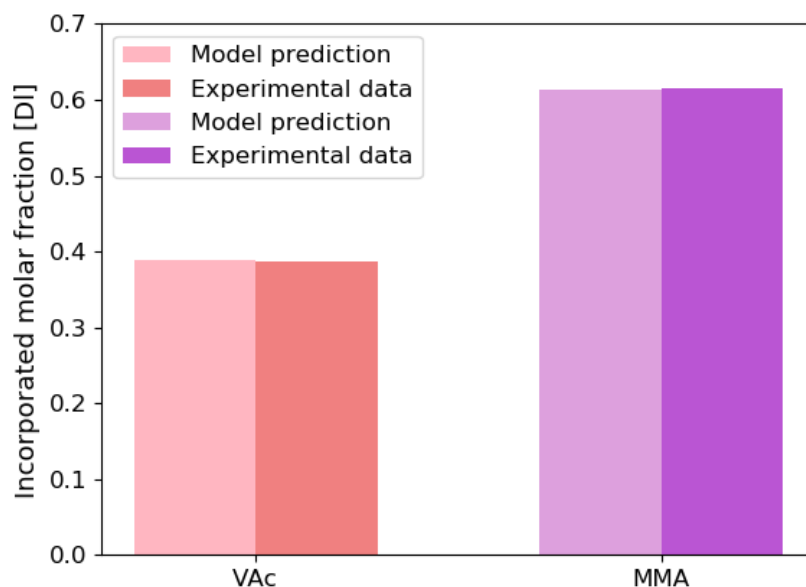


Figure 5.19: Model prediction and experimental data on the copolymer composition.

Figure (5.20) and (5.21) show the model prediction of the average molecular weights specifically at 240 minutes and through out the simulation, respectively.

The simulation returned average molecular weights withing the given precision range, which indicates the model presents good prediction capability for  $M_n$  and  $M_w$ , as presented in Figure (5.20). Additionally, the confidence region stayed close to the optimal model response throughout the simulation, as indicated in Figure (5.21). It is possible to observe that both weight- and number-average molecular weights presented a close value to the homopolymerization of PVAc, although their behavior throughout the reaction has characteristics of both homopolymerizations.

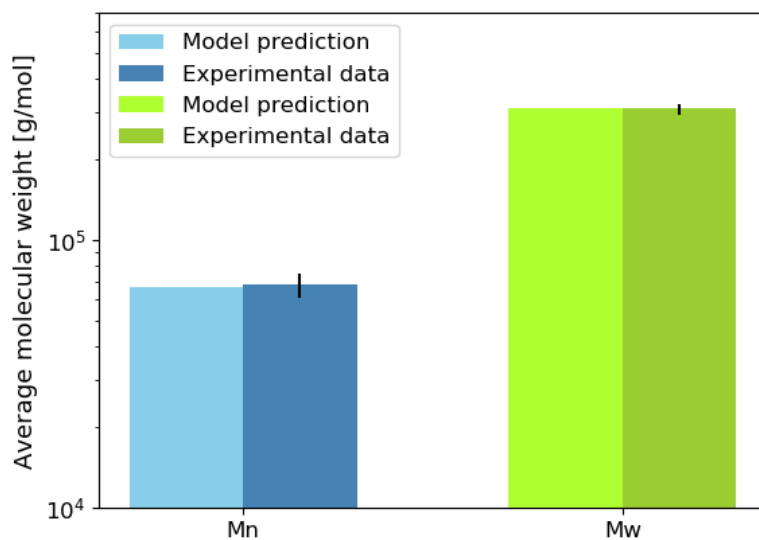


Figure 5.20: Final average molecular weights of experimental data and model prediction in the copolymerization of P(VAc-co-MMA).

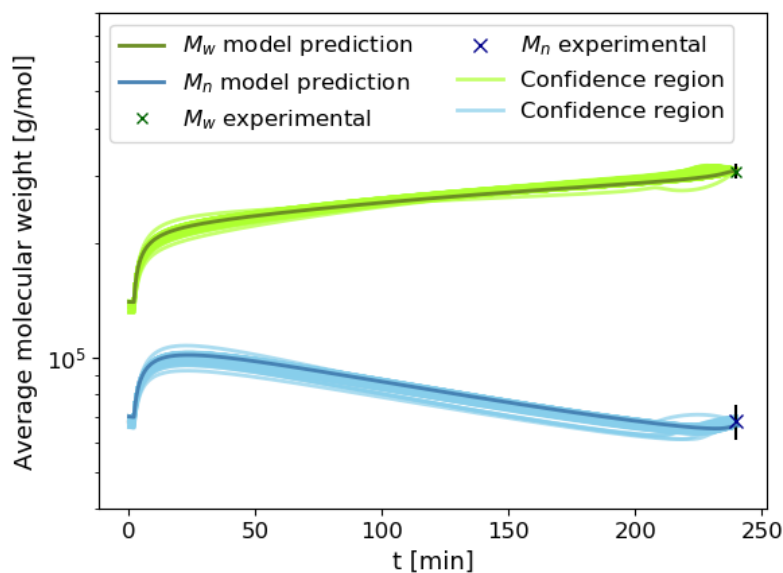


Figure 5.21: Average molecular weights in the simulation of P(VAc-co-MMA).

An initial fast increase of the average molecular weights can be observed, which is related mostly to the consumption of MMA, as indicated in Figure (5.22). This could also explain the decrease in  $M_w$ , since more new polymer chains are formed due to the start of VAc consumption. As MMA is almost

depleted, VAc consumption rate suddenly increases, once again indicating the beginning of the gel effect.

Other charts like volume and initiator variation for both homo- and copolymerizations can be found in Appendix D.

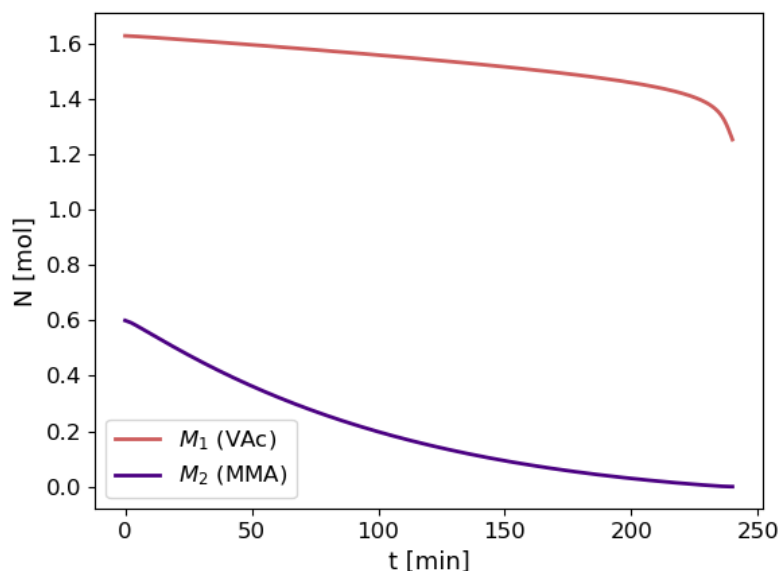


Figure 5.22: Monomers consumption throught the reaction.

### 5.3

#### Concluding remarks

The estimation of the missing parameters was conducted using PSO algorithm. The process took a considerable amount of time, specially for the copolymerization system, since it has more complexities and, therefore, a longer execution time.

It was possible to predict the experimental data for the homopolymerization of vinyl acetate and methyl methacrylate, as well as for the copolymerization of the poly(vinyl acetate-co-methyl methacrylate) with certain precision. In the latter, a range of inaccuracy was approximated for the conversion data using the provided experimental measurements. This approximation assisted on explaining some apparent deviations of the model, meaning more investigation of the system behavior is needed. Nevertheless, it was considered a successful implementation, specially considering how challenging the modeling of copolymerization viscous effects is. Additionally, it was possible to observe the change in composition related to the copolymerization system seems to be much more complex than a linear relation to the homopolymerizations.

For further confirmation of the model's prediction capacity, it would be interesting to perform the copolymerization experiment in a more controlled condition in relation to the sampling precision. Besides, as the model indicates the system was at the beginning of the gel effect when reaction was stopped, meaning higher conversions could probably be achieved by increasing the reaction duration, as indicated in the extrapolation performed.

## 6 Conclusions

A diffusion-controlled free radical suspension copolymerization model has been developed for the synthesis of poly(vinyl acetate-co-methyl methacrylate). The model has been written using the method of moments for the balance equations and the quasi-steady state approach was considered for the free radical species. The gel, cage and glass effects were accounted using diffusion principles of each component according to mathematical frameworks present in the literature. This development was carried out not only for the copolymerization, but also for the homopolymerization of vinyl acetate and methyl methacrylate.

An extensive report research was conducted in order to find the physico-chemical parameters necessary in the modeling. Additionally, the experimental data was also recovered from the literature. Since there was a lack of information regarding the values of some parameters, the particle swarm optimization algorithm was performed to compensate for the absent attributes. It also allowed to retrieve a qualitative region of confidence, considering the quantitative one was not possible, due to lack of experimental variance data.

In relation to the homopolymerization processes, the model has proven to be accurate on the prediction of polymer conversion and on the behavior of the viscous effects, as indicated by the variation of the efficiency, termination and propagation parameters in accordance to the literature. The prediction of the order of magnitude of the number- and weight-average molecular weights were also possible.

Modeling the copolymerization process was a greater challenge, as the mathematical development demands more effort, execution duration is substantially longer and an extra analysis of the experimental data was essential. The model has shown high precision when it comes to average molecular weights, polymer composition and the initial values of conversion. There is a significant amount of evidence indicating the experimental imprecision is not negligible due to the sampling method required, specially for higher conversion values. Nevertheless, the simulation remained in close proximity of the approximated experimental imprecision range.

The model indicates the process could be able to continue, since the gel

effect had barely started when the reaction was stopped. Consequently, polymer production could escalate quickly just by increasing the reaction duration apparently not by much. This is most definitely not guaranteed, but it is an important direction to be investigated for contributing to the improvement of more efficient synthesis of poly(vinyl acetate-co-methyl methacrylate).

All things considered, the main objective of this research was achieved, meaning it was possible to properly predict the suspension copolymerization of vinyl acetate with methyl methacrylate, while also indicating conditions for further experimental investigation. The resulting model is the first step to allow the modeling of particle size distribution of the P(VAc-co-MMA) system, which must be in a specific range for application in vascular embolization procedure.

## 7

### Future perspectives and suggestions

There is still much to be explored in relation to the production of P(VAc-co-MMA) and the following are some suggestions related to this topic.

- Performing experiments for longer reaction times is interesting, but it is probably not enough. Developing a more precise method of measuring reaction conversion is of extreme important. Besides, performing duplicates as well as including average molecular weights and composition measurements throughout the reaction, not only at the end, would allow better statistical evaluation and model validation.
- Measuring the estimated parameters through experiments would reduce uncertainties related to the modeling, as well as provide valuable data to the literature.
- Modeling the posterior hydrolysis process and the particle size distribution, including their relation resulting characteristics of the microspheres would contribute considerably to a more widespread application of this polymeric as an embolic agent.
- Investigating execution time optimization using the implementation of cython and parallel processing.

## Bibliography

- [1] CALLISTER, W.; RETHWISCH, D.. **Materials Science and Engineering: An Introduction, 9th Edition: Ninth Edition**. John Wiley and Sons, Incorporated, ninth edition edition, 2013.
- [2] LOUNIS, M.; LECONTE, S.; ROUSSELLE, C.; BELZUNCES, L. P.; DESAUZIERS, V.; LOPEZ-CUESTA, J.-M.; JULIEN, J. M.; GUENOT, D. ; BOURGEOIS, D.. **Fireproofing of domestic upholstered furniture: Migration of flame retardants and potential risks**. *Journal of Hazardous Materials*, 366:556 – 562, 2019.
- [3] GILBERT, M.. **Chapter 1 - plastics materials: Introduction and historical development**. In: Gilbert, M., editor, *BRYDSON'S PLASTICS MATERIALS (EIGHTH EDITION)*, p. 1 – 18. Butterworth-Heinemann, eighth edition edition, 2017.
- [4] GULATI, K.; RAMAKRISHNAN, S.; AW, M. S.; ATKINS, G. J.; FINDLAY, D. M. ; LOSIC, D.. **Biocompatible polymer coating of titania nanotube arrays for improved drug elution and osteoblast adhesion**. *Acta Biomaterialia*, 8(1):449 – 456, 2012.
- [5] HEINZMANN, C.; WEDER, C. ; DE ESPINOSA, L. M.. **Supramolecular polymer adhesives: advanced materials inspired by nature**. *Chem. Soc. Rev.*, 45:342–358, 2016.
- [6] FELDMAN, D.. **Polymer history**. *Designed Monomers and Polymers*, 11(1):1–15, 2008.
- [7] WANG, N.; GAO, J.; WU, Y. ; HAN, W.. **Study on the application of embolization materials of polyvinyl alcohol particles**. *IOP Conference Series: Materials Science and Engineering*, 587:012006, aug 2019.
- [8] HU, J.; ALBADAWI, H.; CHONG, B. W.; DEIPOLYI, A. R.; SHETH, R. A.; KHADEMHOSEINI, A. ; OKLU, R.. **Advances in biomaterials and technologies for vascular embolization**. *Advanced Materials*, 31(33):1901071, 2019.

- [9] SISKIN, G. P.; DOWLING, K.; VIRMANI, R.; JONES, R. ; TODD, D.. **Pathologic evaluation of a spherical polyvinyl alcohol embolic agent in a porcine renal model.** *Journal of Vascular and Interventional Radiology*, 14(1):89 – 98, 2003.
- [10] SPIES, J. B.; ALLISON, S.; FLICK, P.; CRAMP, M.; BRUNO, J.; JHA, R. C. ; ASCHER, S. A.. **Spherical polyvinyl alcohol versus tris-acryl gelatin microspheres for uterine artery embolization for leiomyomas: Results of a limited randomized comparative study.** *Journal of Vascular and Interventional Radiology*, 16(11):1431 – 1437, 2005.
- [11] POURSAID, A.; JENSEN, M. M.; HUO, E. ; GHANDEHARI, H.. **Polymeric materials for embolic and chemoembolic applications.** *Journal of Controlled Release*, 240:414 – 433, 2016. SI: North America Part II.
- [12] HALLENSLEBEN, M. L.; FUSS, R. ; MUMMY, F.. **Polyvinyl Compounds, Others**, p. 1–23. American Cancer Society, 2015.
- [13] OLIVEIRA, M. A. M.; MELO JR., P. A.; NELE, M. ; PINTO, J. C.. **In-situ incorporation of amoxicillin in pva/pvac-co-pmma particles during suspension polymerizations.** *Macromolecular Symposia*, 299-300(1):34–40, 2011.
- [14] AZEVEDO, G. D.. **Estudo das Propriedades de Micropartículas de Poli(Acetato de Vinila-co-Metacrilato de Metila) Usadas em Procedimentos de Embolização Vascular.** PhD thesis, Federal University of Rio de Janeiro, 2019.
- [15] KRALLIS, A.; MEIMAROGLOU, D. ; KIPARISSIDES, C.. **Dynamic prediction of the bivariate molecular weight–copolymer composition distribution using sectional-grid and stochastic numerical methods.** *Chemical Engineering Science*, 63(17):4342 – 4360, 2008.
- [16] BRANDÃO, A. L. T.; SOARES, J. B. P.; PINTO, J. C. ; ALBERTON, A. L.. **When polymer reaction engineers play dice: Applications of monte carlo models in pre.** *Macromolecular Reaction Engineering*, 9(3):141–185, 2015.
- [17] REGO, A. S. C.; BRANDÃO, A. L. T.. **General method for speeding up kinetic monte carlo simulations.** *Industrial & Engineering Chemistry Research*, 59(19):9034–9042, 2020.

- [18] HOSEN, M. A.; HUSSAIN, M. A. ; MJALLI, F. S.. **Hybrid modelling and kinetic estimation for polystyrene batch reactor using artificial neural network (ann) approach.** *Asia-Pacific Journal of Chemical Engineering*, 6(2):274–287, 2011.
- [19] ZHANG, M.; RAY, W. H.. **Modeling of “living” free-radical polymerization processes. i. batch, semibatch, and continuous tank reactors.** *Journal of Applied Polymer Science*, 86(7):1630–1662, 2002.
- [20] ACHILIAS, D.; KIPARISSIDES, C.. **Development of a general mathematical framework for modeling diffusion-controlled free-radical polymerization reactions.** *Macromolecules*, 25(14):3739–3750, 1992.
- [21] ACHILIAS, D.; KIPARISSIDES, C.. **Modeling of diffusion-controlled free-radical polymerization reactions.** *Journal of Applied Polymer Science*, 35(5):1303–1323, 1988.
- [22] KERAMOPOULOS, A.; KIPARISSIDES, C.. **Development of a comprehensive model for diffusion-controlled free-radical copolymerization reactions.** *Macromolecules*, 35(10):4155–4166, 2002.
- [23] MASTAN, E.; ZHU, S.. **Method of moments: A versatile tool for deterministic modeling of polymerization kinetics.** *European Polymer Journal*, 68:139 – 160, 2015.
- [24] VRENTAS, J. S.; DUDA, J. L.. **Diffusion in polymer—solvent systems. i. reexamination of the free-volume theory.** *Journal of Polymer Science: Polymer Physics Edition*, 15(3):403–416, 1977.
- [25] SOH, S. K.; SUNDBERG, D. C.. **Diffusion-controlled vinyl polymerization. i. the gel effect.** *Journal of Polymer Science: Polymer Chemistry Edition*, 20(5):1299–1313, 1982.
- [26] SOH, S. K.; SUNDBERG, D. C.. **Diffusion-controlled vinyl polymerization. ii. limitations on the gel effect.** *Journal of Polymer Science: Polymer Chemistry Edition*, 20(5):1315–1329, 1982.
- [27] SOH, S. K.; SUNDBERG, D. C.. **Diffusion-controlled vinyl polymerization. iii. free volume parameters and diffusion-controlled propagation.** *Journal of Polymer Science: Polymer Chemistry Edition*, 20(5):1331–1344, 1982.

- [28] SOH, S. K.; SUNDBERG, D. C.. **Diffusion-controlled vinyl polymerization. iv. comparison of theory and experiment.** *Journal of Polymer Science: Polymer Chemistry Edition*, 20(5):1345–1371, 1982.
- [29] SU, W. F.. **Principles of Polymer Design and Synthesis.** Springer, Berlin, Heidelberg, 2013.
- [30] ROUIF, S.. **Radiation cross-linked polymers: Recent developments and new applications.** *Nuclear Instruments and Methods in Physics Research Section B: Beam Interactions with Materials and Atoms*, 236(1):68 – 72, 2005. *Ionizing Radiation Polymers.*
- [31] CRAWFORD, R. J.; THRONE, J. L.. **Rotational molding technology.** William Andrew, 2001.
- [32] KRZYSZTOF MATYJASZEWSKI, T. P. D.. **Handbook of Radical Polymerization.** Wiley-Interscience, 2002.
- [33] TOBITA, H.; HAMIELEC, A. E.. **Modeling of network formation in free radical polymerization.** *Macromolecules*, 22(7):3098–3105, 1989.
- [34] PEREIRA, J. O.. **Modelagem e simulação de reatores de polimerização em massa de estireno com iniciadores multifuncionais.** PhD thesis, Federal University of Rio de Janeiro, 2012.
- [35] VERROS, G. D.; ACHILIAS, D. S.. **Modeling gel effect in branched polymer systems: Free-radical solution homopolymerization of vinyl acetate.** *Journal of Applied Polymer Science*, 111(5):2171–2185, 2009.
- [36] SILVA, F. M.; LIMA, E. L. ; PINTO, J. C.. **Acrylic acid/vinyl acetate suspension copolymerizations. 2. modeling and experimental results.** *Industrial & Engineering Chemistry Research*, 43(23):7324–7342, Nov 2004.
- [37] CURTEANU, S.; BULACOVSKI, V.. **Free radical polymerization of methyl methacrylate: Modeling and simulation under semi-batch and nonisothermal reactor conditions.** *Journal of Applied Polymer Science*, 74(11):2561–2570, 1999.
- [38] KIPARISSIDES, C.. **Polymerization reactor modeling: A review of recent developments and future directions.** *Chemical Engineering Science*, 51(10):1637 – 1659, 1996. *Chemical Reaction Engineering: From Fundamentals to Commercial Plants and Products.*

- [39] KONSTADINIDIS, K.; ACHILIAS, D. ; KIPARISSIDES, C.. **Development of a unified mathematical framework for modelling molecular and structural changes in free-radical homopolymerization reactions.** *Polymer*, 33(23):5019 – 5031, 1992.
- [40] SILVA, F. M.; LIMA, E. L. ; PINTO, J. C.. **Acrylic acid/vinyl acetate suspension copolymerizations. 2. modeling and experimental results.** *Industrial & Engineering Chemistry Research*, 43(23):7324–7342, 2004.
- [41] NESVADBA, P.. **Radical Polymerization in Industry.** American Cancer Society, 2012.
- [42] VIVALDO-LIMA, E.; WOOD, P. E.; HAMIELEC, A. E. ; PENLIDIS, A.. **An updated review on suspension polymerization.** *Industrial & Engineering Chemistry Research*, 36(4):939–965, 1997.
- [43] KALFAS, G.; RAY, W. H.. **Modeling and experimental studies of aqueous suspension polymerization processes. 1. modeling and simulations.** *Industrial & Engineering Chemistry Research*, 32(9):1822–1830, 1993.
- [44] **Endovascular embolization by transcatheter delivery of particles: Past, present, and future.** *Journal of Functional Biomaterials*, 8(2):12, 2017.
- [45] DAWBARN, R. H. M.. **The starvation operation for malignancy in the external carotid area. its failures and successes.** *Journal of the American Medical Association*, XLIII(12):792–795, 09 1904.
- [46] LUESSENHOP, A. J.; VELASQUEZ, A. C.. **Observations on the tolerance of the intracranial arteries to catheterization.** *Journal of Neurosurgery*, 21(2), 1964.
- [47] SELVARAJ, M.; TAKAHATA, K.. **Electrothermally driven hydrogel-on-flex-circuit actuator for smart steerable catheters.** *Micromachines*, 11(1):68, 2020.
- [48] RÖSCH, J.; DOTTER, C. T. ; BROWN, M. J.. **Selective arterial embolization.** *Radiology*, 102(2):303–306, 1972. PMID: 4536688.
- [49] RÖSCH, J.; DOTTER, C. T. ; BROWN, M. J.. **Selective arterial embolization.** *Radiology*, 102(2):303–306, 1972. PMID: 4536688.

- [50] HORÁK, D.; ŠEKŠVEC, F.; KÁLAL, J.; ADAMYAN, A. A.; VOLYNSKII, Y. D.; VORONKOVA, O. S.; KOKOV, L. S. ; GUMARGALIEVA, K. Z.. **Hydrogels in endovascular embolization. ii. clinical use of spherical particles.** *Biomaterials*, 7(6):467 – 470, 1986.
- [51] MANN, W. J.; JANDER, H.; PARTRIDGE, E. E.; RUSSINOVICH, N.; HATCH, K. D.; TAYLOR, P. T. ; SHINGLETON, H. M.. **Selective arterial embolization for control of bleeding in gynecologic malignancy.** *Gynecologic Oncology*, 10(3):279 – 289, 1980.
- [52] TAKEMURA, M.; YAMASAKI, M.; TANAKA, F.; SHIMIZU, H.; OKAMOTO, E.; HISAMATU, K.; OHAMA, K.; TUJI, S.; HADA, Y. ; NOSAKI, T.. **Transcatheter arterial embolization in the management of gynecological neoplasms.** *Gynecologic Oncology*, 34(1):38 – 42, 1989.
- [53] COLLINS, C.; JACKSON, J.. **Pelvic arterial embolization following hysterectomy and bilateral internal iliac artery ligation for intractable primary post partum haemorrhage.** *Clinical Radiology*, 50(10):710 – 714, 1995.
- [54] JONES, K.; MEYERS, P.; GOBIN, P. ; LIU, A.-H.. **Embolization of spinal tumors.** *Operative Techniques in Neurosurgery*, 6(3):156 – 162, 2003. *Vascular Lesions Affecting the Spine*.
- [55] REINHART, H. A.; GHALEB, M. ; DAVIS, B. R.. **Transarterial embolization of renal tumors improves surgical outcomes: A case series.** *International Journal of Surgery Case Reports*, 15:116 – 118, 2015.
- [56] MURRAY, T. E.; DOYLE, F. ; LEE, M.. **Transarterial embolization of angiomyolipoma: A systematic review.** *Journal of Urology*, 194(3):635–639, 2015.
- [57] MONLEÓN, J.; CAÑETE, M. L.; CABALLERO, V.; DEL CAMPO, M.; DOMÉNECH, A.; ÁNGEL LOSADA, M. ; CALAF, J.. **Epidemiology of uterine myomas and clinical practice in spain: An observational study.** *European Journal of Obstetrics Gynecology and Reproductive Biology*, 226:59 – 65, 2018.
- [58] LOBEL, M. K.; SOMASUNDARAM, P. ; MORTON, C. C.. **The genetic heterogeneity of uterine leiomyomata.** *Obstetrics and Gynecology Clinics*, 33(1):13–39, Mar 2006.

- [59] BOCLIN, K. L. S.; FAERSTEIN, E.. **Prevalence of self-reported medical diagnosis of uterine leiomyomas in a brazilian population: Demographic and socioeconomic patterns in the pro-saúde study.** *Revista Brasileira de Epidemiologia*, 16(2):301–313, 2013.
- [60] SPARIC, R.; MIRKOVIC, L.; MALVASI, A. ; TINELLI, A.. **Epidemiology of uterine myomas: A review.** *International journal of fertility & sterility*, 9(4):424–435, 2016. 26985330[pmid].
- [61] FOURIE, P.. **Intravascular approach to the treatment of cerebral arteriovenous malformations and dural arteriovenous fistulae.** *South African Journal of Radiology*, 1(3):18–22, 1996.
- [62] LEYON, J. J.; LITTLEHALES, T.; RANGARAJAN, B.; HOEY, E. T. ; GANESHAN, A.. **Endovascular embolization: Review of currently available embolization agents.** *Current Problems in Diagnostic Radiology*, 43(1):35–53, 2014.
- [63] SHETH, R. A.; SABIR, S.; KRISHNAMURTHY, S.; AVERY, R. K.; ZHANG, Y. S.; KHADEMHOSEINI, A. ; OKLU, R.. **Endovascular embolization by transcatheter delivery of particles: Past, present, and future.** *Journal of functional biomaterials*, 8(2):12, Apr 2017. 28368345[pmid].
- [64] CEDERSTAV, A. K.; NOVAK, B. M.. **Investigations into the chemistry of thermodynamically unstable species. the direct polymerization of vinyl alcohol, the enolic tautomer of acetaldehyde.** *Journal of the American Chemical Society*, 116(9):4073–4074, 1994.
- [65] PEIXOTO, L. D. S.. **Produção de partículas esféricas de pva/pvac com morfologia casca-núcleo para uso em embolização vascular.** Master's thesis, Federal University of Rio de Janeiro, 2007.
- [66] AL-HARTHI, M. A.. **Highlight on the mathematical modeling of controlled free radical polymerization.** *International Journal of Polymer Science*, 2015:469353, May 2015.
- [67] VRENTAS, J. S.; DUDA, J. L.. **Diffusion in polymer—solvent systems. i. reexamination of the free-volume theory.** *Journal of Polymer Science: Polymer Physics Edition*, 15(3):403–416, 1977.
- [68] VRENTAS, J. S.; DUDA, J. L.. **Diffusion in polymer—solvent systems. ii. a predictive theory for the dependence of diffusion coefficients on temperature, concentration, and molecular weight.** *Journal of Polymer Science: Polymer Physics Edition*, 15(3):417–439, 1977.

- [69] DE GENNES, P. G.. **Dynamics of entangled polymer solutions. i. the rouse model.** *Macromolecules*, 9(4):587–593, 1976.
- [70] DE GENNES, P. G.. **Kinetics of diffusion-controlled processes in dense polymer systems. ii. effects of entanglements.** *The Journal of Chemical Physics*, 76(6):3322–3326, 1982.
- [71] SUZUKI, H.; MATHOT, V. B. F.. **An insight into the barton equation for copolymer glass transition.** *Macromolecules*, 22(3):1380–1384, 1989.
- [72] CROWLEY, T. J.; CHOI, K. Y.. **Control of copolymer hydrodynamic volume distribution in a semibatch free radical copolymerization process.** *Computers Chemical Engineering*, 23(9):1153 – 1165, 1999.
- [73] BRANDRUP, J.; IMMERGUT, E.. **Polymer Handbook.** Interscience Publishers, fourth edition edition, 1999.
- [74] NORTH, A. M.. **Polymer chain end accessibility in bimolecular reactions.** *Die Makromolekulare Chemie*, 83(1):15–22, 1965.
- [75] ACHILIAS, D. S.. **A review of modeling of diffusion controlled polymerization reactions.** *Macromolecular Theory and Simulations*, 16(4):319–347, 2007.
- [76] RUSSELL, G. T.; NAPPER, D. H. ; GILBERT, R. G.. **Termination in free-radical polymerizing systems at high conversion.** *Macromolecules*, 21(7):2133–2140, 1988.
- [77] BUBACK, M.; HUCKESTEIN, B. ; RUSSELL, G. T.. **Modeling of termination in intermediate and high conversion free radical polymerizations.** *Macromolecular Chemistry and Physics*, 195(2):539–554, 1994.
- [78] BRANDÃO, A. L. T.. **Mathematical modeling of chain branching reactions in olefin coordination polymerizations.** PhD thesis, Federal University of Rio de Janeiro, 2017.
- [79] KENNEDY, J.; EBERHART, R.. **Particle swarm optimization.** In: *PROCEEDINGS OF ICNN'95 - INTERNATIONAL CONFERENCE ON NEURAL NETWORKS*, volumen 4, p. 1942–1948 vol.4, 1995.
- [80] RINI, D. P.; SHAMSUDDIN, S. M. ; YUHANIZ, S.. **Particle swarm optimization: Technique, system and challenges.** *International Journal of Computer Applications*, 1, 09 2011.

- [81] DA ROS, S.; SCHWAAB, M. ; PINTO, J. C.. **Parameter estimation and statistical methods**. In: REFERENCE MODULE IN CHEMISTRY, MOLECULAR SCIENCES AND CHEMICAL ENGINEERING. Elsevier, 2017.
- [82] HULBURT, H.; KATZ, S.. **Some problems in particle technology: A statistical mechanical formulation**. Chemical Engineering Science, 19(8):555 – 574, 1964.
- [83] IEDEMA, P. D.; HOEFSLOOT, H. C. J.. **Molecular-weight-distribution modelling of radical polymerization in batch and continuous reactors with transfer to polymer leading to gel formation**. Macromolecular Theory and Simulations, 11(4):410–428, 2002.
- [84] PINTO, J.; RAY, W.. **The dynamic behavior of continuous solution polymerization reactors—vii. experimental study of a copolymerization reactor**. Chemical Engineering Science, 50(4):715 – 736, 1995.
- [85] ROBERT C. REID, JOHN M. PRAUSNITZ, B. E. P.. **The properties of gases and liquids**. McGraw-Hill, 4th ed edition, 1987.
- [86] KALFAS, G.; YUAN, H. ; RAY, W. H.. **Modeling and experimental studies of aqueous suspension polymerization processes. 2. experiments in batch reactors**. Industrial & Engineering Chemistry Research, 32(9):1831–1838, 1993.
- [87] KERAMOPOULOS, A.; KIPARISSIDES, C.. **Mathematical modeling of diffusion-controlled free-radical terpolymerization reactions**. Journal of Applied Polymer Science, 88(1):161–176, 2003.
- [88] VICTORIA-VALENZUELA, D.; HERRERA-ORDONEZ, J.; LUNA-BARCENAS, G.; VERROS, G. D. ; ACHILIAS, D. S.. **Bulk free radical polymerization of methyl methacrylate and vinyl acetate: A comparative study**. Macromolecular Reaction Engineering, 10(6):577–587, 2016.
- [89] DUBÉ, M. A.; PENLIDIS, A.. **A systematic approach to the study of multicomponent polymerization kinetics: the butyl acrylate/methyl methacrylate/vinyl acetate example, 2. bulk (and solution) terpolymerization**. Macromolecular Chemistry and Physics, 196(4):1101–1112, 1995.
- [90] PINTO, L.. **Efeito das condições de operação e da geometria do reator sobre a distribuição de tamanhos de partícula de uma**

- polimerização em suspensão. Master's thesis, Universidade Federal de Santa Catarina, 2006.
- [91] ULIANA, M.. Soluções de equações de balanço populacional pelo método de classes com aplicação a processo de polimerização em suspensão. Master's thesis, Universidade de São Paulo, 2007.
- [92] ROBERT A. LEWIS, MICHAEL D. LARRAÑAGA, R. J. L. S.. *Hawley's Condensed Chemical Dictionary*. Wiley, 16 edition, 2016.
- [93] TEYMOUR, F.; RAY, W.. The dynamic behavior of continuous solution polymerization reactors—iv. dynamic stability and bifurcation analysis of an experimental reactor. *Chemical Engineering Science*, 44(9):1967 – 1982, 1989.
- [94] ZIELINSKI, J. M.; DUDA, J. L.. Predicting polymer/solvent diffusion coefficients using free-volume theory. *AIChE Journal*, 38(3):405–415, 1992.
- [95] FERRY, J. D.. *Viscoelastic Properties of Polymers*. Wiley, 3d edition, 1980.
- [96] ZHANG, S. X.; RAY, W. H.. Modeling and experimental studies of aqueous suspension polymerization processes. 3. mass-transfer and monomer solubility effects. *Industrial & Engineering Chemistry Research*, 36(4):1310–1321, 1997.
- [97] MAYO, F. R.; GREGG, R. A. ; MATHESON, M. S.. Chain transfer in the polymerization of styrene. vi. chain transfer with styrene and benzoyl peroxide; the efficiency of initiation and the mechanism of chain termination1. *Journal of the American Chemical Society*, 73(4):1691–1700, 1951.
- [98] AZEVEDO, G. D.; MELO JR., P. A. ; PINTO, J. C.. Influence of sonication on morphological properties of poly(vinyl acetate) particles produced through suspension polymerization. *Macromolecular Symposia*, 368(1):78–83, 2016.
- [99] SANTOS JÚNIOR, J. G. F.. Monitoramento e controle dos tamanhos de partículas em Polimerizações em suspensão do MMA usando NIRS. PhD thesis, Federal University of Rio de Janeiro, 2012.

- [100] AZEVEDO, G. D.; DA SILVA PINTO, J. C. C.. Particle size distributions of p(vac-co-mma) beads produced through nonconventional suspension copolymerizations. *Powder Technology*, 355:727 – 737, 2019.
- [101] AZEVEDO, G. D.; DA SILVA PINTO, J. C. C.. Particle size distributions of p(vac-co-mma) beads produced through nonconventional suspension copolymerizations ii. use of focused beam reflectance measurements for in-line monitoring of chord size distributions. *Powder Technology*, 364:963 – 970, 2020.
- [102] AZEVEDO, G. D.; PINTO, J. C.. Alkaline hydrolysis of p(vac-co-mma) particles for vascular embolization procedures. *Journal of Applied Polymer Science*, 137(42):49298, 2020.

## A Mathematical equivalences

$$\sum_{i=2}^{N_t} \sum_{j=1}^{i-1} P_j^\bullet P_{i-j}^\bullet = \sum_{i=1}^{N_t} P_i^\bullet \sum_{j=1}^{N_t} P_j^\bullet \quad (\text{A-1})$$

$$\sum_{i=2}^{N_t} i \sum_{j=1}^{i-1} P_j^\bullet P_{i-j}^\bullet = \sum_{i=1}^{N_t} \sum_{j=1}^{N_t} (i+j) P_i^\bullet P_j^\bullet = \sum_{i=1}^{N_t} i P_i^\bullet \sum_{j=1}^{N_t} P_j^\bullet + \sum_{i=1}^{N_t} P_i^\bullet \sum_{j=1}^{N_t} j P_j^\bullet \quad (\text{A-2})$$

$$\begin{aligned} \sum_{i=2}^{N_t} i^2 \sum_{j=1}^{i-1} P_j^\bullet P_{i-j}^\bullet &= \sum_{i=1}^{N_t} \sum_{j=1}^{N_t} (i+j)^2 P_i^\bullet P_j^\bullet = \\ \sum_{i=1}^{N_t} i^2 P_i^\bullet \sum_{j=1}^{N_t} P_j^\bullet &+ 2 \sum_{i=1}^{N_t} i P_i^\bullet \sum_{j=1}^{N_t} j P_j^\bullet + \sum_{i=1}^{N_t} P_i^\bullet \sum_{j=1}^{N_t} j^2 P_j^\bullet \end{aligned} \quad (\text{A-3})$$

## B

### Copolymerization moments valid combinations

- **Live moments:**

$$\gamma_{k,w} = \sum_i^{\infty} \sum_j^{\infty} i^k j^w P_{i,j}^{\bullet} \quad \text{for all valid combinations of } i \text{ and } j \quad (\text{B-1})$$

$$\gamma_{0,0} = \sum_{i=1}^{\infty} \sum_{j=0}^{\infty} i^0 j^0 P_{i,j}^{\bullet} = \sum_{i=1}^{\infty} \sum_{j=0}^{\infty} P_{i,j}^{\bullet} \quad (\text{B-2})$$

$$\pi_{0,0} = \sum_{i=0}^{\infty} \sum_{j=1}^{\infty} i^0 j^0 Q_{i,j}^{\bullet} = \sum_{i=0}^{\infty} \sum_{j=1}^{\infty} Q_{i,j}^{\bullet} \quad (\text{B-3})$$

$$\gamma_{1,0} = \sum_{i=1}^{\infty} \sum_{j=0}^{\infty} i^1 j^0 P_{i,j}^{\bullet} = \sum_{i=1}^{\infty} \sum_{j=0}^{\infty} i P_{i,j}^{\bullet} \quad (\text{B-4})$$

$$\pi_{1,0} = \sum_{i=0}^{\infty} \sum_{j=1}^{\infty} i^1 j^0 Q_{i,j}^{\bullet} = \sum_{i=0}^{\infty} \sum_{j=1}^{\infty} i Q_{i,j}^{\bullet} = \sum_{i=1}^{\infty} \sum_{j=1}^{\infty} i Q_{i,j}^{\bullet} \quad (\text{B-5})$$

$$\gamma_{0,1} = \sum_{i=1}^{\infty} \sum_{j=0}^{\infty} i^0 j^1 P_{i,j}^{\bullet} = \sum_{i=1}^{\infty} \sum_{j=0}^{\infty} j P_{i,j}^{\bullet} = \sum_{i=1}^{\infty} \sum_{j=1}^{\infty} j P_{i,j}^{\bullet} \quad (\text{B-6})$$

$$\pi_{0,1} = \sum_{i=0}^{\infty} \sum_{j=1}^{\infty} i^0 j^1 Q_{i,j}^{\bullet} = \sum_{i=0}^{\infty} \sum_{j=1}^{\infty} j Q_{i,j}^{\bullet} \quad (\text{B-7})$$

$$\gamma_{2,0} = \sum_{i=1}^{\infty} \sum_{j=0}^{\infty} i^2 j^0 P_{i,j}^{\bullet} = \sum_{i=1}^{\infty} \sum_{j=0}^{\infty} i^2 P_{i,j}^{\bullet} \quad (\text{B-8})$$

$$\pi_{2,0} = \sum_{i=0}^{\infty} \sum_{j=1}^{\infty} i^2 j^0 Q_{i,j}^{\bullet} = \sum_{i=0}^{\infty} \sum_{j=1}^{\infty} i^2 Q_{i,j}^{\bullet} = \sum_{i=1}^{\infty} \sum_{j=1}^{\infty} i^2 Q_{i,j}^{\bullet} \quad (\text{B-9})$$

$$\gamma_{0,2} = \sum_{i=1}^{\infty} \sum_{j=0}^{\infty} i^0 j^2 P_{i,j}^{\bullet} = \sum_{i=1}^{\infty} \sum_{j=0}^{\infty} j^2 P_{i,j}^{\bullet} = \sum_{i=1}^{\infty} \sum_{j=1}^{\infty} j^2 P_{i,j}^{\bullet} \quad (\text{B-10})$$

$$\pi_{0,2} = \sum_{i=0}^{\infty} \sum_{j=1}^{\infty} i^0 j^2 Q_{i,j}^{\bullet} = \sum_{i=0}^{\infty} \sum_{j=1}^{\infty} j^2 Q_{i,j}^{\bullet} \quad (\text{B-11})$$

$$\gamma_{1,1} = \sum_{i=1}^{\infty} \sum_{j=0}^{\infty} i^1 j^1 P_{i,j}^{\bullet} = \sum_{i=1}^{\infty} \sum_{j=0}^{\infty} ij P_{i,j}^{\bullet} = \sum_{i=1}^{\infty} \sum_{j=1}^{\infty} ij P_{i,j}^{\bullet} \quad (\text{B-12})$$

$$\pi_{1,1} = \sum_{i=0}^{\infty} \sum_{j=1}^{\infty} i^1 j^1 Q_{i,j}^{\bullet} = \sum_{i=0}^{\infty} \sum_{j=1}^{\infty} ij Q_{i,j}^{\bullet} = \sum_{i=1}^{\infty} \sum_{j=1}^{\infty} ij Q_{i,j}^{\bullet} \quad (\text{B-13})$$

• **Dead moments:**

$$\mu_{k,w} = \sum_i^{\infty} \sum_j^{\infty} i^k j^w D_{i,j} \quad \text{for all valid combinations of } i \text{ and } j \quad (\text{B-14})$$

$$\mu_{0,0} = \sum_{i=1}^{\infty} \sum_{j=1}^{\infty} D_{i,j} + \sum_{i=1}^{\infty} D_{i,0} + \sum_{j=1}^{\infty} D_{0,j} \quad (\text{B-15})$$

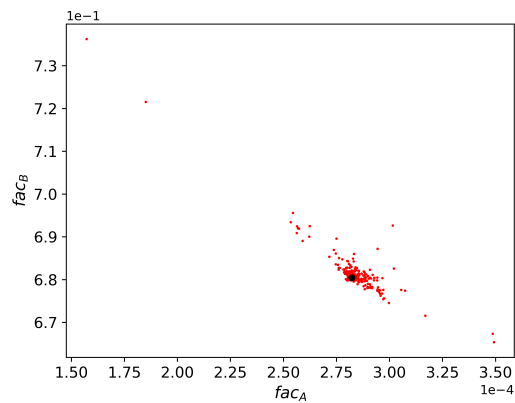
$$\mu_{1,0} = \sum_{i=1}^{\infty} \sum_{j=0}^{\infty} i D_{i,j} \quad ; \quad \mu_{0,1} = \sum_{i=0}^{\infty} \sum_{j=1}^{\infty} j D_{i,j} \quad (\text{B-16})$$

$$\mu_{2,0} = \sum_{i=1}^{\infty} \sum_{j=0}^{\infty} i^2 D_{i,j} \quad ; \quad \mu_{0,2} = \sum_{i=0}^{\infty} \sum_{j=1}^{\infty} j^2 D_{i,j} \quad (\text{B-17})$$

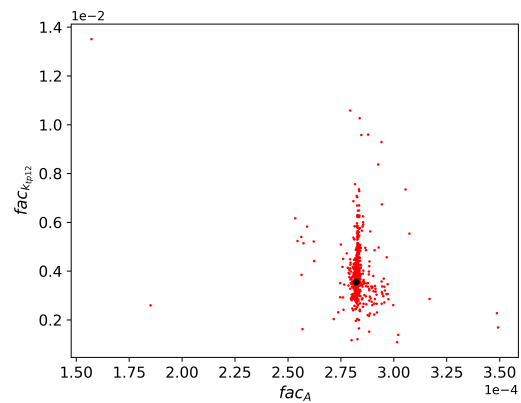
$$\mu_{1,1} = \sum_{i=1}^{\infty} \sum_{j=1}^{\infty} ij D_{i,j} \quad (\text{B-18})$$

# C

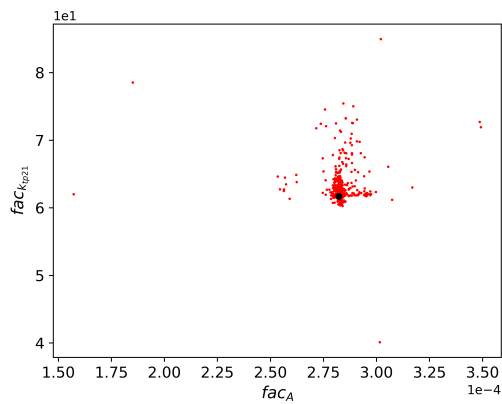
## Values of model parameter in the confidence regions



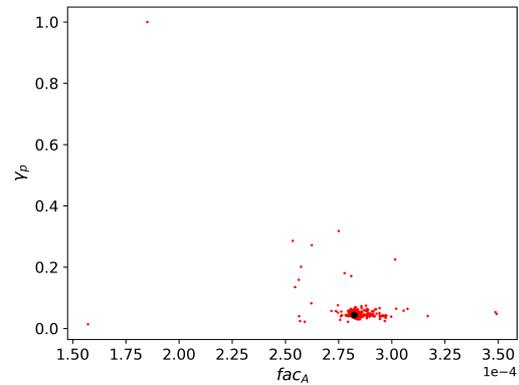
(C.1(a))



(C.1(b))

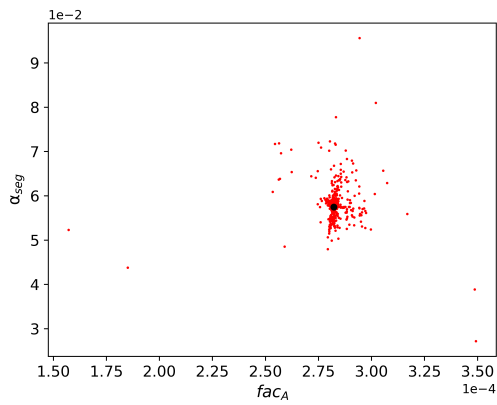


(C.1(c))

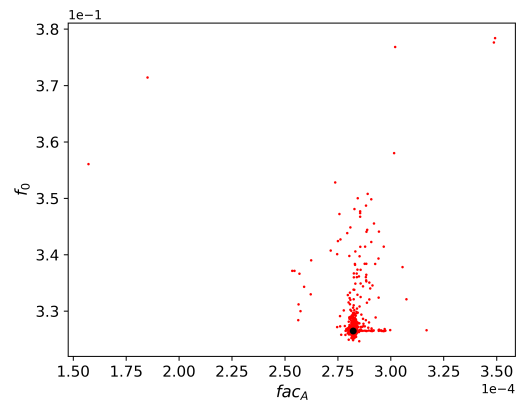


(C.1(d))

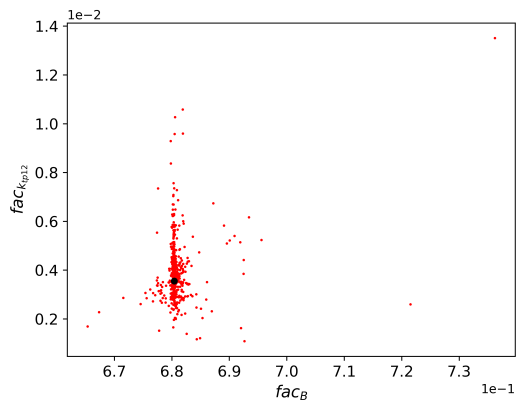
Figure C.1: Values of the coordinates that were considered to be inside the confidence region.



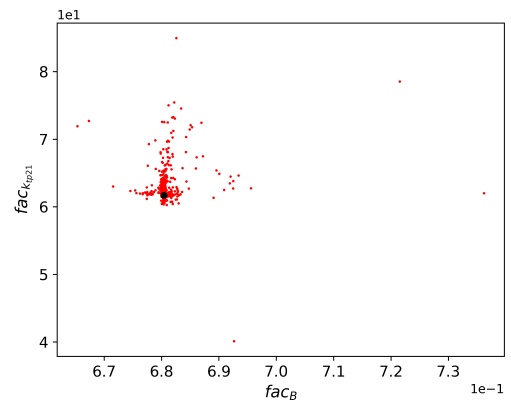
(C.2(a))



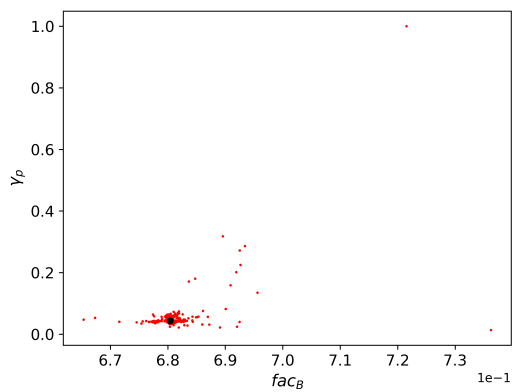
(C.2(b))



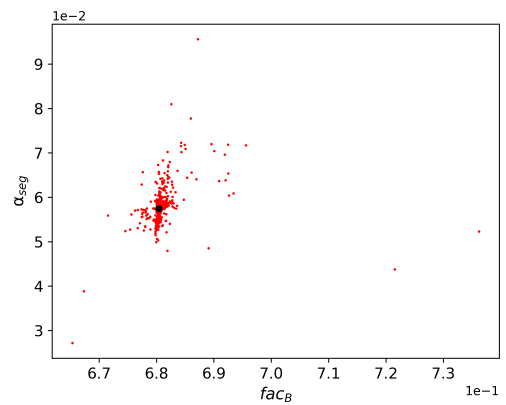
(C.2(c))



(C.2(d))

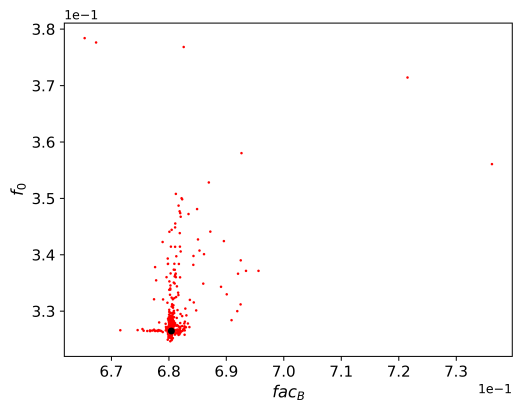


(C.2(e))

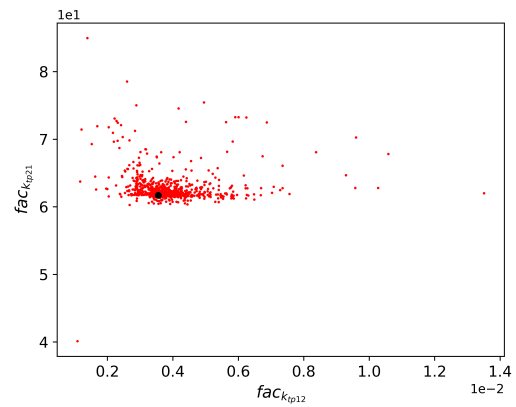


(C.2(f))

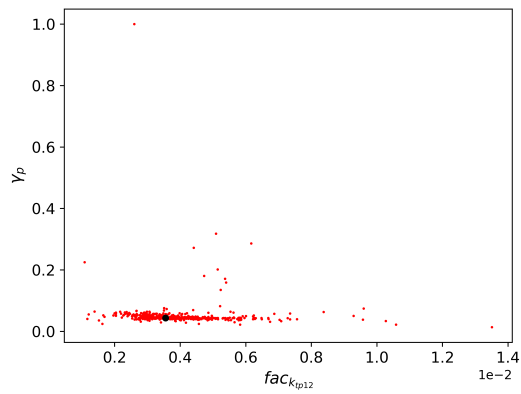
Figure C.2: Values of the coordinates that were considered to be inside the confidence region, continuation.



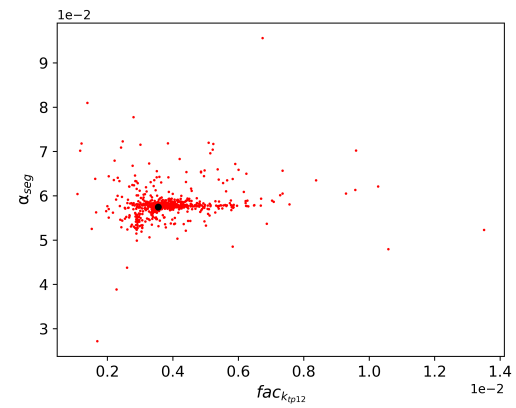
(C.3(a))



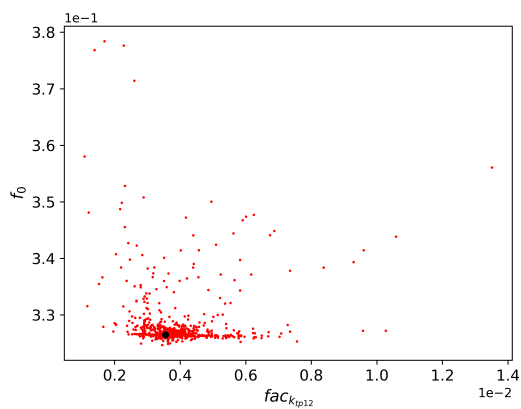
(C.3(b))



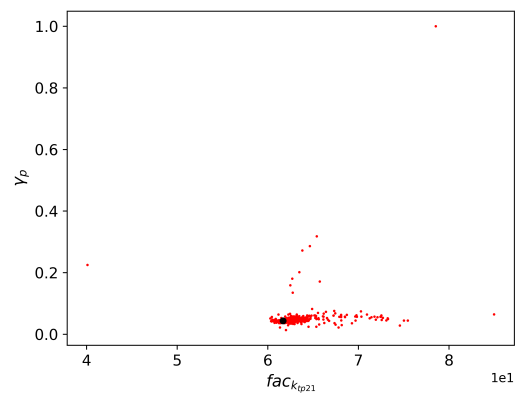
(C.3(c))



(C.3(d))



(C.3(e))



(C.3(f))

Figure C.3: Values of the coordinates that were considered to be inside the confidence region, continuation.

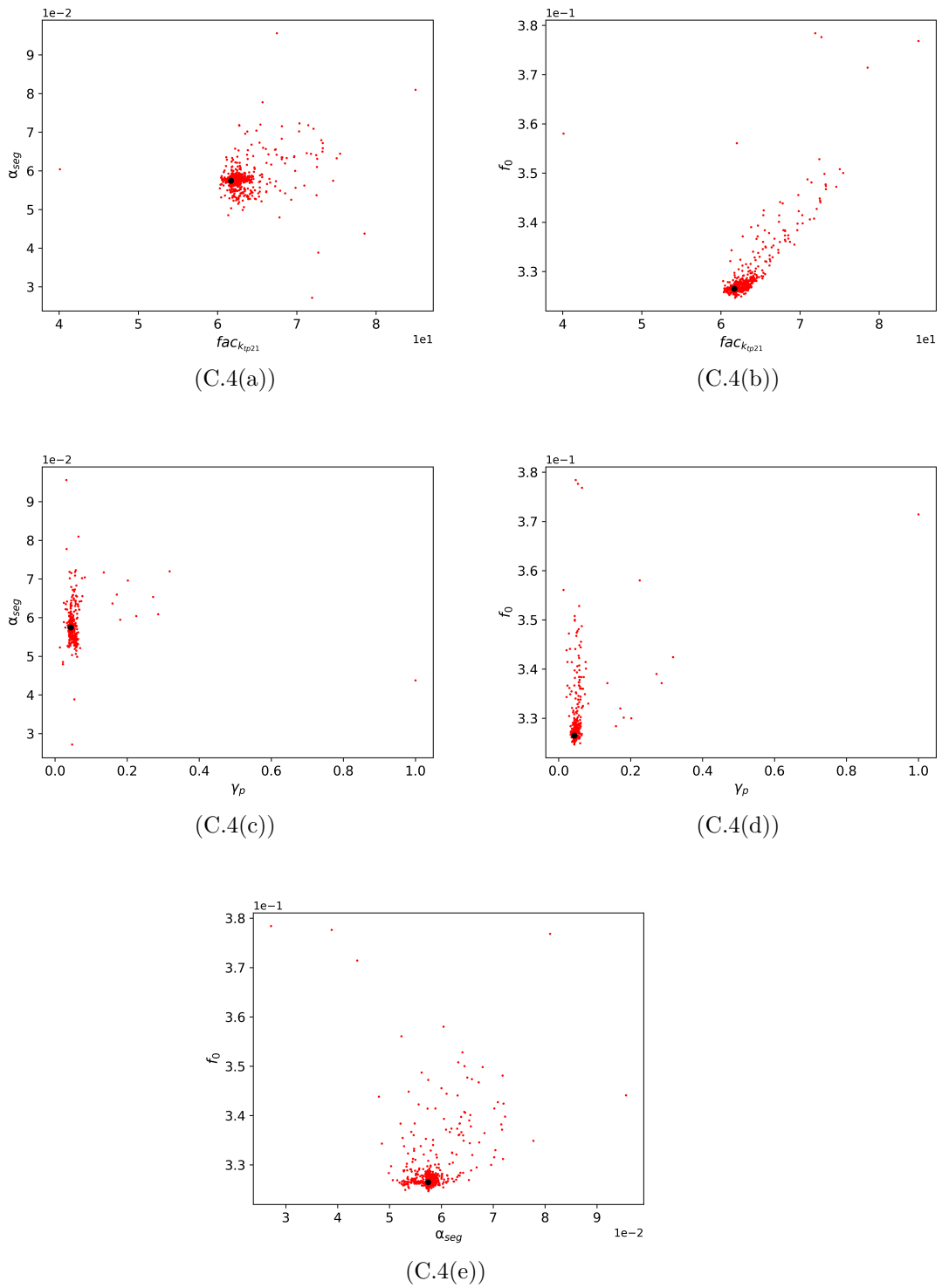


Figure C.4: Values of the coordinates that were considered to be inside the confidence region, continuation.

## D

### Monomer, volume and initiator charts

- Poly(vinyl acetate) homopolymerization

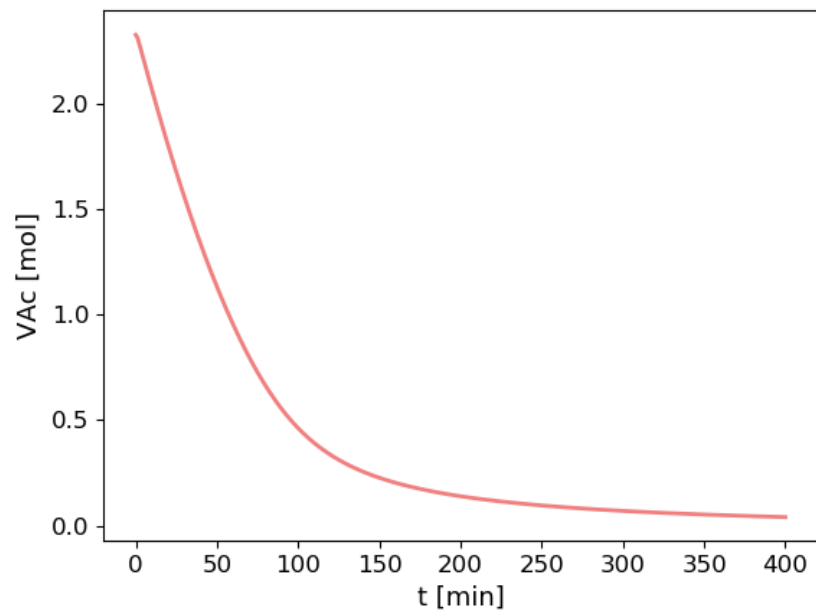


Figure D.1: Vinyl acetate molar behavior.

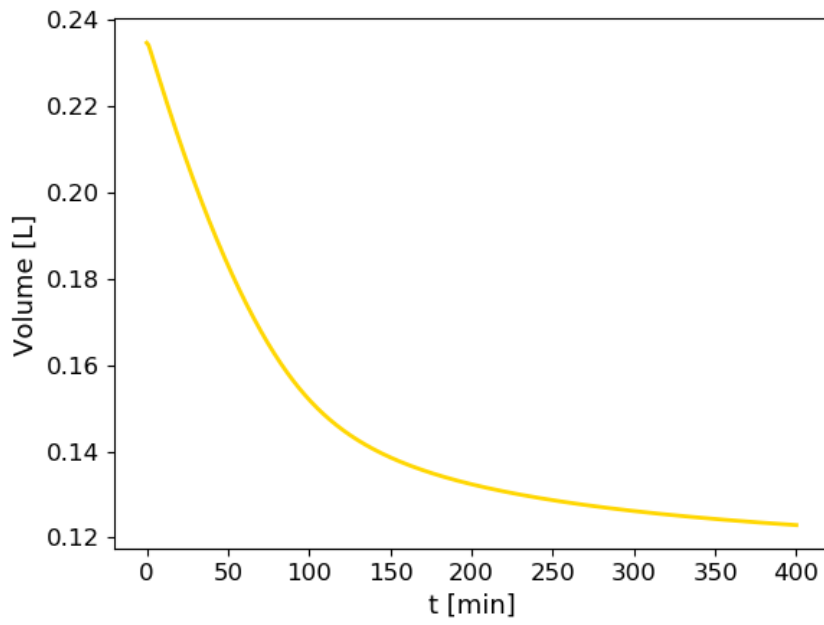


Figure D.2: Volume behavior.

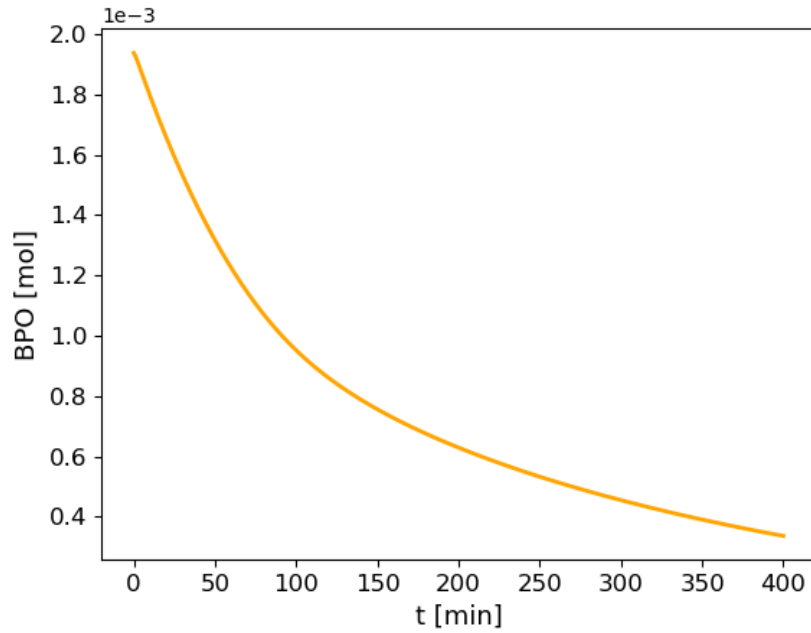


Figure D.3: Initiator molar behavior.

- Poly(methyl methacrylate) homopolymerization

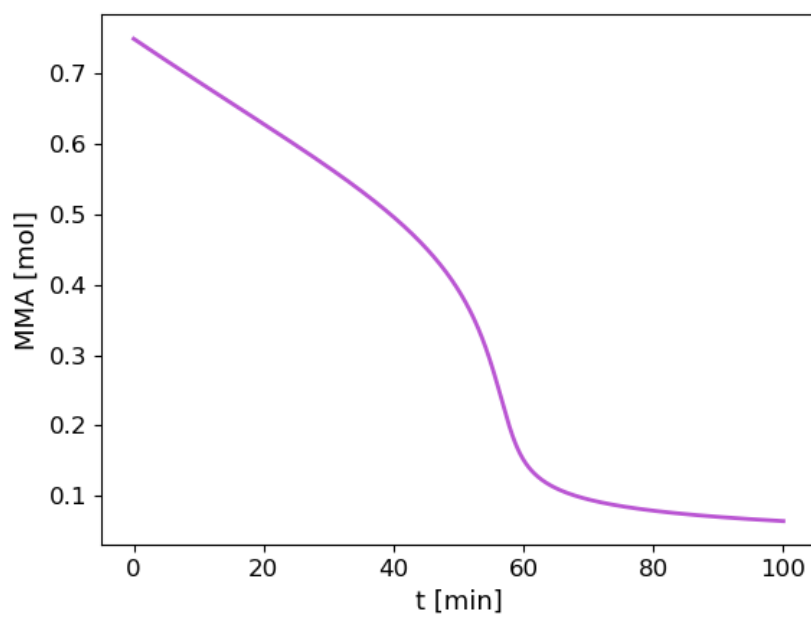


Figure D.4: Methyl methacrylate molar behavior.

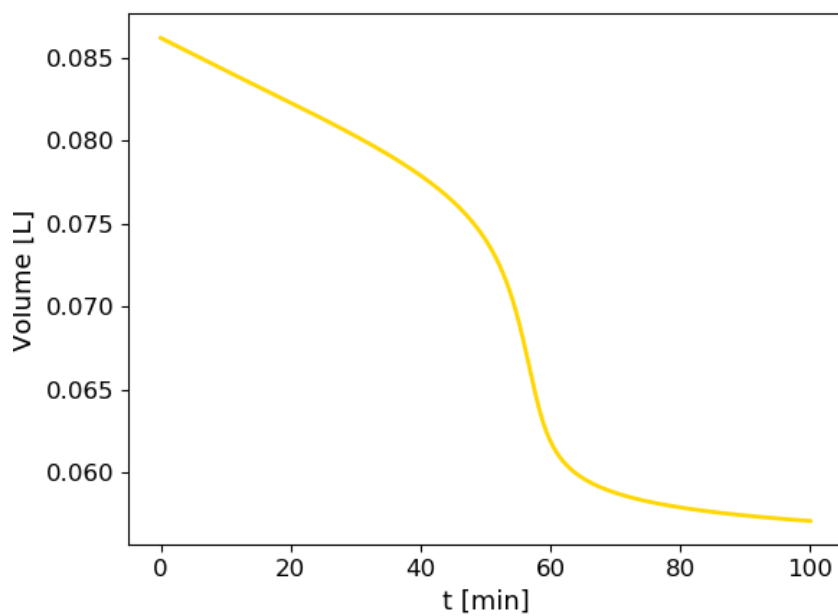


Figure D.5: Volume behavior.

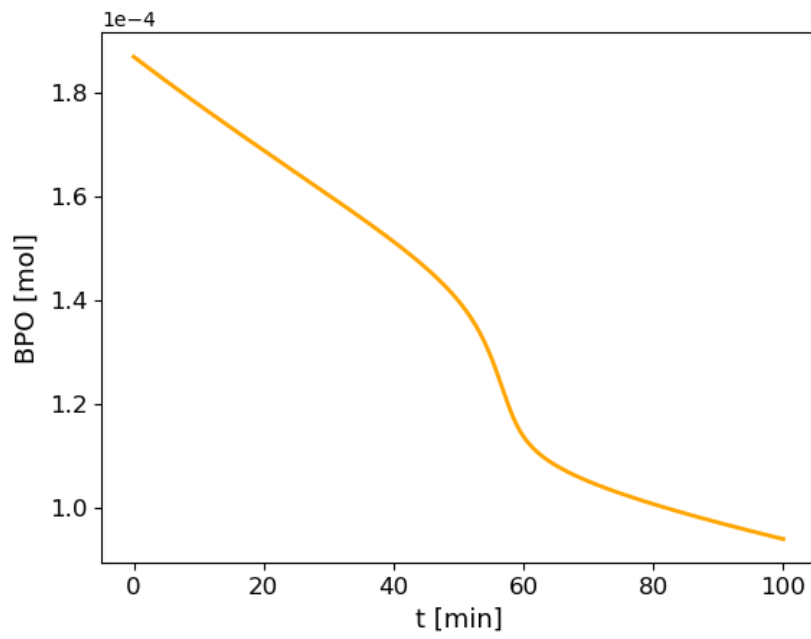


Figure D.6: Initiator molar behavior.

- Poly(vinyl acetate-co-methyl methacrylate) copolymerization

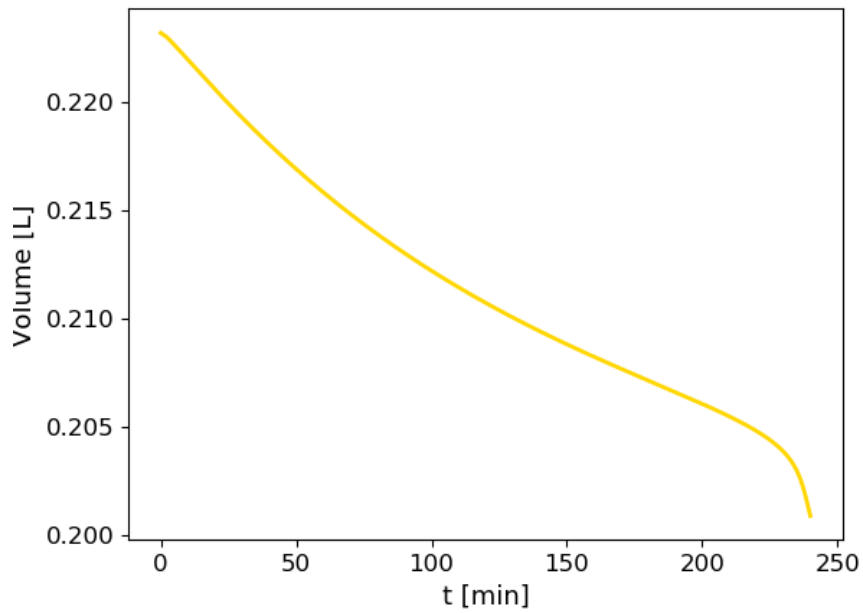


Figure D.7: Volume behavior.

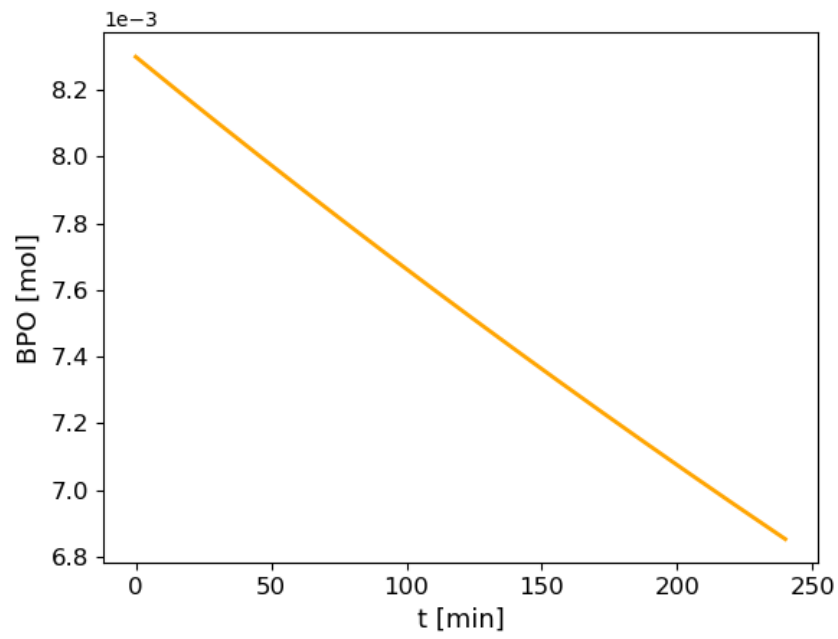


Figure D.8: Initiator molar behavior.